The influence of spring-neap cycles on sediment trapping in tide-dominated estuaries

Dennis Bouwman

TU Delft

The influence of spring-neap cycles on sediment trapping in tide-dominated estuaries

by

Dennis Derek Bouwman

to obtain the degree of Master of Science in Applied Mathematics
with a specialization in Computational Science and Engineering
at the faculty of Electrical Engineering, Mathematics and Computer Science
at the Delft University of Technology.
To be defended publicly on Friday June 7, 2019 at 13:15.

Student number: 4240596

Project duration: September 3, 2018 – June 7, 2019

Thesis committee:

Dr. ir. H.M. Schuttelaars,	Technische Universiteit Delft, Supervisor
Dr. ir. W.T. van Horssen,	Technische Universiteit Delft
Ir. T.J. Zitman,	Technische Universiteit Delft
Dr. ir. Y.M. Dijkstra,	Technische Universiteit Delft, Supervisor

An electronic version of this thesis is available at `http://repository.tudelft.nl/`.

TU Delft

Contents

Preface

Prior to presenting my thesis, I would like to steal the reader's attention and to explain how this thesis came to be and dedicate a few words to sentimentality.

First of all, I would like to tell a story about this document that would not be clear for any reader other than my roommates. At the start of this thesis I concluded that the lifestyle of a stay-at-home-mathematician would be a good fit for me, and subsequently I decided to complete the entire thesis from my student room. A consequence of this decision is that the act of getting dressed is instantly reduced to a purely hypothetical part of daily life. As a result, I estimate that more than 90% of the work that went into this thesis was performed by a deranged-looking adolescent in pyjamas with his peculiar taste of music blasting on max volume. Since the combination of pyjamas with music is a necessary and sufficient condition for a pyjama-party, I cannot help but conclude that this thesis is the outcome of the single most productive pyjama-party of my life.

Of course this deranged-looking adolescent is not the sole contributor to this thesis. Multiple people have helped me both directly and indirectly. Thus some acknowledgements are in order.
First of all I would like thank my daily supervisors Henk and Yoeri. I really enjoyed our weekly meetings and I learned a great many things during them. In particular, I would like to thank Yoeri for helping me when iFlow would not and I would like to thank Henk for the innumerable lessons you taught me and for convincing the people at CWI that they should hire me to do a PhD. I hope that both of you enjoyed our cooperation as much as I did.
I would like to thank Piotr for listening to me rambling on about the tides more often than proper manners dictate, pretending to be good at chess and introducing me to the word *kurwa*.
I owe an apology and an acknowledgement to my roommates, who courageously put up with four-coffee-in-the-morning-Dennis during my regular microbreaks.
Further, I would like to thank Ties for our coffee-thesis sessions and insightful conversations.
Als laatste wil ik graag mijn ouders bedanken: Guido en Joke, als het over mijn studievoortgang gaat dan zeggen jullie soms wel eens tegen mij: 'dat heb je van een vreemde gekregen', maar dit doet onder aan de positieve invloed die jullie op mij hebben gehad. Jullie zijn voor mij hét toonbeeld van doorzettingsvermogen, volharding en toewijding, ook al zeg ik dat eigenlijk nooit hardop. Zonder jullie goede voorbeeld, liefde en steun was ik nooit de persoon geworden die ik nu ben. Meer dan jullie misschien zouden willen toegeven en meer dan ik ooit zal kunnen begrijpen is dit document te danken aan jullie.

If the reader permits, I will redirect their attention one final time in the following abrupt manner: After being confronted with my inevitable retreat from Delft several months ago, I spent some alone-time in retrospection of my life as a student between the years 2012 and 2019. This reexamination forces me to disagree with the credo: 'time flies too fast', since the deeper I sink into memories the more I am astounded by the sheer number of experiences and events that were squeezed into these seven years. (Probably I should be astounded by the number of questionable decisions that have led to great stories, but those will not be treated within the confines of this formal document...) The memories of these past seven years would not have been mine if it were not for the great friends whom I've met along the way. Sadly, this group is too numerous for me to address individually, but to the unlucky few who felt obligated to "scan" the preface of my thesis I would like to say: I am sincerely and deeply grateful for the time we spent together.

With a heavy heart and a blissful mind I turn towards the next chapter of my life.

Delft, June 2019

Abstract

Using an idealized width-averaged model, the influence of spring-neap cycles on the transport and trapping of suspended fine sediment in tide-dominated estuaries is investigated. To this end we introduce a multiple time scale expansion. This provides a mathematically sound argument for treating the fast ebb-flood cycle and the slow spring-neap variations as independent time scales. With this expansion, semi-analytical approximations of the water motion and suspended sediment concentrations can be found as functions of the spring-neap time scale. The advantage of this is that the transport of sediment is then investigated in a tidally-averaged sense using analytically obtained temporal dependencies and model simulations based on the conditions in 2005 of the Ems-Dollard estuary. We found that sediment import is strongly enhanced during spring tide and that a combination of vanishing import processes and sediment export due to river discharge resulted in a net export of sediment during neap tide. Furthermore the spring-neap varying deposition of fine sediment in a bottom pool on the river bed is investigated. We found that the time needed for the system to adjust to new equilibrium conditions can not be neglected within a spring-neap cycle as temporal lag effects are clearly visible in the dynamic behaviour of the bottom pool and suspended sediment concentrations. These temporal lag effects are sensitive to the choice of the parameter governing erosion. Assuming different values of the erosion parameter we have shown that the long-term characteristics of the bottom pool are sensitive to these temporal lag effects. Choosing a low value of the erosion parameter results in the presence of a bottom pool throughout the spring-neap cycle. With a high value of the erosion no bottom pool is formed at any time in the spring-neap cycle.

1 Introduction

1.1. Estuaries: where rivers meet the seas

As a river flows towards the sea, the characteristics of the river change due to the connection with the sea. For example, the fresh river-water and the salt sea-water tend to mix resulting in a region of brackish water. Also, the tides enter the river at the seaward connection and have a measurable influence many kilometers upstream. To distinguish this transition region, the definition of an estuary will be introduced:
An estuary is defined as a semi-enclosed coastal body of water, which has a free connection with the open sea and within which saline sea water is measurably diluted with fresh water from land drainage, often in the form of a river [Pritchard, 1967].

A typical feature of most estuaries is the propagation of tidal waves originating from the seas. These tidal waves can be observed much further upstream than the salt-intrusion, thus forming a fresh-water region where the water elevation is still influenced by the tides. In this thesis, the definition of an estuary is extended to include this region, which is formally named the tidal river [Fairbridge, 1980]. Figure 1.1 illustrates a general transition from river to sea. In some estuaries the influence of tidal waves on the water motion and surface elevation is much greater than the influence of river discharge and wind-induced shear stress at the surface. Such estuaries are the focus of this research and will be named: tide-dominated estuaries.

Because of the water motion due to tidal forcing and river outflow, suspended fine sediment is transported in estuaries. Fine sediment is considered as silt or flocculated groups of clay particles with a typical settling velocity of the order of 1 mm/s, that can be kept in suspension due to turbulent mixing. When in suspension the fine sediment is transported by the water motion through a variety of physical processes, for instance due to advection with the ebb-flood water motion. These transport mechanisms are not necessarily balanced. Hence, over the course of an ebb-flood cycle, many estuaries exhibit a net non-zero total transport of sediment. As a result an estuary can act as a natural sediment retainer, where sediment is imported from the sea or river and kept within the estuary. Examples of estuaries that have strong importing characteristics are the

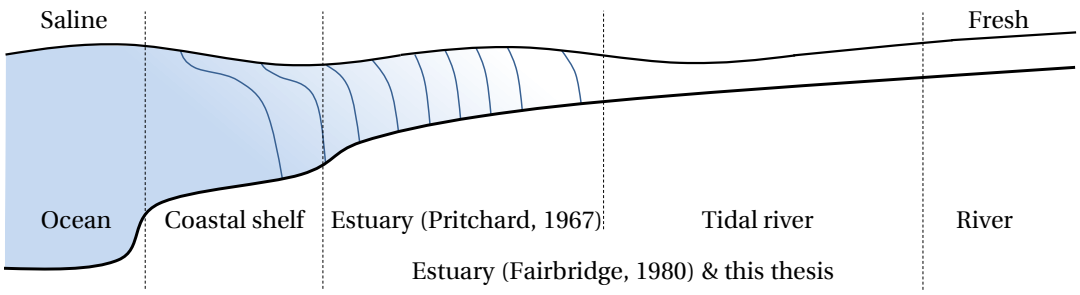

Figure 1.1: Sketch of a river connecting to the sea, with different transition regions indicated. The blue color represent the gradual transition from salt to fresh water, blue lines indicate lines of equal salinity. (Figure from Dijkstra [2019])

Ems (The Netherlands-Germany) and the Loire (France) [Winterwerp and Wang, 2013]. Due to gravitational forces suspended sediment tends to be deposited on the river bed in regions with low turbulence, as the vertical mixing processes cannot keep the sediment in suspension. Therefore we observe an accumulation of sediment on the river bed in the still waters near dams, weirs and harbors. In some importing estuaries such an accumulation can also be observed in more energetic regions [Burchard et al., 2018]. In such scenarios, a complex interplay of deposition, resuspension and longitudinal transport of sediment results in the formation of a region where concentrations of suspended sediment exceeds those in the direct surroundings; such a region is called an estuarine turbidity maximum (ETM). More formally an ETM is defined as a local maximum of the cross-sectionally averaged and tidally averaged suspended sediment concentration [Burchard et al., 2018]. For ETMs with sufficiently high suspended sediment concentrations (SSC) an accumulation of sediment on the river bed is observed. Within this research, sediment deposited on the river bed is only allowed to be transported by resuspension into the water through a process of erosion. In the case that such a layer of deposited sediment persists throughout an ebb-flood cycle we say that the sediment is trapped. The associated layer of fluid mud on the river bed is then referred to as the bottom pool.

1.1.1. Why Study Estuarine Sediment Dynamics?

Estuaries are important from both economic and ecological perspectives. The accumulation of suspended sediment can greatly affect the monetary and natural value of these environments. Therefore, we study sediment dynamics to understand and forecast the underlying processes that govern of ETM and bottom pool formation. This will now be elaborated:

In an estimate of the monetary value of various ecosystems Costanza et al. [1997] have ranked the estuary amongst one of the most productive. In part this is due to the potential of an estuary to support large productions of organic compounds through photosynthesis by phytoplankton. In turn, the availability of these organic compounds provides the basis of the estuarine food chain and is beneficial for commercialized fishing and shell-fish farming in estuaries. However, photosynthesis requires sunlight which is blocked by suspended sediment concentrations exceeding $10-100$ mg/L [Wofsy, 1983]. Thus it follows that high suspended sediment concentrations, as observed in an ETM for example, impose limitations on the productivity of estuaries [Colijn, 1982]. Another important factor contributing to the economical value of estuaries is the support of the world's biggest ports, for example the ports of Shanghai (China), Rotterdam (The Netherlands) and Antwerp (Belgium) are all located in estuaries. The accessibility of these ports is provided by deep navigation channels. The deposition of sediment on the river bed results in channel siltation reducing the accessibility of the port. As a result, the depth of these navigation channels must be regularly maintained by expensive dregding activities.

Aside from economic value, estuaries also support many important ecological functions and are a vital connection between river and sea for many anadromous (ocean dwelling but spawning in estuaries and rivers) and catadromous (freshwater dwelling but spawning in seawater) species (Meire et al. [2005] and references therein). The migration of these species is severely affected by the presence of ETMs. The high concentrations of suspended sediment are associated with depleted oxygen levels [Talke et al., 2009a] leading to hypoxia. Most aquatic life-forms cannot survive in or traverse hypoxic regions, which is why they are commonly referred to as 'dead-zones'. Persistence of dead-zones result in the habitat loss of migrating species accompanied by detrimental consequences for the estuarine ecosystem [Diaz and Rosenberg, 2011].

1.1.2. Subject of this Study

The combination of lunar and solar tidal waves introduces strong fortnightly amplitude variations of the sea surface elevation associated with the ebb-flood cycle. These periodic amplitude variations are commonly referred to as the spring-neap cycle. The effects of spring-neap cycles on stratification, circulation, sediment trapping and bottom consolidation in estuaries has been speculated by Allen et al. [1980]. More recent results, see Sutherland and MacCready [2011], Li et al. [2017] and Hunt et al. [2017], have confirmed the influence of spring-neap variations on a variety of estuarine processes. However, a thorough study on the influence of spring-neap variations on sediment trapping and bottom-pool formation in the context of idealized modelling of estuaries is as of yet not available. Instead most idealized approaches, such as Dijkstra et al. [2017], Brouwer et al. [2018], Dijkstra et al. [2019] and Meerman et al. [2019] only account for purely lunar tidal forcing, usually resulting in an asymmetric ebb-flood cycle (i.e. the falling time of ebb is different than the rising time of flood). In this thesis we will alleviate the assumptions concerning the prescribed tidal wave by in-

cluding the solar tidal constituents and provide a detailed study of the influence of spring-neap cycles on sediment trapping and bottom-pool evolution in an idealized context.

In the remaining parts of this chapter, we will introduce the reader to some important concepts used in this thesis. The implications of combined lunar and solar semidiurnal tidal forcing is described in Section 1.2. Section 1.3 contains a discussion on equilibrium solutions accompanied by a qualitative explanation of the influence of a bottom pool on the adaptation time of dynamic solutions converging to an equilibrium. The characteristics of an idealized model and the application to the Ems estuary are discussed in Section 1.4. Finally, the research questions will be formulated in Section 1.5.

1.2. Spring-Neap Tidal Cycles

Tidal waves are generated due to the gravitational forces of the sun and the moon. As a result we have distinct tidal waves associated with the sun and the moon. The period of these waves differs by a mere matter of minutes, as the period of the principal solar tidal wave is 12 hours while the principal lunar tidal wave has a period of 12 hours and 25 minutes. When these two waves interfere with each other, this small difference in their wave periods introduces a physical phenomenon known as a beat frequency. The idea behind this phenomenon is that, as time progresses, the relative phase between the two waves changes gradually. This results in a change in the alignment of the extreme values of the two waves. Hence an alternating pattern between constructive interference, when peaks align with peaks, and destructive interference, when peaks align with troughs, arises due to the small difference between their wave periods. The resulting wave is then perceived as an ebb-flood cycle with slow-varying amplitude and phase changes known as the spring-neap cycle. In Figure 1.2 this concept is qualitatively illustrated by presenting a regular ebb-flood cycle and an ebb-flood cycle with slow-varying amplitudes.

The perceived spring-neap variations occur with a period of 14 days. Thus the spring-neap variations and the ebb-flood cycles oscillate on vastly different time scales. This allows the reformulation of the tidal forcing in terms of an amplitude modulated function. The amplitude modulated tidal wave is written as a regular ebb-flood cycle multiplied by an envelope representing the gradual sping-neap variations. The benefit of this approach is that by employing this reformulation the time scales are disentangled, thus allowing for the study of an ebb-flood cycle independent of variations introduced by the spring-neap cycle.

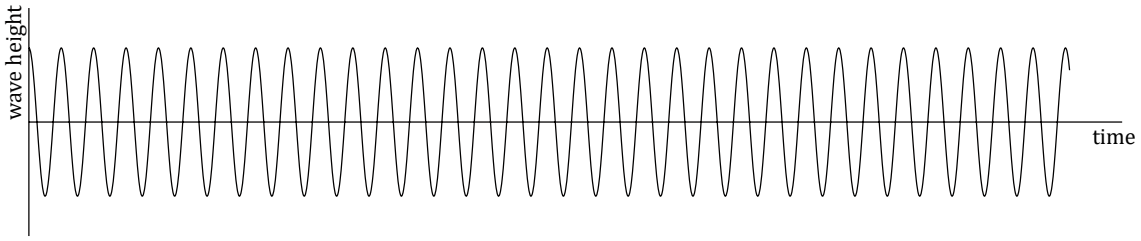

(a) Regular ebb-flood cycle

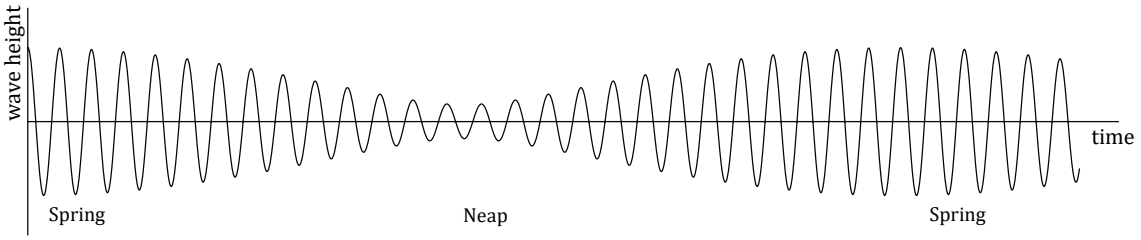

(b) Ebb-flood cycle with spring-neap variations

Figure 1.2: These two figures qualitatively illustrate the difference between regular and spring-neap varying ebb-flood cycles. In Figure 1.2a the wave height of the principal component of the lunar tidal wave is shown. In Figure 1.2b the principal components of the lunar and solar waves are combined. This can be written as the product of the regular ebb-flood cycle with a slow-varying amplitude function.

Previous studies have shown that the ebb-flood cycle is one of the crucial aspects of sediment transport in some estuaries [Chernetsky et al., 2010, Dijkstra et al., 2019]. The trapping of sediment only occurred under a specific interplay of conditions, for example regarding tidal forcing, bathymetry and river discharge. By introducing the spring-neap cycle, one of these crucial aspects governing sediment trapping, namely tidallu forced water motion, is subjected to periodic changes. Thus transport mechanisms, sediment trapping and bottom pool evolution also vary on the spring-neap timescale. As a result, it is possible that the total transport of sediment alternates between an importing phase, where sediment is transported upstream and accumulates in an ETM, and exporting phase, when the sediment in the ETM is depleted and transported to the sea.

1.3. Equilibria on Multiple Time Scales

1.3.1. Concentration Equilibrium

The conditions in an estuary are subject to constant change due to the tidally forced movement of water. Due to the introduction of solar tidal constituents, the tidal forcing consists of a relatively fast time scale associated with the ebb-flood cycle with spring-neap variations on the long time scale. The big gap between the two time scales allows us to interpret the transport processes in a tidally averaged sense with respect to the ebb-flood cycle. In this interpretation the intertidal transport of sediment, that is the sediment transport during an ebb-flood cycle, is not subjected to analysis. Instead this behaviour will be represented by a tidally averaged quantity. This has two advantages; First, many transport processes vanish in the tidally averaged sense and can therefore be omitted, greatly simplifying the analysis. Second, we can formulate a concentration equilibrium condition [Dijkstra et al., 2019]. The concentration equilibrium can be interpreted as the solution where tidally averaged SSC is constant on the fast time scale of an ebb-flood cycle for fixed tidal conditions. Variations of the slower spring-neap time scales affect the tidally averaged steady state of SSC.

1.3.2. Adaptation Time

Although the concentration equilibrium is defined as a steady-state solution on the ebb-flood time scale, it does not necessarily follow that a similar equilibrium condition also holds for variations on the spring-neap time scale. In general, a tidally averaged solution requires an adaptation time to adjust to new equilibrium conditions associated with a different tidal forcing. In the theory of dynamical system such a solution is called exponentially stable and the adaptation time corresponds to the inverse rate of convergence.

If the adaptation time is of the same order as or larger than the typical time scale of the spring-neap variations, then the solution is expected to lag behind the changing equilibrium conditions. This is called a temporal lag effect. An example of a mechanism that introduces temporal lag effects is the time needed to resuspend the sediment deposited in the bottom pool, since the concentration can only reach the new equilibrium position if the bottom pool is completely depleted (this example will be discussed more extensively below). Temporal lag effects can also arise in the absence of a bottom pool, for example if the tidally averaged transport of sediment is relatively small compared to the SSC since a relatively long time is needed to redistribute suspended sediment.

1.3.3. Temporal Lag Effects due to a Bottom Pool

The strength of temporal lag effects due to the presence of a bottom pool is affected by the rate of erosion, which is related to the dimensionless erosion parameter $\hat{M}$ within the context of this thesis. For example, if $\hat{M}$ is large, then the rate of erosion is large and the temporal lag effect is weak, since only a short time is needed to resuspend a given amount of sediment in the bottom pool. It would hold that the bottom pool would be rapidly resuspended in the exporting phase of the spring-neap cycle. On the other hand, if $\hat{M}$ is small then the rate of erosion is small and the temporal lag effect is strong. In this case, we would find a bottom pool even during parts of the exporting phase of the spring-neap cycle. In the extreme, if $\hat{M}$ is sufficiently small then the temporal lag effect persists throughout the exporting phase of the spring-neap cycle upon which the bottom pool will be resupplied in the importing phase and thus continues to grow with each spring-neap cycle. Therefore, the dimensionless erosion parameter is regarded as an important parameter determining the long-term characteristics of bottom pool evolution. However this parameter is not yet properly understood nor has there been any research in which this parameter is properly calibrated or prescribed using field observations, see Section 8.3.2. of Dijkstra [2019].

1.3.4. Assessing the Importance of Temporal Lag Effects

To assess the importance of temporal lag effects associated with spring-neap variations of the tidal forcing, we will compare two types of solutions for different values of $\hat{M}$. The first solution type corresponds to the concentration equilibrium, that is the solution that would instantly adapt to a new equilibrium condition. The second type is a dynamic equilibrium, defined as solution in which the adaptation time is taken into account. By comparison of these types of solutions, the influence of temporal lag effects introduced by spring-neap variations on the trapping of sediment will be investigated. We will show that different values of $\hat{M}$ yield vastly different long-term characteristics of bottom pool evolution, thereby underlining the importance of a proper estimation for the dimensionless erosion parameter.

1.4. Modeling Approach

1.4.1. Complex versus Idealized

The research field of estuarine dynamics is broad and a vast amount of modeling studies exist. These models can be categorized, by their approach and purpose, ranging from *complex* to *exploratory* (sometimes referred to as *idealized*) [Murray, 2003].

Complex models aim at obtaining a highly accurate quantitative comparison between model output and observations of estuarine dynamics. To this end, complex models use state-of-the-art parametrizations to account for unresolved processes, high-resolution meshing of the geometrical domain and rigorous model calibration. However this comes at the cost of lengthy computation times thus restraining the extent of sensitivity studies. Furthermore, results of complex models are less suitable for qualitative analysis as different processes cannot be studied in isolation.

On the other side of the spectrum, idealized models are effective tools for developing fundamental understanding of estuarine processes. These models often involve elaborate (semi-)analytical methods reducing calculation time and thus allowing for in-depth sensitivity studies. Furthermore, in idealized models the individual processes can be studied in isolation, greatly aiding the analysis of model results. However, these models require considerable simplifications and model assumptions. Hence these exploratory models aim at qualitatively explaining trends of the estuarine processes instead of a detailed quantitative reproduction of observations.

Since the goal of this study is to gain qualitative understanding of the influence of spring-neap cycles on sediment trapping, the model and solution method presented in the following chapters will be on the idealized end of the spectrum. Our focus is on the longitudinal balance of transport mechanisms, therefore a width-averaged model (2DV) is taken as the vantage point. Characteristic for the spring-neap cycle, is the emergence of a fast ebb-flood cycle with slow-varying amplitude and phase changes. Within the idealized context, these two time scales can be simplified by approximating them as distinct and independent. Then using a multiple time scale expansion, the spring-neap variations can be incorporated into the semi-analytical solution method.

1.4.2. Application to the Ems-Dollard Estuary

Although the theory developed in this thesis is general in nature, results will be obtained by applying the model to the Ems-Dollard estuary in particular. The Ems-Dollard estuary is located on the Dutch-German border (see Figure 1.3) where the Ems river discharges in the shallow coastal Wadden Sea. A series of islands bordering the coast act as a natural barrier between the Wadden Sea and the North Sea. In Figure 1.3b one can find Borkum, one of these barrier islands. The part between Borkum and the city of Knock is called the outer Ems estuary. The domain of focus in this thesis extends from the city Knock, 64 kilometers upstream, to a tidal weir at Herbrum. Based on observations, we prescribe a tidal forcing at Knock and a constant river discharge at Herbrum. Further, in between Knock and Pogum the shallow Dollard bay is located. A semi-permeable dam (Geisedamm) partly seperates the course of the river from this bay. The influence of the Dollard bay on the estuarine dynamics is neglected, the role of the Dollard bay on the ETM dynamics is at this moment unclear and subject to active research. The estuary is relatively narrow and slowly converging allowing for a focus on the width-averaged dynamics.

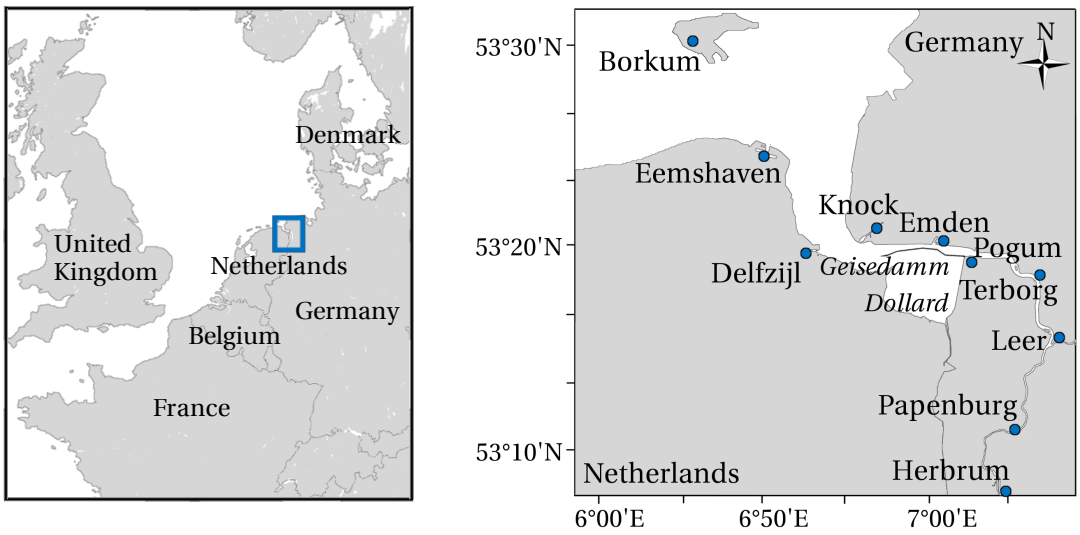

(a) Location of the Ems in Europe

(b) The Ems-Dollard estuary

Figure 1.3: The Ems-Dollard estuary is located on the Dutch-German border. The island Borkum marks the transition between Wadden Sea and the North Sea. The estuarine domain under consideration in this thesis stretches from the city Knock to the tidal weir at Herbrum. Further, between Knock and Pogum the shallow Dollard bay is located. A semi-permeable dam (Geisedamm) partly seperates the course of the river from this bay. (Figures from Dijkstra [2019])

1.5. Research Questions and Outline of this Thesis

As mentioned in Section 1.1.2 the main goal of this study is to investigate the influence of the spring-neap variations on sediment trapping. To that end we define the following research questions:

1. Can the solar semi diurnal tidal constituents be incorporated in a semi-analytical modeling framework?
2. What are the effects of the spring-neap cycle on the transport of sediment?
3. How are the long-term characteristics of bottom pool evolution affected by temporal lag effects associated with the spring-neap cycle?

These research questions will be answered in the following chapters. The thesis is structured as follows:

- **Chapter 2** presents the idealized geometrical features, the systems of equations describing water motion and sediment transport and the evolution equation of the bottom pool.
- **Chapter 3** contains an overview of the semi-analytical solution method used to solve the water motion and sediment dynamics under the influence of the spring-neap cycle. Further this chapter contains an analytical description of the influence of spring-neap variations on sediment transport.
- **Chapter 4** consists of two simulation studies based on the characteristics of the Ems estuary. First the tidal-averaged equilibrium solution within a single spring-neap cycle is obtained accompanied by a process-based study of the transport of sediment. Second the influence of temporal lag effects is shown by comparing the dynamic solutions with the aformentioned tidal averaged equilibrium solution.
- **Chapter 5** concludes the obtained results and answers the research questions. Moreover, possibilities for future research are discussed.

2

Model Description

A width-averaged model that describes the interaction between water motion and sediment transport will be presented to investigate the influence of a spring-neap cycle on sediment trapping in tidally dominated estuaries. The domain considered consists of a single channel with prescribed width- and depth-profiles. On this domain, the water motion is governed by the width- and Reynolds-averaged shallow-water equations. Suspended sediment concentrations follow from a width-averaged transport equation. Lastly, sediment fluxes at the river bed and bottom pool evolution follow from a concentration equilibrium condition.

2.1. Domain and Geometry

The domain under consideration consists of a single channel estuary of finite length L, see Figure 2.1. The along-channel coordinate x extends from the seaward boundary, denoted by $x = 0$, to a tidal weir located at $x = L$. The width of the estuary $B(x)$ is assumed to be exponentially converging [Savenije, 2012]:

$$B(x) = B_0 e^{-x/L_b}, \tag{2.1}$$

with B_0 the width at the seaward boundary and L_b the convergence length. Further, the bottom profile at $z = -H(x)$ is allowed to vary gradually in the along-channel direction. The free surface elevation is located at $z = \zeta(t,x)$ with t denoting time and $z = 0$ the reference water level. An external tidal wave is prescribed at the seaward boundary. A depth-integrated transport of water is prescribed at the tidal weir, representing the river discharge. It is assumed that no water or sediment leaves the domain through the side-banks. Similarly, it is assumed that the river bed is impermeable for water.

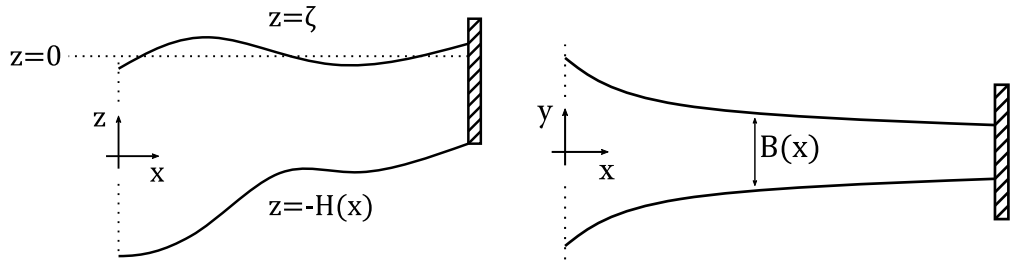

(a) Side view (b) Top view

Figure 2.1: Sketches of the geometry of an idealized single-channel estuary.

2.2. Width-Averaged Water Motion

The water level $\zeta(t,x)$, horizontal velocity $u(t,x,z)$ and vertical velocity $w(t,x,z)$ are determined by the width- and Reynolds-averaged shallow water equations. These coupled partial differential equations follow from the Reynolds-averaged Navier-Stokes equations together with the Boussinesq approximation, the hydrostatic assumption and a turbulence closure model. Here a prescribed time- and depth-independent vertical eddy

viscosity coefficient $A_v(x)$ will be used. Following Friedrichs and Hamrick [1996], we take the vertical eddy viscosity to be linearly proportional to the local water depth:

$$A_v = A_{v0}\frac{H(x)}{H_0}, \tag{2.2}$$

with A_{v0} the eddy viscosity coefficient at the seaward boundary and H_0 the depth at the seaward boundary. Furthermore, Coriolis effects are neglected and the estuary is assumed to be well-mixed, hence the salinity and density are independent of the vertical coordinate. We assume that the along-channel density only varies due to a prescribed time-independent salinity, thus neglecting density variations due to temperature, suspended sediment concentration and temporal variations of salinity. Following these assumptions, the along-channel density can be expressed as:

$$\rho(x) = \rho_0\Big(1+\beta_s\langle S(x)\rangle\Big), \tag{2.3}$$

with ρ_0 is the reference density and β_s a parameter converting salinity to a density increment and $\langle S(x)\rangle$ the depth- and tidal averaged salinity expressed as [Talke et al., 2009b]:

$$\langle S(x)\rangle = \frac{S_{\text{sea}}}{2}\left(1-\tanh\left(\frac{x-x_c}{x_L}\right)\right), \tag{2.4}$$

with S_{sea} the seaward salinity, x_c the location of maximum salinity gradient and x_L the typical length scale of the salt intrusion. The tidal average $\langle\cdot\rangle$ is defined as the average over the period associated with the lunar semi diurnal tidal constituent (M_2):

$$\langle\cdot\rangle \equiv \frac{1}{P}\int_0^P \cdot\, dt, \tag{2.5}$$

with P the M_2 tidal period, see Section 3.1 for an elaborate discussion. The resulting equations read (for details see Appendix A):

$$u_x + w_z - \frac{u}{L_b} = 0, \tag{2.6a}$$

$$u_t + uu_x + wu_z + g\zeta_x + \frac{g\rho_x}{\rho_0}(z-\zeta) - (A_v u_z)_z = 0, \tag{2.6b}$$

where g is the gravitational acceleration.

2.2.1. Boundary Conditions

At the seaward boundary the water motion is forced by both the semi-diurnal lunar (M_2) and solar (S_2) tidal constituents and their respective first overtides (M_4 and S_4):

$$\zeta(t,0) = \sum_{i\in\mathcal{G}} A_i\cos(\sigma_i t+\phi_i). \tag{2.7}$$

Here, A_i denotes the tidal amplitude, σ_i the angular frequency, $\phi_i \in [0,\, 2\pi)$ the phase and $\mathcal{G} = (M_2,\, S_2,\, M_4,\, S_4)$ the set containing the harmonic tidal constituents.

At the landward boundary at $x = L$, a constant river discharge $Q > 0$ is prescribed:

$$B(L)\int_{-H}^{\zeta} u(t,L,z)\,dz = -Q. \tag{2.8}$$

At the free surface, the effects of wind shear stress are neglected, requiring the free surface to be stress-free:

$$A_v u_z = 0, \qquad \text{at } z=\zeta. \tag{2.9}$$

Furthermore, the kinematic boundary condition is imposed:

$$w = \zeta_t + u\zeta_x, \qquad \text{at } z=\zeta. \tag{2.10}$$

The river bed is considered to be impermeable regarding water motion:

$$w = -uH_x, \qquad \text{at } z=-H(x), \tag{2.11}$$

and the shear stress at the bed τ_b is taken proportional to the near-bed velocity squared. Following Zimmerman [1982], we replace this quadratic relation by a linearized condition, $\tau_b = \rho_0 s_f u$, with s_f the partial slip parameter. This results in the following dynamic boundary condition:

$$A_v u_z = s_f u, \qquad \text{at } z = -H(x). \tag{2.12}$$

Following Schramkowksi et al. [2002], we use a linear relation for the partial slip parameter:

$$s_f = s_{f0} \frac{H(x)}{H_0}, \tag{2.13}$$

with s_{f0} partial slip parameter at seaward boundary.

2.3. Width-Averaged Sediment Transport

The transport of width-averaged suspended sediment concentration (SSC), denoted by $c(t,x,z)$, is governed by the following advection-diffusion equation (for details see Appendix B):

$$c_t + uc_x + (w - w_s)c_z = (K_h c_x)_x + (K_v c_z)_z - \frac{1}{L_b} K_h c_x, \tag{2.14}$$

with w_s a constant settling velocity and the functions K_h and K_v horizontal and vertical eddy diffusivity coefficients. The vertical eddy diffusivity can be related to the vertical eddy-viscosity by taking $K_v = \sigma_P A_v$, with σ_P the Prandtl-Schmidt number. In this research $\sigma_P = 1$ is chosen for simplicity. Furthermore, the horizontal eddy diffusivity K_h is assumed to be constant.

2.3.1. Boundary Conditions

At the seaward boundary we prescribe a depth averaged and tidally averaged concentration c_{sea}. On the landward side, a constant tidally averaged transport due to sediment import across the tidal weir is prescribed, denoted by $\mathcal{F}_{\text{river}}$. At the free surface we require that the sediment flux vanishes:

$$-w_s c - K_v c_z + K_h c_x \zeta_x = 0, \qquad \text{at } z = \zeta. \tag{2.15}$$

The sediment flux at the bottom is governed by the tidally averaged difference in deposition and erosion flux. The deposition flux, which is a result of the gravitational force resulting in a settling velocity w_s, is written as:

$$D = w_s c, \qquad \text{at } z = -H(x).$$

The erosion flux is expressed as $E = \hat{E} f$ [Brouwer et al., 2018], with $\hat{E}$ denoting the potential erosion, i.e. the total erosion that would occur if an abundance of sediment is present, and f the tidally averaged erodibility function. Following Brouwer et al. [2018], the potential erosion can be modeled as:

$$\hat{E} = \frac{w_s \rho_s \hat{M} s_f}{g' d_s} \left| u(t,x,-H) \right|, \tag{2.16}$$

with ρ_s and d_s denoting sediment density and grain size respectively, $g' = g(\rho_s - \rho_0)/\rho_0$ the reduced gravity and $\hat{M}$ the dimensionless erosion parameter. The tidally averaged erodibility function $0 \le f \le 1$ accounts for the amount of erodible sediment on the bottom. If no sediment is present on the bottom at any time in the tidal cycle, $f = 0$ and no sediment can be eroded. If sediment is available on the bed throughout an entire tidal cycle, the erosion flux equals the potential erosion and we find $f = 1$. This is known as an erosion-limited state, since there is still sediment at the bed that can be eroded under different hydrodynamic conditions. If there is a net horizontal convergence of sediment transport at these locations, sediment will accumulate at the bottom resulting in the formation of a bottom pool. For values of f in between these extrema the erodibility indicates the coexistence of an erodible muddy state and an inerodible sandy state within each tidal cycle. This is known as an availability-limited state.

Then by equating the sediment flux at the bottom, Eq. (2.14), to the difference in deposition and erosion we find that the bottom boundary condition can be expressed as:

$$w_s c + K_v c_z - K_h c_x H_x = D - E, \qquad \text{at } z = -H(x). \tag{2.17}$$

2.3.2. Concentration Equilibrium

The net sediment flux at the river bed, Eq. (2.17), governs the growth of a bottom pool. This sediment flux will vary due to changing hydrodynamical conditions induced by the periodic tidal forcing. Hence the total mass of sediment deposited in the bottom pool fluctuates associated with the time scales of the ebb-flood and spring-neap cycles. In this study, we only focus on the bottom pool evolution on the time scale associated with the spring-neap cycle. It is assumed that the difference between tidally averaged erosion and deposition only slowly changes the bottom pool. With this assumption, it holds that the tidally averaged SSC and the tidally averaged bottom pool are in a steady state (associated with the ebb-flood cycle) but are allowed to vary on the much longer time scale associated with the spring-neap cycle. Hence the bottom pool is described by the tidally averaged erodibility f (see definition above). This erodibility is the result of the tidally varying velocity and SSC. Moreover, the erodibility can vary on the spring-neap cycle.

The formulation for the bottom pool evolution starts by assuming that the river bed consists of an impermeable sandy layer not subjected to erosion. Due to deposition of suspended sediment a bottom pool can be formed on the river bed. By taking resuspension into the water column as the only mechanism transporting sediment out of the bottom pool we find that the evolution of the bottom pool is governed by the difference in deposition and erosion fluxes, D and E respectively:

$$(\mathcal{S}_{\text{bed}})_t = D - E, \tag{2.18}$$

with $\mathcal{S}_{\text{bed}}$ the width-averaged mass of sediment per surface area in the bottom pool. Next, the total stock is denoted by $\mathcal{S}$ and corresponds to the sum of width averaged and tidally averaged amount of sediment in the bottom pool and suspended in the water column:

$$\mathcal{S}(t,x) = \left\langle \mathcal{S}_{\text{bed}} + \int_{-H}^{\zeta} c(t,x,z)\, dz \right\rangle. \tag{2.19}$$

Since no sources or sinks are present within a water column, $\mathcal{S}$ can only change due to a divergence in the depth-integrated longitudinal sediment transport. An explicit relation between the total stock and longitudinal sediment transport can be found by integrating Eq. (2.14) over the depth, using the Leibniz integral rule and applying the boundary conditions from Eqs. (2.10), (2.11) and (2.15). Next this expression is substituted in Eq. (2.18), then by tidally averaging and using Eq. (2.19) we find (See Appendix B for a detailed derivation):

$$B\mathcal{S}_t = -\left\langle B \int_{-H}^{\zeta} (uc - K_h c_x)\, dz \right\rangle_x. \tag{2.20}$$

This can be interpreted as the tidally averaged depth-integrated version of Eq. (2.18). Eq. (2.20) will be referred to as the concentration equilibrium condition, since the tidally averaged total stock and SSC are in steady state on the time scale associated with the ebb-flood cycle [Dijkstra et al., 2019]. Variations of the total stock and SSC due to spring-neap variations occur on a time scale that is long compared to the ebb-flood cycle. Note that the right-hand side of Eq. (2.20) is dependent on the tidally averaged erodibility f due to the contribution of the erosion flux in Eq. (2.17). Then, with given hydrodynamic conditions, Eq. (2.20) completely determines the tidally averaged SSC and evolution of the bottom pool. Note that Eq. (2.20) was found by requiring an equilibrium in the tidally averaged sense. Thus it follows the solutions of Eq. (2.20) are allowed to vary on the time scale associated with the spring-neap cycle.

3

Solution Method

Continuing on the approaches of Dijkstra et al. [2017] and Brouwer et al. [2018] a perturbation approach will be applied to find semi-analytic approximate solutions to the full system of equations. These perturbation methods allow the original nonlinear system of equations to be approximated by a set of asymptotically ordered linear systems of equations. The linearity of the approximation enables a systematic analysis of the longitudinal transport processes in isolation. A novelty of this thesis, compared to Brouwer et al. [2018], is the introduction of a multiple time scale expansion which allows the analysis of the effects of spring-neap cycles on individual transport processes that underlie sediment trapping dynamics.

3.1. Perturbation Approach

Solving the system of nonlinear equations (2.6a) and (2.6b) using the perturbation approach consists of four steps. We briefly mention these steps and later discuss each step in detail. First, we scale the system of equations and identify a small perturbation parameter ($\varepsilon \ll 1$). Second, we substitute an asymptotic expansion of the unknown variables in terms of this small parameter into the system of equations. Third, we introduce asymptotically ordered time scales corresponding to the fast ebb-flood time scale and the slow spring-neap time scales. Finally, the resulting ordered set of linear equations describing water motion and suspended sediment concentrations can be solved semi-analytically in a systematic manner, while the erodibility and bottom-pool evolution will result from numerically solving the concentration equilibrium condition.

In the first step, we scale the system of equations by making the physical variables dimensionless using their typical scales (for a detailed derivation see Appendix C). The resulting non-dimensional system of equations contains a number of dimensionless parameters whose magnitudes are estimated based on field observations in the Ems estuary (See Section 4.1 for further references). One of these parameters, denoted by ε and defined as the ratio between M_2 amplitude and the entrance depth H_0:

$$\varepsilon = \frac{A_{M_2}}{H_0} \ll 1, \tag{3.1}$$

measures the relative importance of the nonlinear terms in the scaled equations and is typically small in the estuaries under consideration. Using the conditions of the Ems as presented in Table 4.1, we find $\varepsilon \approx 0.14$. Remaining parameters are related to orders of ε, allowing the assessment of their relative importance. It is assumed that the amplitudes of the principal tidal constituents, i.e. the semi diurnal M_2 and S_2 tidal constituents, are of the same order, i.e. $A_{S_2}/A_{M_2} = \mathcal{O}(1)$. The ratio of the amplitudes of the first overtides, M_4 and S_4, with the principal constituents, M_2 and S_2 respectively, is assumed to be of first order, i.e. $A_{S_4}/A_{M_2} = \mathcal{O}(\varepsilon)$ and $A_{M_4}/A_{M_2} = \mathcal{O}(\varepsilon)$. Moreover, the velocities induced by river discharge and baroclinicity are assumed to be of order $\mathcal{O}(\varepsilon)$ compared to the M_2 and S_2 velocity amplitudes.

In the second step the asymptotic expansions in terms of ε for the hydrodynamic variables u, w, ζ and the suspended sediment concentration c are substituted in the system of equations. In this research, only the first two orders turn out to be essential for answering the research questions defined in Section 1.5. Thus the

asymptotic expansions take the form:

$$\begin{aligned} u(t,x,z) &\approx u^0(t,x,z) + u^1(t,x,z), \\ w(t,x,z) &\approx w^0(t,x,z) + w^1(t,x,z), \\ \zeta(t,x) &\approx \zeta^0(t,x) + \zeta^1(t,x), \\ u(t,x,z) &\approx c^0(t,x,z) + c^1(t,x,z), \end{aligned} \tag{3.2}$$

with $[\cdot]^0$ denoting a quantity at leading order and $[\cdot]^1$ a first order quantity. Using the estimated orders of the dimensionless parameters, the full system of equations can now be separated in linear order equations.

3.1.1. Spring-Neap Variations

In the third step the linear order equations will be complemented by the multiple time scale expansion, allowing the definition of a well-defined tidal-average.

An external tidal forcing consisting of both lunar and solar semidiurnal constituents (Eq. (2.7)) results in a combination of a relatively fast ebb-flood cycle of the sea surface elevation multiplied with a slow amplitude modulation. To address these slow variations, we propose a novel aspect of the solution method compared to Brouwer et al. [2018], namely the introduction of a multiple time scale expansion.

The time variable is decomposed in two distinct time scales t_1 and t_2 with $t_1 \ll t_2$. The fast ebb-flood time scale corresponds to $t_1 = t$ and the slow time scale, related to the spring-neap cycle, is defined as $t_2 = \frac{\sigma_{S_2} - \sigma_{M_2}}{\sigma_{M_2}} t$. The use of this multiple time scale expansion is justified since the relative order of the dimensionless spring-neap time scale is indeed much smaller than 1:

$$\frac{\sigma_{S_2} - \sigma_{M_2}}{\sigma_{M_2}} = \mathcal{O}(\delta), \tag{3.3}$$

where δ is a small parameter unrelated to ε. Using the conditions of the Ems as presented in Table 4.1, we find $\delta \approx 0.04$. For practical purposes it is useful to relate δ to the order of ε, this comparison leads to: $\delta = \mathcal{O}(\varepsilon^2)$. Hence the time scales can be regarded as distinct and independent, resulting in a redefinition of the time-derivative operator as:

$$\frac{\partial}{\partial t} = \frac{\partial}{\partial t_1} + \frac{\sigma_{S_2} - \sigma_{M_2}}{\sigma_{M_2}} \frac{\partial}{\partial t_2}, \tag{3.4}$$

Since Eq. (3.3) indicates that the slow time scale only adds $\mathcal{O}(\varepsilon^2)$ terms to the time derivative and since our focus is solely on leading and first order solutions, the t_2 contributions of the time derivative operator can be neglected. More importantly the introduction of these distinct time scales validates the notion of a well-defined M_2 tidal average as given by Eq. (2.5), since variations on the long time scale can be neglected within a single M_2 wave period, resulting in tidally averaged quantities that are still functions of t_2.

The two time scales enable the reformulation of the leading order sea surface elevation at $x = 0$ (see Eq. (2.7)) in terms of a complex spring-neap amplitude modulation $A_{SN_2}(t_2)$ multiplied with a regular ebb-flood cycle:

$$\begin{aligned} \zeta^0(t_1,t_2,0) &= \Re\left\{ A_{M_2} e^{it + i\phi_{M_2}} + A_{S_2} e^{i\frac{\sigma_{S_2}}{\sigma_{M_2}} t + i\phi_{S_2}} \right\}, \\ &= \Re\left\{ \left(A_{M_2} e^{i\phi_{M_2}} + A_{S_2} e^{i\frac{\sigma_{S_2} - \sigma_{M_2}}{\sigma_{M_2}} t + i\phi_{S_2}} \right) e^{it} \right\}, \\ &= \Re\left\{ \left(A_{M_2} e^{i\phi_{M_2}} + A_{S_2} e^{it_2 + i\phi_{S_2}} \right) e^{it_1} \right\}, \\ &= \Re\left\{ A_{SN_2}(t_2) e^{it_1} \right\}, \end{aligned} \tag{3.5}$$

with:

$$A_{SN_2}(t_2) = A_{M_2} e^{i\phi_{M_2}} + A_{S_2} e^{it_2 + i\phi_{S_2}}. \tag{3.6}$$

Similarly, the first order tidal forcing can be expressed as multiplication of the regular first overtide with an amplitude modulation $A_{SN_4}(t_2)$:

$$\zeta^1(t_1,t_2,0) = \Re\left\{ A_{SN_4}(t_2) e^{2it_1} \right\}, \tag{3.7}$$

with:

$$A_{SN_4}(t_2) = A_{M_4} e^{i\phi_{M_4}} + A_{S_4} e^{it_2 + i\phi_{S_4}}. \tag{3.8}$$

As a result of the multiple time scale expansion the seaward tidal forcing of the surface elevation is no longer expressed in lunar and solar tidal constituents, instead this forcing term is expressed as a single set of tidal constituents corresponding to the ordered amplitude modulated contributions. Thus the amplitude modulated tidal forcing consists of a principal component, denoted by D_2, and a first overtide, denoted by D_4. The fast time scale of the principal component of the amplitude modulated tidal forcing is still associated with the ebb-flood cycle. However, to distinguish it from the purely lunar or purely solar semi diurnal tidal constituents it is denoted by D_2, where the D stands for 'Daily'. This extends to the higher order modulated harmonics D_4, D_6, etc. As a consequence of this reformulation, the solar resonance modes cannot be resolved anymore because the solar tidal waves are incorporated in the modulation functions $A_{SN_2}(t_2)$ and $A_{SN_4}(t_2)$.

In conclusion, as a result of the multiple time scale expansion we have found asymptotically ordered contributions of the time-derivative operator, a well-defined tidal-average and expressions for the seaward tidal forcing of the free surface in terms of amplitude modulated tidal constituents D_2 and D_4. This allows us to formulate the system of order equations of Eqs. (2.6a), (2.6b), see Appendix C for an elaborate derivation of the order equations.

3.1.2. Harmonic Decomposition

In the fourth step, the system of linear order equations will be solved. However, not all tidal constituents result in a non-zero tidally averaged contribution to longitudinal sediment transport as described in Eq. (2.20). Decomposing the ordered solutions of water motion and SSC in harmonic tidal constituents allows the identification of sediment transport terms that vanish in the tidally averaged sense. Since the focus of this thesis is on tidally averaged longitudinal sediment transport we will omit these terms, thereby greatly simplifying the analysis. In this section we will elaborate on the harmonic decomposition of the water motion and SSC in components that lead to non-zero tidally averaged sediment transport. Details concerning the solution method of the individual components can be found in Appendix C.

The time dependency of the physical variables is solved in terms of a modulated residual component (D_0) and the modulated tidal constituents D_2, D_4, D_6, etc. This can be done since the system of order equations are linear, separable and only forced by the externally prescribed D_2 and D_4 tidal waves. Note that infinitely many even-integer higher harmonics arise due to internally generated nonlinear interactions, for example higher order harmonics for the SSC arise due to the nonlinear relation between erosion flux and horizontal water motion (see Eq. (2.16)). Then the physical variables, for example c^0, can be rewritten in terms of tidal harmonics:

$$c^0 = \sum_{n=0}^{\infty} \Re\left\{ a_n(t_2) \cdot c_n^0(x,z) \cdot e^{int_1} \right\}, \tag{3.9}$$

where $n = 0$ denotes the D_0 component, $n = 1$ the D_2 component, $n = 2$ the D_4 component etc. Furthermore, $a_n(t_2)$ denotes the complex spring-neap variations of the nth tidal constituent of c^0 and $\hat{c}_n^0(x,z)$ denotes the complex amplitude function of the nth tidal constituent of c^0. A similar decomposition is made for the other physical variables. As a consequence of this decomposition, the physical variables can be solved per tidal constituent.

Inspection of the advective transport terms in Eq. (2.20) (i.e. terms of the form $\int_{-H}^{\zeta} \langle uc \rangle \, dz$) shows that only products corresponding to the same tidal constituent (i.e. $u_{D_0} \cdot c_{D_0}$, $u_{D_2} \cdot c_{D_2}$ etc.) have a nonzero tidally averaged contribution, since $\langle u_{D_i} \cdot c_{D_j} \rangle = 0$ for $i \neq j$. Furthermore, the leading order contribution[1] of these advective transport terms are of order $\mathcal{O}(\varepsilon^2)$. Sediment transport mechanisms that do not have a net nonzero tidally averaged $\mathcal{O}(\varepsilon^2)$-contribution to Eq. (2.20) can therefore be omitted.

Then, as shown in Appendix D, it follows that leading order tidally averaged sediment transport is determined by: the D_2 component of leading order water motion, the D_0 and D_4 components of first order water motion, the D_0 and D_4 components of leading order SSC and the D_2 component of first order SSC. These tidal constituents and their respective orders are shown in Table 3.1. Thus, without loss of generality within the context of leading order tidally averaged sediment transport, the asymptotic expansions of Eqs. (3.2) can

[1] In the first step, scaling the system of equations, the dimensionless parameter describing the relative magnitude of advective transport processes was already estimated as $\mathcal{O}(\varepsilon)$.

Table 3.1: The only tidal constituents resulting in leading order contributions to the tidally averaged transport

	ζ	u	c
$\mathcal{O}(1)$	D_2	D_2	D_0, D_4
$\mathcal{O}(\varepsilon)$	D_0, D_4	D_0, D_4	D_2

be written as:

$$u \approx u^{02} + u^{10} + u^{14}, \tag{3.10}$$

$$\zeta \approx \zeta^{02} + \zeta^{10} + \zeta^{14}, \tag{3.11}$$

where the first subscript denotes the corresponding order of ε and the second the tidal components, e.g. u^{02} corresponds to the leading order D_2 component. For the suspended sediment concentration we find:

$$c \approx c^{00} + c^{04} + c^{12}. \tag{3.12}$$

To indicate the mechanism forcing each physical quantity, sub-scripts are used. Table 3.2 contains a summary of such forcing mechanisms. For example, the physical quantity $u^{14}_{\text{ext.-tide}}$ denotes the first order D_4 component that arises due to the externally prescribed tidal forcing.

As a result of the amplitude modulation of the tidal forcing Eq. (3.5), each component still depends on the long time scale. To indicate the respective (complex) dependency of the physical variable on the amplitude modulation, the proportionality symbol will be used, e.g. for the proportionality of the residual component of leading order concentration as given by the $n = 0$ term of Eq. (3.9) we can write $c^{00} \propto a_0(t_2)$. In Table 3.3 and Table 3.4 an overview is given of these subtidal dependencies for the water motion and sediment concentrations, respectively. See appendix D for a detailed derivation.

Table 3.2: List of forcing mechanisms to the water and sediment motion

Abbreviation	Explanation
Hydrodynamics	
ext.-tide	External tidal forcing of water elevation at the seaward boundary
river	Constant river discharge at landward boundary
grav-circ	Residual forcing due to a salinity-induced pressure gradient
adv	Effect of momentum advection term $uu_x + wu_z$
stokes	Flow induced by Stokes-forcing, i.e. by correlations between water velocity and surface level elevation
no-stress	Correction for applying the no-stress condition at $z = 0$ instead of at the real surface $z = \zeta$
Sediment Dynamics	
ero	Local resuspension of sediment at the river bed due to net erosion flux induced by any of the horizontal velocity components
sedadv	Effect of sediment advection term $uc_x + wc_z$
no-flux	Correction for applying the no-flux condition at $z = 0$ instead of at the real surface $z = \zeta$

Table 3.3: Overview of subtidal hydrodynamical dependencies

u^{02}	$\propto$	A_{SN_2}
ζ^{02}	$\propto$	A_{SN_2}
$u^{10}_{\text{grav-circ}}$	$\propto$	1
u^{10}_{river}	$\propto$	1
u^{10}_{adv}	$\propto$	$\lvert A_{SN_2}\rvert^2$
u^{10}_{stokes}	$\propto$	$\lvert A_{SN_2}\rvert^2$
$u^{10}_{\text{no-stress}}$	$\propto$	$\lvert A_{SN_2}\rvert^2$
u^{14}_{adv}	$\propto$	$(A_{SN_2})^2$
u^{14}_{stokes}	$\propto$	$(A_{SN_2})^2$
$u^{14}_{\text{no-stress}}$	$\propto$	$(A_{SN_2})^2$
u^{14}_{tide}	$\propto$	A_{SN_4}

Table 3.4: Overview of subtidal dependencies of individual concentration components*

c^{00}_{ero}	$\propto$	$\lvert A_{SN_2}\rvert$
c^{04}_{ero}	$\propto$	$\lvert A_{SN_2}\rvert \frac{A_{SN_2}}{A^*_{SN_2}}$
c^{12}_{sedadv}	$\propto$	$A_{SN_2}\lvert A_{SN_2}\rvert$
$c^{12}_{\text{no-flux}}$	$\propto$	$A_{SN_2}\lvert A_{SN_2}\rvert$
$c^{12}_{\text{ero, river}}$	$\propto$	$\text{sgn}(A_{SN_2})$
$c^{12}_{\text{ero, grav-circ}}$	$\propto$	$\text{sgn}(A_{SN_2})$
$c^{12}_{\text{ero, adv}}$	$\propto$	$A_{SN_2}\lvert A_{SN_2}\rvert$
$c^{12}_{\text{ero, stokes}}$	$\propto$	$A_{SN_2}\lvert A_{SN_2}\rvert$
$c^{12}_{\text{ero, no-stress}}$	$\propto$	$A_{SN_2}\lvert A_{SN_2}\rvert$
$c^{12}_{\text{ero, tide}}$	$\propto$	$\text{sgn}(A_{SN_2})^* A_{SN_4}$

*For first order concentration due to erosion, only the dominant contribution is analyzed.

3.1.3. Solving the Concentration Equilibrium

By inspection of the dependencies of the suspended sediment concentration, as shown in Appendix C, it follows that only terms proportional to f or to f_x are obtained. Thus any concentration component can be further decomposed as:

$$c(t_1, t_2, x, z) = f c_f + f_x c_{f_x}, \tag{3.13}$$

with c_f the part of the concentration that scales linearly with f and c_{f_x} scales linearly with f_x. With the leading and first order solutions of the water motion and sediment concentrations explicit and the decomposition from Eq. (3.13) we can express the leading order contribution of the concentration equilibrium (Eq. (2.20)) as [Brouwer et al., 2018]:

$$B\mathcal{S}_{t_2} = -(BTf + BFf_x)_x, \tag{3.14}$$

where:

$$T = \left\langle \int_{-H}^{0} u^{02} c_f^{12} + u^{14} c_f^{04} + u^{10} c_f^{00} - K_h (c_f^{00})_x \, dz + [\zeta^{02} u^{02} c_f^{00}]_{z=0} \right\rangle, \tag{3.15a}$$

$$F = \left\langle \int_{-H}^{0} u^{02} c_{f_x}^{12} - K_h c_f^{00} \, dz \right\rangle. \tag{3.15b}$$

Note that the leading order contributions to the functions T and F are fully determined by leading and first order water motion [Chernetsky, 2012]. Furthermore, an explicit relation between the total stock $\mathcal{S}$ and the tidally averaged erodibility f is presented in Brouwer et al. [2018] and shown in Figure 3.1. In this figure, the region $\mathcal{S} < \mathcal{S}_a$ corresponds to the state in which all sediment is in suspension throughout (almost) an entire ebb-flood cycle. In this case the bed shear stress is strong enough to erode all fine sediment deposited on the river bed, resulting in a sandy bed throughout an ebb-flood cycle. For this region we find the approximated relation $f \approx \mathcal{S}$. The region $\mathcal{S} > \mathcal{S}_b$ corresponds to the state in which a bottom pool of erodible sediment is found at any time of the ebb-flood cycle. This region corresponds to the erosion limited state (defined in Section 2.3.1). Then due to equality of the erosion flux and the potential erosion, i.e. $E = \hat{E}$, we find $f = 1$ for all stock values exceeding $\mathcal{S}_b$ by definition. Values of the total stock in between these these regions, $\mathcal{S}_a < \mathcal{S} < \mathcal{S}_b$, correspond to the coexistence of an erodible muddy state and an inerodible sandy state within each ebb-flood cycle. In this region, the relation between f and $\mathcal{S}$ can be approximated by a sublinear function (See Appendix A of Brouwer et al. [2018] for further details).

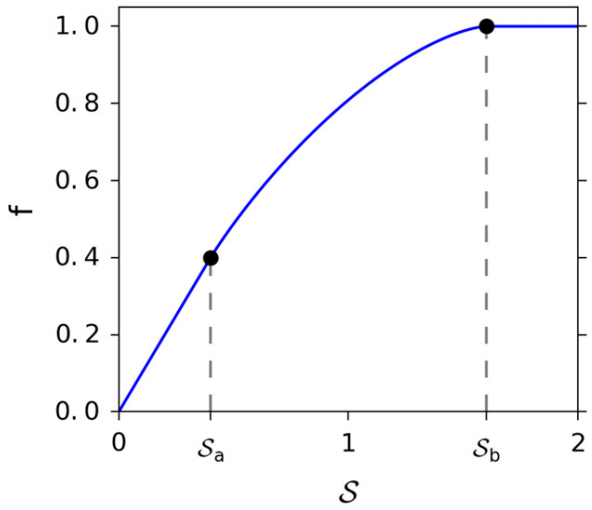

Figure 3.1: The functional relation between the erodibility f and the total stock $\mathcal{S}$. (Figure from Brouwer et al. [2018])

The horizontal boundary conditions of Eq. (3.14) are specified in terms of the erodibility. At the seaward boundary a prescribed erodibility f_{sea} follows from the prescribed seaward concentration:

$$f_{\text{sea}} = \frac{H_0 c_{\text{sea}}}{\left\langle \int_{-H}^{0} c(t,0,z)\big|_{f=1}\, dz \right\rangle}. \tag{3.16}$$

At the landward side, the total net tidally averaged suspended sediment transport equals the sediment import from the riverine side:

$$(BTf + BFf_x)_{x=L} = -\mathcal{F}_{\text{river}} \tag{3.17}$$

Then, with the boundary conditions specified, the concentration equilibrium as initial condition and $\mathcal{S}_{\text{bed}} \equiv 0$ at $t_2 = 0$, Eq. (3.14) will be solved numerically.

3.1.4. Equilibrium and Temporal Lag Effects

Two types of solutions of Eq. (3.14) will be considered, the concentration equilibrium and the dynamic equilibrium.

- The concentration equilibrium is defined as the solution of Eq. (3.14) such that the tidally averaged SSC is in steady-state on the time scale of the ebb-flood cycle for fixed tidal conditions.
- The dynamic equilibrium is defined as the solution of Eq. (3.14) such that the tidally averaged SSC requires an adaptation time (defined in Section 1.3.2) to converge to concentration equilibrium. Note that this solution is not subject to fixed tidal conditions, hence slow variations of the concentration equilibrium associated with the spring-neap cycle introduce temporal lag effects.

Note that for the concentration equilibrium the bottom pool can be omitted indirectly, as the amount of sediment in the bottom pool does not affect the tidally averaged erodibility (i.e. $f = 1$ if a bottom pool is present regardless of the amount of sediment deposited in the bottom pool) and thus has no influence on the steady-state solutions of the SSC. It also follows that the temporal behaviour of the concentration equilibrium on the spring-neap time scale is not affected by temporal lag effects since the prescribed concentration at the seaward boundary is assumed to be constant. This type of solution can be found by assuming constant tidal amplitudes (i.e. $A_{SN_2}(t_2')$ and $A_{SN_4}(t_2')$ are chosen for *fixed* t_2') and by assuming exponential stability of the dynamic solution [Brouwer et al., 2018]. By comparison of the dynamic equilibrium and the concentration equilibrium the temporal lag effects will be investigated.

3.2. Analyzing Subtidal Behaviour of Sediment Trapping

The introduction of the spring-neap amplitude modulation not only leads to subtidal dependencies of water motion and sediment concentrations but also results in subtidal variations of the sediment transport. However, the total transport of sediment, i.e. the right-hand side of Eq. (3.14), is dependent on the tidally averaged erodibility. This means that a comparison of the individual transport processes is coupled to the location of the ETM and the magnitude of sediment concentrations. As a consequence an analysis of individual transport processes independent of the precise distribution of erodible sediment at the bed is not possible.

To overcome this problem we will analyze the subtidal behaviour of sediment trapping using the transport capacity T [Dijkstra et al., 2019]. This notion corresponds to the total transport that would occur if an abundance of sediment was available throughout the estuary, i.e. $f \equiv 1$ for all x and t_2. The transport capacity can therefore be interpreted as the system's initial tendency to redistribute a layer of sediment covering the entire river bed. Unlike the total transport, the transport capacity is mainly dependent on the hydrodynamical conditions and sediment parameters (such as settling velocity and dimensionless erosion parameter), thus the analysis is not complicated by the precise distribution of sediment in the water column or bottom pool. Furthermore, the transport capacity is an insightful concept for analyzing sediment trapping as the zeros of T correspond with the extreme values of f, which are indicative for the extreme values of c. More specifically, zeros of T with a negative first derivative indicate that upstream export (i.e. seaward transport) converges with downstream import (i.e. landward transport) possibly resulting in an ETM. As such, determining the subtidal dependency of the transport capacity gives insight in the behaviour of sediment trapping locations during a spring-neap cycle.

Contributions to the Transport Capacity

The total transport capacity comprises a myriad of contributions related to specific physical mechanisms. Six different transport processes are explained and analyzed, because of a high relative magnitude (specific to this thesis) or significance in literature. These mechanisms are introduced below accompanied by a physical interpretation:

- T_{stokes}: the sediment transport due to velocities associated with the Stokes-forcing. Stokes-forcing produces residual-inward and D_4 water flows localized at the surface known as the Stokes-drift velocity. Associated with this water velocity is a sediment importing contribution to the transport capacity. The import of water due to Stokes drift is exactly compensated by the tidal return flow. This velocity causes a sediment importing or exporting contribution to the total transport capacity depending on the phase-lag with the D_2 tidal wave. Due to the inherent connection between these two transporting mechanisms (Stokes-drift and tidal return flow) their contributions will be considered collectively.

- $T_{\text{no-stress}}$: applying the no-stress condition at $z = 0$ instead of at the free surface induces a correction velocity profile resulting in a subtidal transport of tidally resuspended sediment.

- T_{sedadv}: sediment advection arises due to correlation between velocities and concentration gradients of the same tidal constituent. The resulting concentration profile due to sediment advection will be transported by the D_2 tidal wave.

- T_{river}: the prescribed river discharge at the weir results in an export of sediment by two mechanisms. First, the time-independent velocity profile induced by river discharge flushes tidally resuspended sediment seawards. Second, the velocity profile induced by river discharge exerts stress at the bottom resulting of the resuspension of deposited sediment in the water column that is exported by the D_2 wave.

- $T_{\text{grav-circ}}$: the velocity profile related to gravitational circulation consists of residual inward velocities near the bed and a seaward velocities near the surface. This results in a net import of tidally resuspended sediment due to a spatial asymmetry in the vertical concentration profile. Because gravitational circulation is driven by the presence of a salt intrusion, the resulting importing mechanism will be largest at the point of the highest salinity gradient.

- $T_{\text{ext.-tide}}$: the sediment transport as a result of the externally applied sea surface elevation due to D_2 and D_4 tidal constituents. The relative phase difference between the externally applied surface elevations of the tidal constituents introduces a velocity asymmetry [Festa and Hansen, 1978]. As a result the velocities during ebb and flood are different, resulting in residual sediment transport [Chernetsky et al.,

2010]. $T_{\text{ext.-tide}}$ can be further decomposed into the distinct tidal constituents. The first component $T_{\text{ext.-}D_2}$ denotes the transport of tidally resuspended sediment by the external D_2 water motion. Vice-versa, the second component $T_{\text{ext.-}D_4}$ denotes the transport of D_2 resuspended sediment by the external D_4 water motion. These mechanisms can result in both import and export of suspended sediment during a single spring-neap cycle depending on the relative phase difference between the prescribed D_2 and D_4 tidally forced sea surface elevation.

The intensity of each transport mechanisms depends on the magnitude of the externally prescribed sea surface elevation. Hence the spring-neap cycle introduces clear subtidal variations in the sediment transport capacity (for a derivation see Appendix D) see Table 3.5. Notably, due to the complex amplitude modulation, the spring-neap cycle results in time-dependent phases of the D_2 and D_4 constituents. Hence the relative phase difference fluctuates throughout a spring-neap cycle. Under specific conditions this can result in profound time-dependent behaviour of the tidal transport capacity and hence trapping characteristics.

Table 3.5: Overview of subtidal dependencies of the dominant contributions to the transport capacity

T_{stokes}	$\propto$	$\lvert A_{SN_2}\rvert^3$
$T_{\text{no-stress}}$	$\propto$	$\lvert A_{SN_2}\rvert^3$
T_{sedadv}	$\propto$	$\lvert A_{SN_2}\rvert^3$
T_{river}	$\propto$	$\lvert A_{SN_2}\rvert$
$T_{\text{grav-circ}}$	$\propto$	$\lvert A_{SN_2}\rvert$
$T_{\text{ext.-}D_2}$	$\propto$	$\lvert A_{SN_2}\rvert \cdot \lvert A_{SN_4}\rvert e^{-i(\phi_{SN_4}-2\phi_{SN_2})}$
$T_{\text{ext.-}D_4}$	$\propto$	$\lvert A_{SN_2}\rvert \cdot \lvert A_{SN_4}\rvert e^{i(\phi_{SN_4}-2\phi_{SN_2})}$

4

Model Simulations

In this chapter the influence of the spring-neap variation on sediment trapping in the Ems estuary will be investigated. The general characteristics and model parameters for the Ems are discussed in Section 4.1. This section is followed by an analysis of the steady-state solutions using the subtidal transport capacity in Section 4.3. In Section 4.4 a comparison is made between steady-state solutions and the dynamic behaviour to illustrate the importance of temporal lag effects. Further, the sensitivity of the long-term dynamic behaviour on the dimensionless erosion parameter $\hat{M}$ will be investigated.

4.1. Characteristics of the Ems and Model Calibration

The model domain we consider consists of the upper estuary and the tidal river part of the Ems-Dollard estuary. The seaward boundary, corresponding to $x = 0$ in our coordinate system, is taken at the city of Knock. Here, the estuary has a width of 800 m. The domain extends 64 km upstream to a tidal weir situated at the city of Hebrum. Along this stretch, neglecting shallow areas and the Dollard Bay, the estuary is taken to be exponentially converging with a convergence length of 30 km. The bottom profile is approximated by a smooth curve fit of depth measurements from WSA Emden (see also de Jonge et al. [2014]) and presented in Figure 4.1. The smooth fit averages over bottom variations related to sand-dunes with maximum height of 3 meters and length of 10 km. Hence the model does not resolve their influence on the hydro- and sediment dynamics.

Measurements by the Lower Saxony state department for water management, coastal and nature conservation (NLWKN) of the water elevation at the seaward boundary in 2005 are analyzed by T-TIDE [Pawlowicz et al., 2002] using a classical harmonic analysis method in order to obtain the amplitudes and phases of the tidal constituents under consideration. For the principal components, year-averaged amplitudes of $A_{M_2} = 1.39$ m and $A_{S_2} = 0.35$ m are found with corresponding phases $\phi_{M_2} = 334.68°$ and $\phi_{S_2} = 47.33°$. For

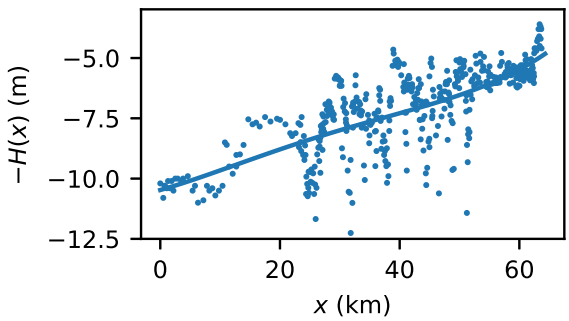

Figure 4.1: Measured channel depth of the Ems in 2005 and smooth fit used in the model (WSA Emden, see also de Jonge et al. [2014])

the first overtide we find year-averaged amplitudes of $A_{M_4} = 0.17$ m and $A_{S_4} = 0.013$ m with corresponding phases $\phi_{M_4} = 138.03°$ and $\phi_{S_4} = 356.33°$. Using these parameters, the magnitude of the spring-neap variations of the prescribed sea surface elevation and the relative phase difference at the seaward boundary are shown in Figure 4.2

The river discharge of the Ems is determined by a measuring station at Versen, approximately 40 km upstream from the weir at Hebrum. Data collected by WSA Meppen show a year-averaged discharge of 80 m^3/s. However, for this research we assume an average discharge of 45 m^3/s corresponding to summer conditions (Jul-Sep). Furthermore, the river Leda discharges into the main channel at km 36. Even though this tributary has a significant mass flow into the Ems, its influence will be ignored in this study.

We follow observations from Talke et al. [2009b] and prescribe a hyperbolic tangent salinity profile with a seaward salinity of 30 psu. The year-averaged spatial features of the salt intrusion are determined by the $x_c = -3.5$ km and $x_L = 11.5$ km, see Eq. (2.4). By prescribing this diagnostically, we have ignored effects of deviations on the year-averaged river discharge on the salinity profile. Finally, the salinity becomes zero near the weir since the estuary transitions to complete fresh water.

Consistent with the measurements of seaward concentration presented by de Jonge et al. [2014], we prescribe a depth- and tidally averaged seaward concentration of 20 mg/L and a settling velocity of 0.002 m/s. Further, to study the effect of sediment import from the seaward boundary in isolation, we require the sediment transport across the weir to vanish. The erosion formulation, see Eq. (2.16), introduces the erosion parameter $\hat{M}$, the efficiency of resuspension of sediment at the bottom. Dijkstra [2019] identifies this parameter as poorly understood and subsequently uses it as a calibration parameter. In this research a default value of $\hat{M} = 5 \cdot 10^{-5}$ is used. In Section 4.4 this value will be varied to investigate the sensitivity of subtidal bottom pool formation on this dimensionless erosion parameter.

The vertical eddy viscosity and bottom friction coefficients follow from calibration [Chernetsky, 2012] and are given by $A_{v0} = 0.012$ m^2/s and $s_{f0} = 0.049$ m/s. In Dijkstra et al. [2019], it is verified that the model results are insensitive to the choice of the constant horizontal eddy diffusivity. Following Dijkstra et al. [2019] we take $K_h = 100$ m^2/s. Moreover, we also assume that the Prandtl-Schmidt number σ_P equals 1 (i.e. $A_v = K_v$).

The default values of model parameters are summarized in Table 4.1.

Table 4.1: Default model parameter values for the Ems in 2005

Parameter	Description	Value
L	Length	64 km
B_0	Width at the entrance	0.8 km
L_b	Convergence length	30 km
H_0	Depth at the entrance	10.2 m
A_{M_2}	Amplitude of M_2 tidal wave	1.39 m
A_{S_2}	Amplitude of S_2 tidal wave	0.35 m
A_{M_4}	Amplitude of M_4 tidal wave	0.17 m
A_{S_4}	Amplitude of S_4 tidal wave	0.013 m
ϕ_{M_2}	Phase of M_2 tidal wave	334.68°
ϕ_{S_2}	Phase of S_2 tidal wave	47.33°
ϕ_{M_4}	Phase of M_4 tidal wave	138.03°
ϕ_{S_4}	Phase of S_4 tidal wave	356.33°
σ_{M_2}	M_2 angular frequency	$1.4 \cdot 10^{-4}$ rad/s
σ_{S_2}	S_2 angular frequency	$1.35 \cdot 10^{-4}$ rad/s
g	Gravitational acceleration	9.81 m/s^2
ρ_0	Reference density of water	1000 kg/m^3
Q	River discharge	45 m^3/s
S_{sea}	Seaward salinity	30 psu
β_s	Conversion parameter	$7.6 \cdot 10^{-4}$ psu^{-1}
x_c	Maximum salinity gradient	−3.5 km
x_L	Salt intrusion length scale	11 km
c_{sea}	Seaward SSC	20 mg/L^3
$\mathcal{F}_{\text{river}}$	Transport across weir	0 kg m^{-1} s^{-1}
d_s	Sediment grain size	20 μm
ρ_s	Sediment density	2650 kg/m^3
g'	Reduced gravity	16.2 m/s^2
$\hat{M}$	Erosion parameter	$5 \cdot 10^{-5}$
w_s	Settling velocity	0.002 m/s
A_{v0}	Eddy viscosity	0.012 m^2/s
s_{f0}	Bottom friction coefficient	0.049 m/s
σ_P	Prandtl-Schmidt number	1
K_h	horizontal eddy diffusivity	100 m^2/s

(a) Prescribed amplitude of ζ^0 at $x = 0$

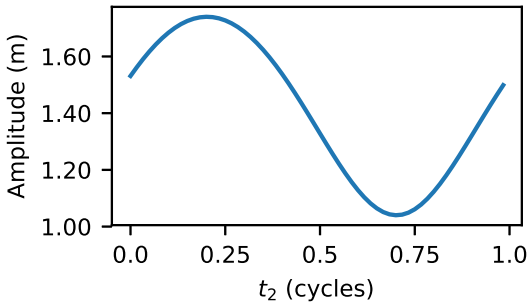

(b) Prescribed phase of ζ^0 at $x = 0$

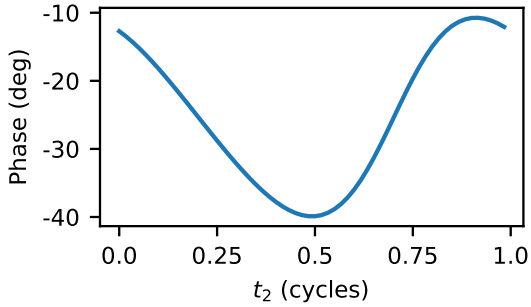

(c) Prescribed amplitude of ζ^1 at $x = 0$

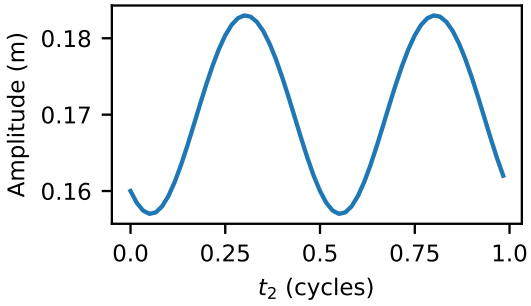

(d) Prescribed phase of ζ^1 at $x = 0$

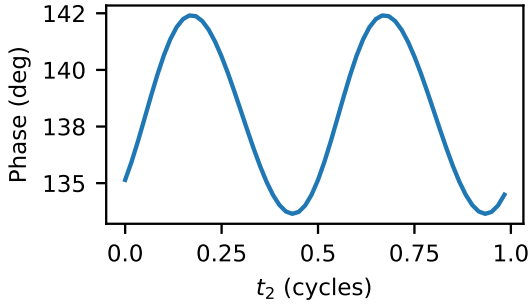

(e) Prescribed amplitude of $\zeta^0 \cdot \zeta^1$ at $x = 0$

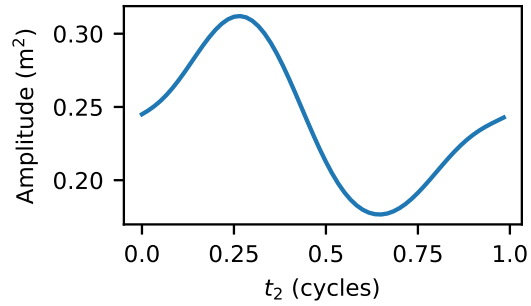

(f) Prescribed relative phase difference at $x = 0$

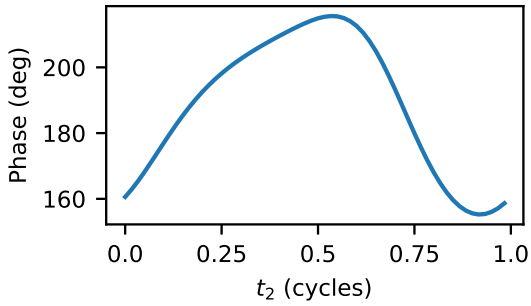

Figure 4.2: Using the parameters for the seaward forcing from Table 4.1, the prescribed sea surface elevation is shown in terms of the amplitude and phase. The leading and first order contributions, ζ^0 and ζ^1, correspond to D_2 and D_4 respectively. Furthermore, in Figure 4.2e the product of the leading and first order amplitudes, describing the amplitude of tidal transport of sediment (see Table 3.5), is shown. Figure 4.2f shows the relative phase difference between the prescribed D_2 and D_4 sea surface elevation, describing the phase of tidal transport of sediment (see Table 3.5).

4.2. Spring-Neap Variations of Water Motion

In this section we will investigate the spring-neap variations of the width-averaged horizontal water velocity u. The subtidal variations of the components due to various forcing mechanisms were presented in Table 3.3. In this section we will not analyze each individual component, instead we will investigate the magnitude of the total width-averaged horizontal water velocity as a result of the combined effect of individual components. High magnitudes of u indicate strong oscillatory water motion and thus high typical velocities. Low magnitudes of u indicate that the water is (relatively) stationary and thus low typical velocities.

In Figures 4.3a and 4.3b the magnitude of the u is given during spring tide ($t_2 = 0.25$ cycles) and neap tide ($t_2 = 0.75$ cycles), respectively. We find that the magnitude of u decreases close to the river bed and near the tidal weir and reaches a maximum at the surface at km 35. During spring tide we find a maximum absolute horizontal velocity of 1.0 m/s, whereas during neap the maximum absolute horizontal velocity equals 0.5 m/s. Since the horizontal water velocity is associated with the transport capacity T (see Section 3.2), the higher typical velocities during spring tide are expected to result in more enhanced sediment transport.

(a) $|u|$ at spring tide

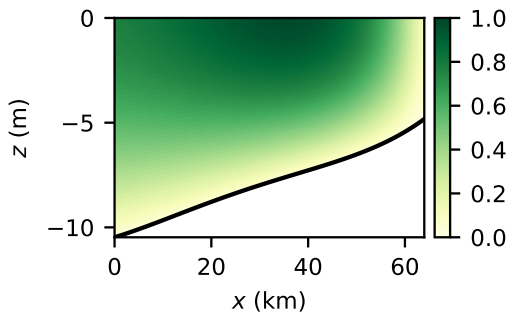

(b) $|u|$ at neap tide

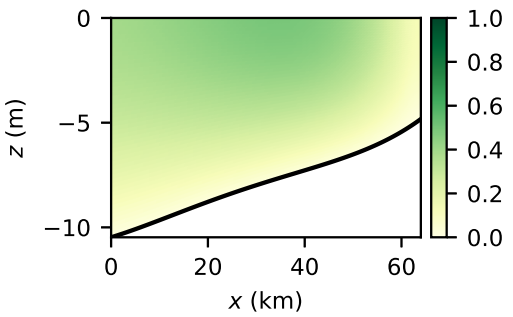

Figure 4.3: The magnitude of the width-averaged horizontal water velocity u (in m/s) throughout the estuary during spring and neap tide.

The magnitude of the horizontal water velocity at the river bed throughout the estuary as a function of the long time scale is shown in Figure 4.4a. The maximum magnitude of u is 0.06 m/s during spring tide ($t_2 = 0.25$ cycles) and 0.03 m/s during neap tide ($t_2 = 0.75$ cycles) at km 45. The transition of the magnitude of u between spring and neap conditions at the river bottom for $x = 45$ km is shown in Figure 4.4b. Furthermore, since the potential erosion $\hat{E}$ (see Eq. (2.16)) is proportional to the absolute value of the velocity at the river bed this result suggests that erosion flux is more enhanced during spring tide.

(a) $|u|$ in m/s at the river bed

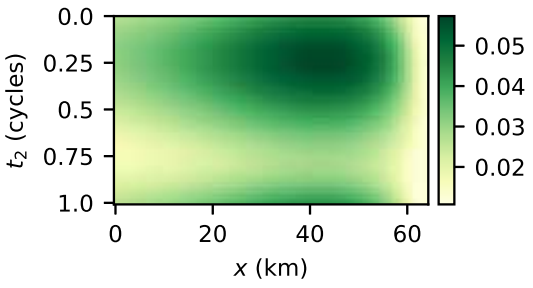

(b) $|u|$ in m/s at the river bed for $x = 45$ km

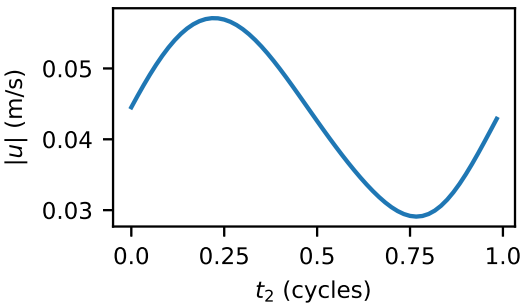

Figure 4.4: The magnitude of the width-averaged horizontal water velocity u (in m/s) throughout the estuary as a function of the long time scale t_2. The values at km 45 are shown separately.

4.3. Results for the Concentration Equilibrium

In this section, we will analyze the steady-state erodibility solutions $f_{\text{eq}}(t_2, x)$ of the concentration equilibrium condition, which are assumed to be exponentially stable (See Appendix C of Brouwer et al. [2018]). To this end, the amplitude functions, $A_{SN_2}(t_2)$ and $A_{SN_4}(t_2)$ are varied with t_2 but kept fixed when calculating the concentration equilibrium resulting from Eq. (3.14) through numerical time-integration. This implies that the steady-state erodibility is independent of any temporal lag effects.

Furthermore, a comparison is made between the (numerically obtained) steady-state erodibility and the (analytically obtained) subtidal dependency of the transport capacity, presented in Table 3.5. This process-based analysis enables the formulation of the main balance of transport mechanisms governing sediment dynamics, thus underlining the influence of the spring-neap cycle on sediment trapping.

Lastly, the components of the transport capacity due to externally prescribed sea surface elevation will be studied and the direction of transport will be related to the prescribed relative phase difference of the D_2 and D_4 tidal constituents of the seaward forcing.

4.3.1. Suspended Sediment Concentration during the Spring-Neap Cycle

Figure 4.5 shows the SSC throughout the estuary during spring (t_2 = 0.25 cycles) and neap tide (t_2 = 0.75 cycles), respectively. During spring tide (Figure 4.5a) we observe a narrow ETM around km 55 with near-bed concentrations up to 450 mg/L. During neap tide (Figure 4.5b) the ETM is found more downstream than during spring. Moreover, the ETM becomes wider, covering an area between km 30 and 45 with relatively low near-bed concentrations up to 45 mg/L.

By comparison of the SSC during spring and neap tide we find that spring tide is associated with the formation of a narrow ETM close to the tidal weir, whereas during neap the ETM moves downstream and becomes wider. Furthermore the concentration of suspended sediment is an order of magnitude larger during spring than during neap tide. Both of these observations indicate that the importing transport mechanisms are dominant during spring tide and tend to vanish during neap, as is proposed in Table 3.5 by the subtidal dependency of the transport capacities on the spring-neap time scale.

Figure 4.6 contains the SSC at the surface as a function of the spring-neap time scale t_2. The strong ETM formation during spring tide, t_2 = 0.25 cycles, is indicated by relatively high surface SSC up to 210 mg/L. As the tidal amplitude decreases the ETM gradually moves downstream and becomes wider, reaching km 45 at t_2 = 0.6 cycles with concentrations up to 150 mg/L. Then, as tidal amplitudes transition to neap tide, the surface concentrations drop abruptly to 25 mg/L during neap tide. These low concentrations are maintained until spring tide, when a sudden transition to the previously noted narrow ETM with surface concentrations up to 200 mg/L is observed.

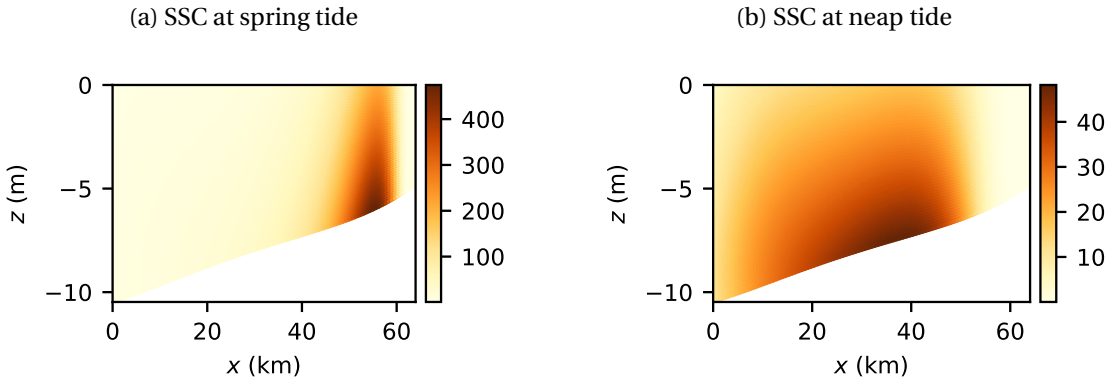

Figure 4.5: The SSC in mg/L is shown for two instances during the spring-neap cycle. First during spring tide (t_2 = 0.25 cycles) and then during neap tide (t_2 = 0.75 cycles). Note that the SSC during spring tide is an order of magnitude larger than during neap tide.

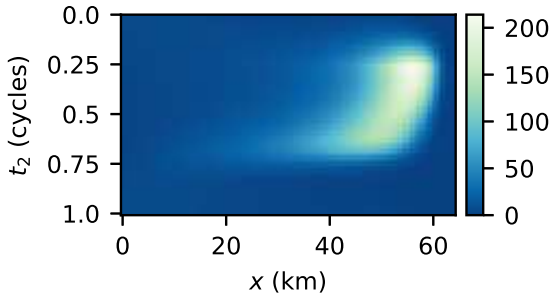

Figure 4.6: Concentrations of suspended sediment (in mg/L) at the surface as a function of the spring-neap time scale t_2. Spring and neap tide correspond to $t_2 = 0.25$ cycles and $t_2 = 0.75$ cycles, respectively. The transition from spring to neap and vice versa is characterized by abrupt changes in SSC.

4.3.2. Comparison of the Steady-State Erodibility with the Total Transport Capacity

Figure 4.7 contains the results of the steady-state erodibility $f_{\text{eq}}(t_2, x)$ and the total transport capacity as a function of the position in the estuary (on the horizontal axis) and the long timescale (on the vertical axis). i.e. the spring-neap cycle.

We find that sediment trapping (i.e. $f_{\text{eq}} = 1$) only occurs during the period of enhanced D_2 tidal amplitude of the sea surface elevation i.e. during spring-tide. Sediment trapping first occurs around km 55 during maximum A_{SN_2} amplitude. As the tidal amplitude decreases the trapping location is pushed away from the tidal weir to approximately km 50 at the beginning of neap tide. During neap-tide no clear maximum of the steady-state erodibility is found until the start of next spring tide.

This behaviour is also observed for the transport capacity, see Figure 4.7b. During spring-tide the emergence of the trapping location is due to strongly enhanced import of suspended sediment (denoted in blue). Second when the tidal amplitude decreases, we find that there is a larger region with sediment export near the weir (denoted in red), explaining the downstream movement of the trapping location. Third, the transition to a high export throughout most of the estuary during neap-tide explains the absence of any sediment deposited on the river bed during this period.

(a) Steady-state erodibility

(b) Total transport capacity

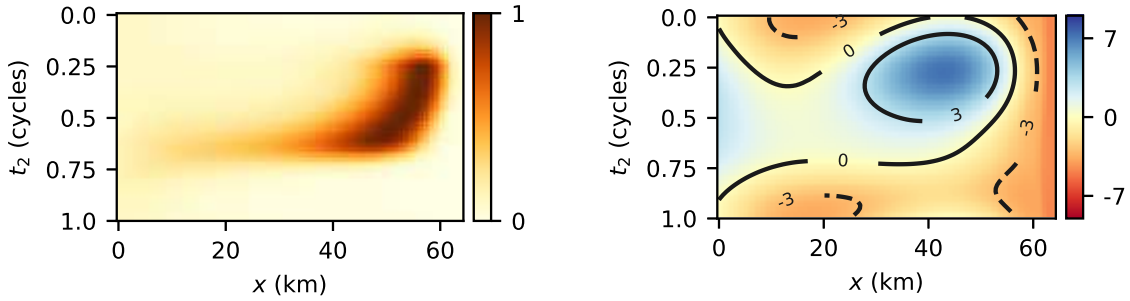

Figure 4.7: The steady-state erodibility and the total transport capacity ($\mathrm{kg\,m^{-1}\,s^{-1}}$) are shown as a function of the spring-neap cycle.

4.3.3. Contributions to the Total Transport Capacity

The total transport capacity is a result of various mechanisms. These mechanisms were discussed in Section 3.2 and the six most important contributions (in magnitude) are shown in Figure 4.8.

The dominant export mechanism throughout the entire spring-neap cycle is the river discharge. Through-

out the entire spring-neap cycle, stokes-forcing (Figure 4.8a) and the no-stress condition (Figure 4.8b) result in sediment export near the seaward boundary and net import from approximately km 25 to the landward boundary with a maximum around km 50. Further, it is found that transport due to the externally prescribed D_4 sea surface elevation (Figure 4.8f) varies between importing and exporting as a result of the spring-neap variations of prescribed amplitudes and phases. Gravitational circulation (Figure 4.8d) results in sediment import located at the salt intrusion. Within the context of this thesis the salt intrusion is relatively short, hence the import due to gravitational circulation only occurs close to the seaward boundary. Finally, we find that sediment advection (Figure 4.8c) results in an importing contribution throughout the estuary, albeit of a relatively small magnitude compared to the other transport mechanisms.

Note that the transport capacities from Figures 4.8a-4.8e all attain maximum values during spring tide and tend to vanish during neap. This is directly explained by the analytically obtained subtidal dependencies of the transport capacities presented in Table 3.5. The same trend is not observed for the tidal transport capacity, as the dependency in Table 3.5 is different. In the following paragraph, the subtidal behaviour of the transport capacity due to the externally prescribed sea surface elevation will be discussed in detail.

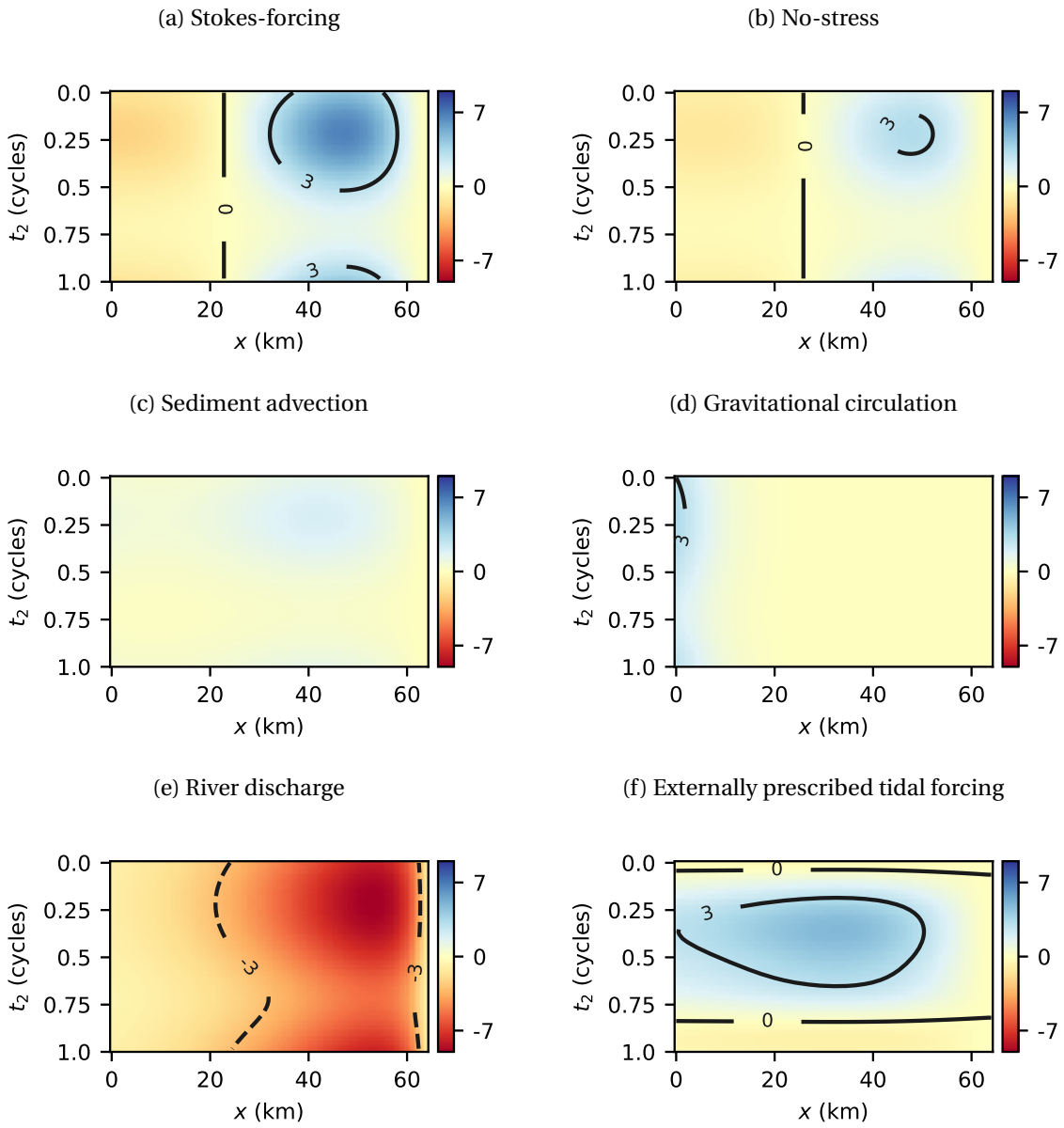

Figure 4.8: Six contributions to the total transport capacity ($\mathrm{kg\,m^{-1}\,s^{-1}}$)

4.3.4. Contributions to the Tidal Transport Capacity

The transport capacities associated with the water motion induced by the externally prescribed sea surface elevation has contributions in terms of D_2 and D_4 tidal constituents, $T_{\text{ext.-}D_2}$ and $T_{\text{ext.-}D_4}$ respectively, which correspond to the advection of tidally resuspended sediment by the externally prescribed D_2 and D_4 components of the water motion. Thus for $T_{\text{ext.-}D_2}$ we find that the transport is due to the advective term $u^{02}_{\text{ext.-tide}} \cdot c^{12}_{\text{ero, tide}}$, similarly $T_{\text{ext.-}D_4}$ corresponds with $u^{14}_{\text{ext.-tide}} \cdot c^{04}_{\text{ero}}$.
From Figure 4.9a it follows that $T_{\text{ext.-}D_2}$ results in an import of sediment. On the other hand, $T_{\text{ext.-}D_4}$ results in an export of sediment, see Figure 4.9b. Since the maxima of $T_{\text{ext.-}D_2}$ and $T_{\text{ext.-}D_4}$ occur at different moments in the spring-neap cycle the combined transport, Figure 4.8f, has an alternating pattern of import and export.

By inspection of the phases of $T_{\text{ext.-}D_2}$ and $T_{\text{ext.-}D_4}$ the direction of these transport capacities and the emergence of an upstream importing region for $T_{\text{ext.-}D_4}$, as can be seen in Figure 4.9b, will be explained. Note that the phase of a tidal wave is shifted as it propagates through the estuary. The phase of the transport due to externally applied tidal waves is the result of the combined effect of these spatially varying phase shifts and the relative phase difference of the prescribed sea surface elevation, see Appendix D for an elaborate discussion. Then, if the phase of a transport process intersects any of the $\pm 90°$-lines, the real part of the associated complex exponential changes sign and the direction of sediment transport changes. In Figure 4.10a we see that the phase of $T_{\text{ext.-}D_2}$ does not cross the $\pm 90°$-lines and hence is associated with sediment import. However in Figure 4.10b, we see that the phase of $T_{\text{ext.-}D_4}$ crosses the $90°$-line for sufficiently large x, resulting in an upstream sediment import region.

(a) Externally prescribed D_2 forcing

(b) Externally prescribed D_4 forcing

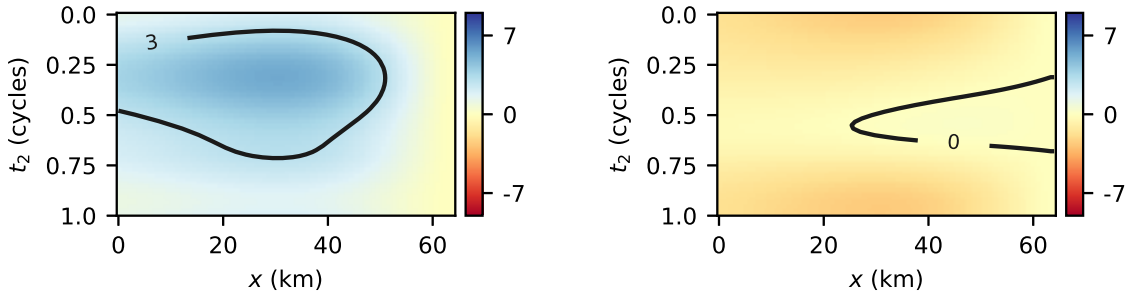

Figure 4.9: The contributions to the transport capacity (kg m^{-1} s^{-1}) due to externally prescribed tidal forcing.

(a) Phase of $T_{\text{ext.-}D_2}$ at various locations.

(b) Phase of $T_{\text{ext.-}D_4}$ at various locations.

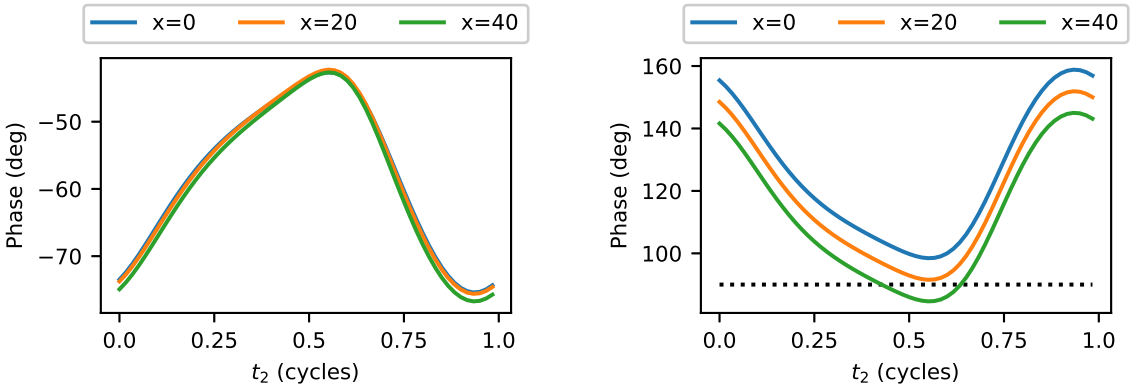

Figure 4.10: The phase of the transport capacities at various locations in the estuary is given as a function of t_2. The phase of $T_{\text{ext.-}D_2}$ does not intersect any of the $\pm 90°$-lines. However for $T_{\text{ext.-}D_4}$ we find that the phase intersects the $90°$-line for increasing x, causing an upstream change in direction of sediment transport.

4.4. The Influence of Temporal Lag Effects

The influence of temporal lag effects within a spring-neap cycle is shown by comparison of the steady-state and dynamic erodibilities. In this section we will present three cases corresponding to the values of the dimensionless erosion parameter $\hat{M} = 1{\cdot}10^{-5}$, $\hat{M} = 5{\cdot}10^{-5}$ and $\hat{M} = 10{\cdot}10^{-5}$, respectively. The dynamic solution is computed with the concentration equilibrium as an initial condition for 10 spring-neap cycles, such that the effects of the initial condition vanish and a periodic solution is obtained. The last spring-neap cycle of the dynamic solution is compared with the steady-state erodibility for all values of $\hat{M}$.

In Figure 4.11 the erodibility and surface SSC of the steady-state and dynamic solutions are shown for a low dimensionless erosion parameter of $\hat{M} = 1 \cdot 10^{-5}$. For the dynamic erodibility (Figure 4.11b) we find that a bottom pool is formed around km 50 which is present during the entire spring-neap cycle. This is the result of temporal lag effects introduced by low erosion flux. Due to the relatively low value of $\hat{M}$ the total sediment that is resuspended from the bottom pool during the exporting phase associated with neap tide is smaller than the amount of sediment that is deposited in the bottom pool in the importing phase associated with spring tide, implying net growth of the bottom pool. Thus for the dynamic solution we find a bottom pool throughout the spring-neap cycle. Since the sediment in the bottom pool can only be transported by resuspension, we find that the location of the bottom pool is stationary, as opposed to the trapping region corresponding to the steady-state erodibility (Figure 4.11a). By inspection of the surface SSC corresponding to the dynamic solutions (Figure 4.11d), we observe a spatially stationary ETM at the location of the bottom pool (km 50). The ETM is present throughout the spring-neap cycle, in contrast with the surface SSC corresponding to the steady-state solution (Figure 4.11c) which tends to vanish during neap tide. The magnitude of the surface SSC corresponding to the dynamic solution is larger during spring tide, up to 50 mg/L, than during neap tide, up to 25 mg/L, as the bottom velocity and therefore the erosion flux are larger during spring tide, hence more sediment is resuspended resulting in an increase in surface SSC.

(a) Steady-state erodibility

(b) Dynamic erodibility

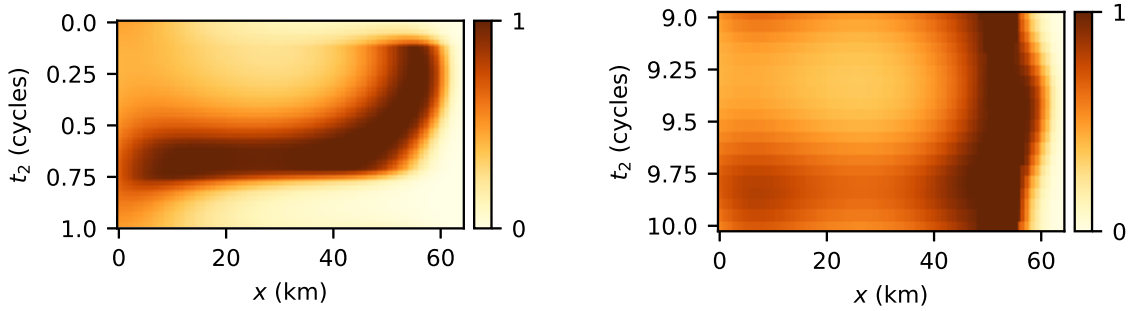

(c) Steady-state surface SSC

(d) Dynamic surface SSC

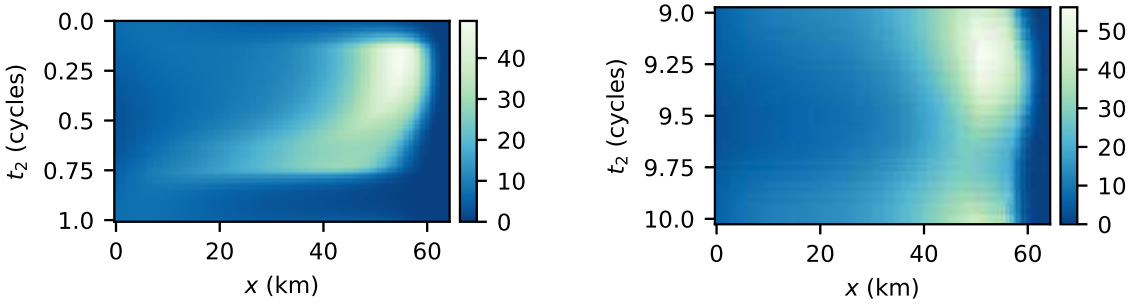

Figure 4.11: The steady-state and dynamic erodibility solutions corresponding to a low rate of erosion ($\hat{M} = 1 \cdot 10^{-5}$). Due to temporal lag effects the bottom pool is present for the entire spring-neap cycle.

In Figure 4.12 the erodibility and surface SSC of the steady-state and dynamic solutions are shown for a dimensionless erosion parameter of $\hat{M} = 5 \cdot 10^{-5}$. For the dynamic erodibility (Figure 4.12b) we find that no bottom pool is formed at any time in the spring-neap cycle even though the steady-state erodibility indicates that sediment trapping occurs during spring tide (Figure 4.12a). From this we conclude that the total sediment imported during spring tide (for the dynamic solution) is subsequently exported in the following neap tide. The balance between import during spring tide and export during neap tide results in no residual growth of the total stock and thus $\mathcal{S}$ is bounded. Since this bound on the total stock occurs for $f < 1$, no bottom pool is observed at any time during the spring-neap cycle. This result indicates that the formation of a bottom pool can be ruled out due to temporal lag effects.

The steady-state and dynamic surface SSC are shown in Figures 4.12c and 4.12d, respectively. We find a profound difference in the magnitude of concentrations between the maximum steady-state surface SSC (up to 200 mg/L) and the maximum dynamic surface SSC (up to 45 mg/L) due to the absence of erodible sediment in the bottom pool. For the dynamic solution we find an ETM throughout the spring-neap cycle which gradually moves from km 55 during spring tide to km 45 during neap tide. Furthermore, due to temporal lag effects, the maximum surface concentration of 45 mg/L of the dynamic solution occurs at the end of the importing phase associated with spring tide (denoted by $t_2 = 9.5$ cycles in Figure 4.12d), when the total amount of imported sediment is at a maximum. Then, as the system transitions to the exporting phase associated with neap tide, the surface SSC decreases to the initial value (i.e. the surface SSC found at the beginning of the spring-neap cycle, denoted by $t_2 = 9.0$ cycles) as the import of sediment during spring tide is subsequently counteracted by the sediment export during neap tide.

(a) Steady-state erodibility

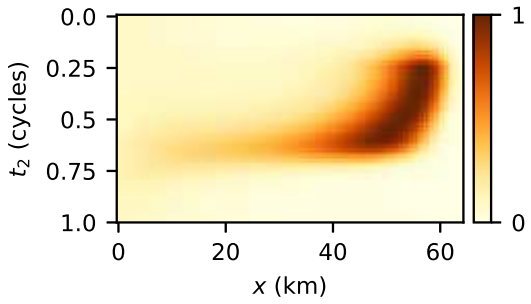

(b) Dynamic erodibility

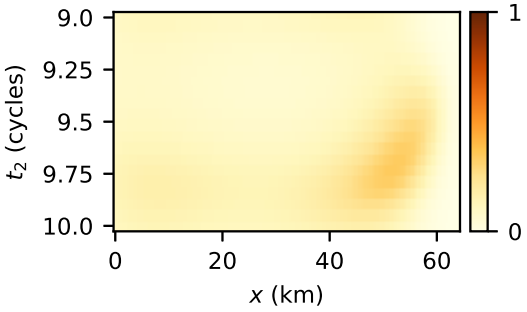

(c) Steady-state surface SSC

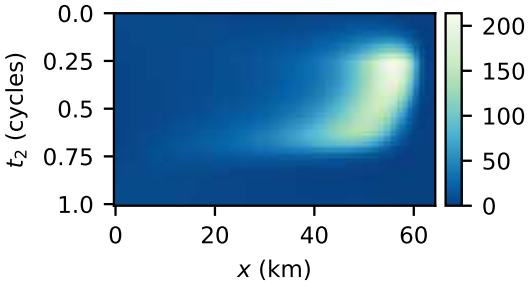

(d) Dynamic surface SSC

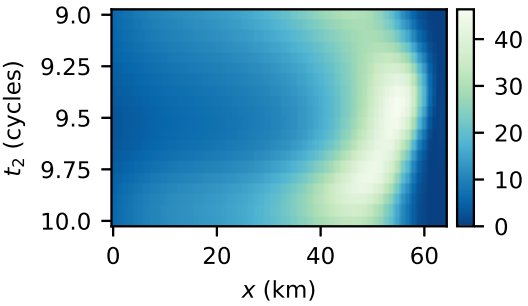

Figure 4.12: The (periodic) steady-state and dynamic erodibility solutions corresponding to a high rate of erosion ($\hat{M} = 5 \cdot 10^{-5}$). Due to temporal lag effects the dynamic solution does not exhibit a bottom pool and therefore surface concentrations are low.

In Figure 4.13 the erodibility and surface SSC of the steady-state and dynamic solutions are shown for a relatively high dimensionless erosion parameter of $\hat{M} = 10 \cdot 10^{-5}$. The steady-state erodibility (Figure 4.13a) indicates that no sediment trapping occurs at any time in the spring-neap cycle. Instead, the steady-state erodibility reaches a maximum of $f_{\text{eq}} = 0.8$ around km 55 during spring tide, indicating the coexistence of an erodible muddy and inerodible sandy state within each ebb-flood cycle. However, due to temporal lag effects, the low value of the dynamic erodibility (Figure 4.13b) indicates that all the sediment is in suspension throughout the spring-neap cycle. This corresponds with the region $\mathcal{S} < \mathcal{S}_a$ in Figure 3.1. This can be explained with a similar argument as was used to explain the absence of a bottom pool for the $\hat{M} = 5 \cdot 10^{-5}$ case: a balance is formed between the total sediment imported during spring tide and the total sediment exported during the subsequent neap tide. Thus it follows that the total stock is bounded. Since this bound occurs for sufficiently low values of $\mathcal{S}$ the coexistence of an erodible muddy bed and an inerodible sandy bed within each ebb-flood cycle is ruled out due to temporal lag effects.

The steady-state and dynamic surface SSC are shown in Figures 4.13c and 4.13d, respectively. A comparison of these solutions shows that the results are similar to solutions obtained with $\hat{M} = 5 \cdot 10^{-5}$. A similar difference between the magnitude of the steady state surface SSC (up to 300 mg/L) and the dynamic surface SSC (up to 45 mg/L) is found, due to the absence of erodible sediment during an ebb-flood cycle. Furthermore the surface SSC of the dynamic solution is indiscernible from the dynamic surface SSC obtained using $\hat{M} = 5 \cdot 10^{-5}$, namely an ETM that gradually and periodically moves from km 55 during spring tide to km 45 during neap tide, with a maximum surface concentration of 45 mg/L at the end of the importing phase associated with spring tide. This result indicates that dynamic solutions in which all sediment is in suspension become insensitive to the specific value of $\hat{M}$. Moreover, these solutions are still heavily influenced by temporal lag effects, as the maximum surface SSC concentration of the dynamic solutions is an order of magnitude smaller than the corresponding steady state surface SSC.

(a) Steady-state erodibility

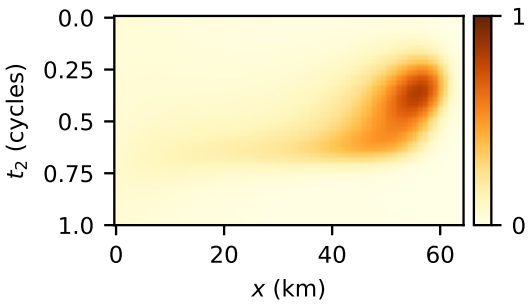

(b) Dynamic erodibility

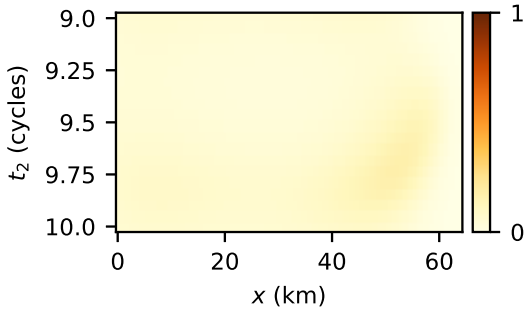

(c) Steady-state surface SSC

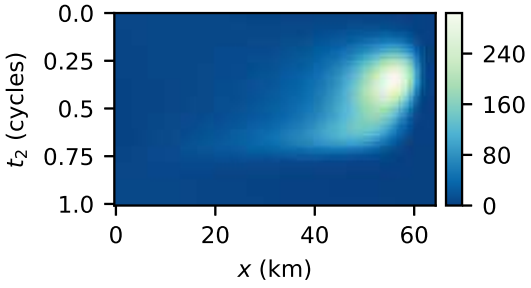

(d) Dynamic surface SSC

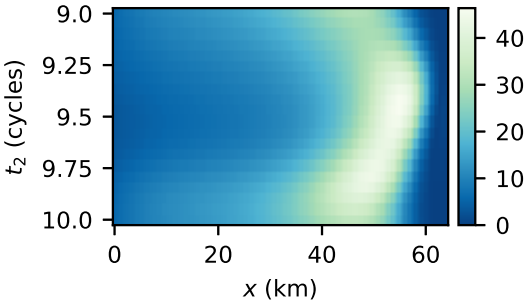

Figure 4.13: The (periodic) steady-state and dynamic erodibility solutions corresponding to a high rate of erosion ($\hat{M} = 10 \cdot 10^{-5}$). Due to temporal lag effects the dynamic solution does not exhibit a sediment deposition during an ebb-flood cycle and therefore surface concentrations are low

In conclusion, we find that temporal lag effects have a profound influence on the dynamic solutions for all investigated values of the dimensionless erosion parameter $\hat{M}$. For a low value, $\hat{M} = 1 \cdot 10^{-5}$, this resulted in the presence of an ETM and a bottom pool at a constant location which persisted throughout the spring-neap cycle. For higher values, $\hat{M} = 5 \cdot 10^{-5}$ and $\hat{M} = 10 \cdot 10^{-5}$, we found that all sediment was kept in suspension throughout a spring-neap cycle, in contrast with the respective steady state solutions which indicated sediment deposition during spring tide. Moreover, the typical dynamic surface SSC are much lower than the respective steady state concentrations. For these high values of $\hat{M}$ a gradually moving ETM was found throughout the spring-neap cycle.

For all investigated values of $\hat{M}$, we found that the surface SSC concentrations were of the same order of magnitude. More specifically the concentrations corresponding to $\hat{M} = 5 \cdot 10^{-5}$ and $\hat{M} = 10 \cdot 10^{-5}$ are exactly similar, indicating that all sediment is in suspension for both solutions. If all sediment is in suspension, the transport of sediment becomes insensitive to the value of $\hat{M}$, thus it is expected that increasing the value of $\hat{M}$ yields the same dynamic surface SSC. Due to higher typical velocities during spring tide, a higher dynamic surface SSC was found for the low rate of erosion, $\hat{M} = 1 \cdot 10^{-5}$. However it holds that surface concentrations vanish as $\hat{M}$ goes to zero.

These results indicate that in order to accurately describe sediment trapping on the spring-neap time scale the influence of temporal lag effects have to be taken into account by obtaining the solutions of suspended sediment concentrations and bottom pool formation using a dynamic model. This holds for all investigated values of the dimensionless erosion parameter $\hat{M}$.

4.5. Evolution of the Total Sediment Mass in the Estuary

In the previous section it was noted that for high values of the dimensionless erosion parameter $\hat{M}$, a balance is formed between the (tidally averaged and width-averaged) sediment mass imported during spring tide and exported in the following neap tide. On the other hand, for low values of $\hat{M}$ a bottom pool was formed due to a net deposition of sediment on the river bed for each spring-neap cycle. In this section we will show this balance for the dynamic solutions by inspection of the time evolution of the total width-averaged and tidally averaged sediment mass in the estuary in suspension and in the bottom pool combined, which is expected to vary on the long time scale due to spring-neap variations.

The total tidally averaged and width-averaged sediment mass $\mathcal{S}_{\text{tot}}(t_2)$ (in kg/m) is defined as:

$$\mathcal{S}_{\text{tot}}(t_2) = \int_0^L \mathcal{S}_{\text{dyn}}(t_2, x)\, dx, \tag{4.1}$$

where we emphasize that $\mathcal{S}_{\text{dyn}}(t_2, x)$ is the total stock corresponding to the dynamic solution. In this section, $\mathcal{S}_{\text{dyn}}(t_2, x)$ is obtained using an empty stock as an initial condition.

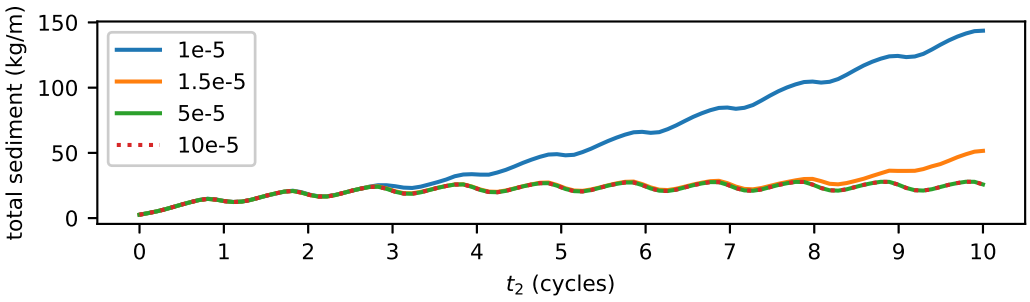

Figure 4.14: The evolution of the total tidally averaged and width-averaged mass of sediment in the estuary for various rates of the dimensionless erosion parameter $\hat{M}$. For low values of $\hat{M}$ we find the formation of a bottom pool leading to residual growth of the total sediment in the estuary. For higher values of $\hat{M}$ we find a periodic solution, indicating a balance between the sediment import during spring-tide and export during neap-tide.

Since $\mathcal{S}_{\text{tot}}(t_2)$ is independent of the spatial coordinate, the analysis is not influenced by the observed movement of the ETM for high values of $\hat{M}$. Moreover, since it is assumed that sediment can only be imported from the sea, fluctuations of $\mathcal{S}_{\text{tot}}(t_2)$ must follow from sediment transport across the seaward boundary. The concentration of suspended sediment at this boundary was prescribed by a constant concentration c_{sea}.

In Figure 4.14 the evolution of the total width-averaged sediment mass $\mathcal{S}_{\text{tot}}(t_2)$ is presented for various rates of erosion, i.e. $\hat{M} = 1 \cdot 10^{-5}$, $\hat{M} = 1.5 = \cdot 10^{-5}$, $\hat{M} = 5 \cdot 10^{-5}$ and $\hat{M} = 10 \cdot 10^{-5}$. For high values, $\hat{M} = 5 \cdot 10^{-5}$ and $\hat{M} = 10 \cdot 10^{-5}$, we find a periodic solution (after the influence of the initial condition vanishes after approximately 3 spring-neap cycles) of $\mathcal{S}_{\text{tot}}(t_2)$, indicating a balance of sediment import during spring and sediment export during neap across the seaward boundary. Moreover, due temporal lag effects explained in the previous section, we observe that the total sediment reaches a maximum value at the end of each importing period associated with spring tide (i.e. $t_2 = 0.75 + n$ where n is the number of cycles) and a minimum value at the end of each exporting period associated with neap tide (i.e. $t_2 = 0.25 + n$). For low values, $\hat{M} = 1 \cdot 10^{-5}$ and $\hat{M} = 1.5 = \cdot 10^{-5}$, we find that the total sediment in the estuary is subject to residual growth. For $\hat{M} = 1 \cdot 10^{-5}$ a bottom pool is formed after 3 spring-neap cycles. Due to a net deposition of sediment in the bottom pool for each spring-neap cycle the total amount of sediment in the estuary grows. Similar behaviour is found for $\hat{M} = 1.5 \cdot 10^{-5}$, although due to the higher rate of erosion a bottom pool is only formed after 8 spring-neap cycles. Moreover the residual growth of the total sediment in the estuary (indicated by the steepness of the linear trend of the solutions) is smaller compared to the dynamic solution corresponding to $\hat{M} = 1 \cdot 10^{-5}$.

5
Conclusion

5.1. Reviewing the Research Questions

Three research questions were defined in Section 1.5. The answers to these questions will be discussed below.

1. Can the solar semi diurnal tidal constituents be incorporated in the semi-analytical modeling framework?

In Chapter 3 the use of a multiple time scale expansion to obtain an approximation of the combined effect of lunar and solar semi diurnal tidal constituents was presented. The introduced asymptotically ordered time scales correspond to the fast ebb-flood cycle and the slow spring-neap variations. These time scales were regarded as distinct and independent, thus allowing a reformulation of the tidal forcing in terms of amplitude modulated tidal constituents, denoted by D_2 and D_4. Furthermore, a well-defined approximated tidal average can be defined as the average over the lunar semi diurnal wave period. Finally approximated solutions of the water motion and sediment dynamics can be found as functions on the time scale associated with the spring-neap variations.

2. What are the effects of the spring-neap cycle on the transport of sediment?

The dependency of sediment transport on the spring-neap variations has been investigated analytically, in Section 3.1.4, and in a simulation study using the conditions of the Ems-Dollard estuary, Section 4.3.2. We found that the import of suspended sediment is strongly enhanced during spring-tide. Furthermore, the direction of sediment transport by the external tidal forcing is determined by the prescribed relative phase difference between the D_2 and D_4 tidal constituents of the sea surface elevation. Based on the tidal forcing observed in the Ems-Dollard estuary we concluded that the external tidal forcing transports sediment seawards during neap-tide. This resulted in an overal export of sediment during neap-tide. Hence the transport of sediment in the Ems-Dollard estuary is characterized by an import-phase during spring-tide and an export-phase during neap-tide.

3. How are the long-term characteristics of bottom pool evolution affected by temporal lag effects?

A profound influence of temporal lag effects was found regardless of the presence of a bottom-pool, as shown in Sections 4.4 and 4.5. Moreover, it was found that the long-term characteristics of the bottom pool evolution is sensitive to the strength of temporal lag effects. We have defined the dimensionless erosion parameter $\hat{M}$ as an important parameter determining long-term bottom pool evolution. For low rates of erosion we found that the bottom pool is present throughout the exporting-phase and is subjected to a residual nonzero growth. Large rates of erosion resulted in the absence of a bottom pool, thus placing a bound on the total mass of sediment in the estuary, even though a convergence of sediment transport is observed during the import-phase of the spring-neap cycle.

5.2. Recommendations for Future Research

Assessing the importance of missing solar resonance modes

With the introduction of the multiple time scale expansion, the tidal forcing is represented by amplitude modulated lunar tidal constituents. As a result, the solar resonance modes can not be resolved with this model. Thus, the approximation presented in this thesis might fail to reproduce the conditions associated with estuaries with lengths close to a solar resonance mode.

Based on rudimentary simulations it is expected that this phenomenon is of little importance for realistic bottom friction coefficients, however this has not been subjected to thorough research

Spring-neap varying eddy-viscosity/diffusivity

The calibrated eddy-viscosity/diffusivity coefficients used in this thesis were assumed to be constant in time. However, the turbulent conditions are expected to vary during the spring-neap cycle and should thus lead to periodic fluctuations of the magnitudes of the eddy-viscosity/diffusivity coefficients. It is expected that the low-energetic conditions associated with neap-tide lead to reduced turbulent vertical mixing, possibly resulting in more enhanced sediment deposition during neap-tide. On the other hand, associated with the high-energetic conditions of spring-tide is an increase in the turbulent vertical mixing resulting in a decrease in sediment deposition. These fluctuations can be incorporated in the model by diagnostically prescribing spring-neap varying eddy-viscosity/diffusivity coefficients or, if sufficient data is present, by interpolating calibrated coefficients for various times in the spring-neap cycle.

Improved calibration of the dimensionless erosion parameter

As discussed in Dijkstra [2019], the dimensionless erosion parameter $\hat{M}$ is poorly understood and a specific value of $\hat{M}$ resembling the efficiency of resuspension in the Ems-Dollard estuary is not available. In this thesis we have performed a sensitivity study with assumed values of $\hat{M}$. This led to the conclusion that the long-term characteristics of bottom pool evolution is sensitive to the dimensionless erosion parameter. In order to accurately explain the spring-neap variations of sediment trapping in the Ems-Dollard estuary the dimensionless erosion parameter must be subjected to further research.

Application to other estuaries

Although the theoretical framework developed in this thesis is general in nature, our model was applied to the conditions of the Ems in 2005. However, we have found that different phases of the prescribed sea surface elevation can lead to profoundly different behaviour of sediment transport (not shown in this thesis). Thus the application of our method to other estuaries should lead to a different description of spring-neap variations of the transport of suspended fine sediment.

A

Width-Averaged Shallow-Water Equations

To describe the water motion in an estuary, we will derive the shallow-water equations, consisting of the continuity and momentum equations. Next, these equations will be averaged over the width resulting in the width-averaged shallow-water equations.

A sketch of the geometry of an idealized estuary is shown in Figure A.1. The seaward boundary, at $x = 0$, is connected to the sea and the landward boundary, at $x = L$, is constrained by a weir. Located at $z = 0$ is the undisturbed water level. The water surface is given by $z = \zeta(t,x)$ and the bed profile is described by $z = -H(x)$. Further, the upper and lower bank are denoted by $B_1(x)$ and $B_2(x)$ respectively, hence the width of the estuary can be written as $B(x) = B_1(x) - B_2(x)$.

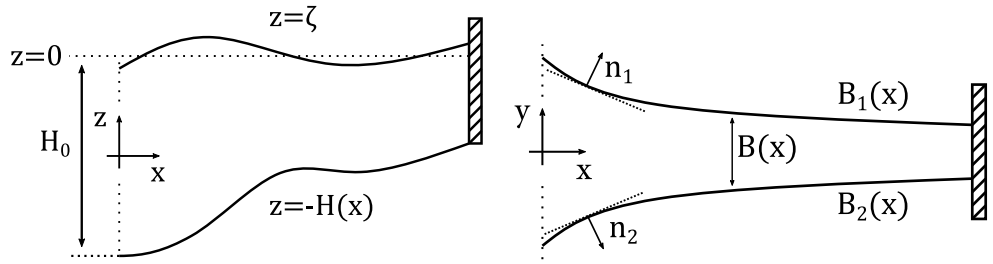

(a) Side view (b) Top view

Figure A.1: Sketches of the model geometry.

Specific to our approach, the total width of the estuary is taken as exponentially converging [Savenije, 2012]:

$$B(x) = B_0 e^{-x/L_b}, \tag{A.1}$$

with B_0 the characteristic width at the seaward boundary and L_b the convergence length. Further, we require that the side banks are impermeable, thus any flux across the banks vanishes:

$$\bar{n}_{1,2} \cdot \bar{J}(t,x,y,z)\big|_{y=\pm B/2} = 0, \tag{A.2}$$

with $\bar{n}_1$, $\bar{n}_2$ outward pointing vectors perpendicular to the side boundaries, see Figure A.1b, and $\bar{J}$ a vector representing either water or sediment flux.

A.1. Shallow-Water Equations

A.1.1. Continuity Equation

The continuity equation is derived from conservation of mass. For a fluid, mass is given in terms of the density ρ. This leads to the classical form of the continuity equation [Rahman, 1995]:

$$\frac{D\rho}{Dt} + \rho \nabla \cdot \bar{U} = 0, \tag{A.3}$$

with the vector, denoted by an upper bar, $\bar{U} = (u, v, w)$ the three-dimensional velocity field and D/Dt the total derivative operator. In the total derivative, spatial coordinates are taken to be a function of time, applying the chain rule results in:

$$\frac{D}{Dt} = \frac{\partial}{\partial t} + \bar{U} \cdot \nabla.$$

In other words, the total derivative takes into account that the fluid is advected by the velocity field.

We can simplify Eq. (A.3) by applying the Boussinesq approximation, see Cushman-Roisin [1994]. The density ρ can be expressed as a mean reference value and a fluctuation part:

$$\rho = \rho_0 + \rho'(t, x, y, z), \tag{A.4}$$

where ρ_0 is the reference density of water and ρ' represents the fluctuations around this reference value, for example caused by salinity differences. It is assumed that the density fluctuations are small compared to the reference value i.e. $\rho' \ll \rho_0$. This assumption allows us to simplify Eq. (A.3) based on a scaling argument. Let $\mathcal{L}$, $\mathcal{T}$ be the characteristic length and time scale of the system. Then, substitution of Eq. (A.4) in Eq. (A.3) and dividing by the reference density results in:

$$\begin{array}{ccccc} \frac{1}{\rho_0}\frac{D\rho'}{Dt} & + & \frac{\rho'}{\rho_0}\nabla\cdot\bar{U} & + & \nabla\cdot\bar{U} = 0, \\ \left[\frac{\rho'}{\rho_0}\frac{1}{\mathcal{T}}\right], & & \left[\frac{\rho'}{\rho_0}\frac{\mathcal{U}}{\mathcal{L}}\right], & & \left[\frac{\mathcal{U}}{\mathcal{L}}\right], \end{array}$$

where the characteristic scales are indicated underneath each term. We find that the first two terms are of the same magnitude, since the characteristic velocity scale is given by $\mathcal{L} \simeq \mathcal{U}\mathcal{T}$. However these two terms are much smaller than the third term, by virtue of the Boussinesq approximation, i.e. $\rho' \ll \rho_0$. Then, in leading order the continuity equation reduces to:

$$\nabla \cdot \bar{U} = 0. \tag{A.5}$$

By this scaling argument it follows that conservation of mass leads to the fluid behaving as being incompressible.

A.1.2. Momentum Equations

Conservation of momentum for a fluid is given by the three-dimensional Navier-Stokes equations [Rahman, 1995]:

$$\begin{cases} \rho\frac{Du}{Dt} = F_1 - \frac{\partial P}{\partial x} + \mu\nabla^2 u, \\ \rho\frac{Dv}{Dt} = F_2 - \frac{\partial P}{\partial y} + \mu\nabla^2 v, \\ \rho\frac{Dw}{Dt} = F_3 - \frac{\partial P}{\partial z} + \mu\nabla^2 w, \end{cases} \tag{A.6}$$

with $\bar{F} = (F_1, F_2, F_3)$ the vector representing external forces and μ is the molecular (dynamic) viscosity. The general form of the momentum equations as given by Eq. (A.6) is impractical, since the behaviour of solutions (if any exist [Fefferman, 2000]) can be chaotic and random in nature due to turbulence. Therefore, following Burchard [2002], we turn our attention towards a statistical approach of turbulence modelling. We start by writing a velocity component in terms of a mean $\hat{u}$ and a fluctuation part u', known as the Reynolds Decomposition:

$$u(t, x, y, z) = \hat{u}(t, x, y, z) + u'(t, x, y, z). \tag{A.7}$$

The mean field $\hat{u}$ can be understood in terms of a random process: Formally we can find repeated realizations of a given flow situation, on the same domain with the same initial conditions and external forcing. Say we have n realizations, due to the apparent random nature of turbulence these realizations would exhibit varying instances of u_i, the ith realization of a velocity component. The mean would then be defined as the ensemble average of all these realizations:

$$\hat{u} \equiv \langle u \rangle = \lim_{n\to\infty} \frac{1}{n} \sum_{i=1}^{n} u_i(t, x, y, z) \tag{A.8}$$

We can find an equations for the mean velocity components by substituting Eq. (A.7) in Eq. (A.6) and then taking the mean, as defined in Eq. (A.8). Writing out the total derivative results in the Reynolds-Averaged

Navier-Stokes equations:

$$\begin{cases} \rho\left(\frac{\partial \hat{u}}{\partial t} + \hat{U}\cdot\nabla\hat{u}\right) = \hat{F}_1 - \frac{\partial \hat{P}}{\partial x} + \mu\nabla^2\hat{u} + \rho\nabla\cdot\langle u'\bar{U}'\rangle, \\ \rho\left(\frac{\partial \hat{v}}{\partial t} + \hat{U}\cdot\nabla\hat{v}\right) = \hat{F}_2 - \frac{\partial \hat{P}}{\partial y} + \mu\nabla^2\hat{v} + \rho\nabla\cdot\langle v'\bar{U}'\rangle, \\ \rho\left(\frac{\partial \hat{w}}{\partial t} + \hat{U}\cdot\nabla\hat{w}\right) = \hat{F}_3 - \frac{\partial \hat{P}}{\partial z} + \mu\nabla^2\hat{w} + \rho\nabla\cdot\langle w'\bar{U}'\rangle. \end{cases} \tag{A.9}$$

Note that the expression for the mean velocity field still depends on (unknown) correlation terms: $u'\bar{U}'$, $v'\bar{U}'$, $w'\bar{U}'$, corresponding to momentum transfer due to turbulent fluctuations. Following Nieuwstadt et al. [2016], we state that this turbulent momentum transfer gives rise to internal frictions, which act in a manner analogous to molecular viscosity, but on a larger scale:

$$\begin{aligned} \nabla\cdot\langle u'U'\rangle &\simeq \nabla\cdot(\bar{A}\nabla\langle u\rangle), \\ \nabla\cdot\langle v'U'\rangle &\simeq \nabla\cdot(\bar{A}\nabla\langle v\rangle), \\ \nabla\cdot\langle w'U'\rangle &\simeq \nabla\cdot(\bar{A}\nabla\langle w\rangle), \end{aligned} \tag{A.10}$$

with $\bar{A} = (A_h,\ A_h,\ A_v)$ the eddy viscosity coefficients (compare with viscosity term in Eq. (A.9)). The eddy viscosity is anisotropic because the vertical length scale is much smaller than the longitudinal and cross-sectional length scales. The rate of momentum transfer will then be different because the size of the eddies is bounded by the characteristic depth, hence constraining the rate of momentum transfer. The eddy viscosity coefficients are to be determined empirically. However, in general it holds that turbulent stresses are orders of magnitude larger then their viscous counterparts. This approach is known as a first moment closure scheme

Having accounted for the unknown correlations terms, we turn towards the remaining undefined terms of Eq. (A.9), the external Reynolds-Averaged forces per unit mass. For geophysical fluid flows, the gravitational force and the Coriolis psuedo-force are important external forces to consider, see Cushman-Roisin [1994]. The gravitational force is given by: $\bar{F}_g = (0,\ 0,\ -\rho g)$. Next, the Coriolis psuedo-force arises due to movement in a rotating frame of reference. In the context of geophysical fluid dynamics, the Coriolis effect results in a deflection of fluid motion due to the Earth's rotation. Let Ω denote the angular rotation of the Earth and ϕ the angle corresponding to a given lattitude. Then the Coriolis psuedo-force is given by $F_c = (f_*\hat{w} - f\hat{u},\ f\hat{u},\ -f_*\hat{u})$, where $f = 2\Omega\sin\phi$ is the Coriolis parameter and $f_* = 2\Omega\cos\phi$.

Combining the eddy-viscosity parametrization, gravity and the Coriolis effect, we find that Eq. (A.9) can be written as:

$$\begin{cases} \rho\left(\frac{\partial \hat{u}}{\partial t} + \hat{U}\cdot\nabla\hat{u} + f_*\hat{w} - f\hat{v}\right) = -\frac{1}{\rho}\frac{\partial \hat{P}}{\partial x} + \rho\nabla\cdot(\bar{A}\nabla\hat{u}), \\ \rho\left(\frac{\partial \hat{v}}{\partial t} + \hat{U}\cdot\nabla\hat{v} + f\hat{u}\right) = -\frac{1}{\rho}\frac{\partial \hat{P}}{\partial y} + \rho\nabla\cdot(\bar{A}\nabla\hat{v}), \\ \rho\left(\frac{\partial \hat{w}}{\partial t} + \hat{U}\cdot\nabla\hat{w} - f_*\hat{u}\right) = -\rho g - \frac{1}{\rho}\frac{\partial \hat{P}}{\partial z} + \rho\nabla\cdot(\bar{A}\nabla\hat{w}), \end{cases} \tag{A.11}$$

where the molecular viscosity terms are neglected as they are much smaller than their turbulent eddy viscosity counterparts. The system of equations defined in Eq. (A.11) can be simplified even further with the shallow water approximation. This approximation is based on a scaling argument for a typical length scales that are much longer than they are deep. The influence of this assumption becomes apparent when we inspect the relative scales of the individual terms of the momentum equation in the vertical direction:

$$\begin{array}{cccccccc} \frac{\partial \hat{w}}{\partial t} + \hat{U}\cdot\nabla\hat{w} & -f_*u & = & -g & - & \frac{1}{\rho}\frac{\partial \hat{P}}{\partial z} & + & \nabla\cdot(\bar{A}\nabla\hat{w}). \\ \left[\frac{\mathcal{W}}{\mathcal{T}}\right], & [\Omega\mathcal{U}], & & [g], & & \left[\frac{\mathcal{P}}{\rho\mathcal{H}}\right], & & \left[A_h\frac{\mathcal{W}}{\mathcal{L}^2}\right], \left[A_h\frac{\mathcal{W}}{\mathcal{B}^2}\right], \left[A_v\frac{\mathcal{W}}{\mathcal{H}^2}\right], \end{array}$$

with $\mathcal{L}$, $\mathcal{B}$, $\mathcal{H}$ the characteristic longitudinal, cross-sectional and vertical length scales, $\mathcal{T}$ the characteristic time scale and the characteristic longitudinal velocity follows from $\mathcal{L} \simeq \mathcal{U}\mathcal{T}$. Then, balancing the longitudinal and vertical velocity terms of the continuity equation, Eq. (A.5), results in the vertical velocity scale $\mathcal{W} \simeq \mathcal{U}\mathcal{H}/\mathcal{L}$. By this balancing observation, we find that $\mathcal{W}/\mathcal{T} \simeq \mathcal{U}\mathcal{H}/\mathcal{L}\mathcal{T}$. With the characteristic values of our system, it holds that $\mathcal{H}/\mathcal{L}\mathcal{T} \ll \Omega$. However, the second term, corresponding to the Coriolis effect, is already magnitudes lower then the gravitational force. Thus the first two terms can be neglected from leading order. By further comparison of the characteristic scales of our system, it becomes apparent that the contribution of the turbulent momentum transfer is dominated by the vertical viscosity term, since $A_h \simeq A_v$ and

$\mathcal{H} \ll \mathcal{B} \leq \mathcal{L}$. Moreover, the vertical momentum transfer is already small compared to the gravitational force. Hence the turbulent eddy viscosity can also be omitted from leading order. Finally taking $\mathcal{P} \simeq \rho g \mathcal{H}$ we find that in leading order, the gravitational force is balanced by the vertical pressure gradient.

Using this approximation, the vertical momentum equation reduces to the hydrostatic pressure balance:

$$\frac{\partial \hat{P}}{\partial z} = -\rho g.$$

We can easily find the hydrostatic pressure by integrating over the depth:

$$\hat{P} = P_a + g \int_z^\zeta \rho \, dz,$$

with P_a the atmospheric pressure at the free surface which we take to be constant. Then, the pressure gradient in the longitudinal direction can be found by the Leibniz integral rule:

$$\frac{\partial \hat{P}}{\partial x} = \rho g \zeta_x \big|_{z=\zeta} + g \int_z^\zeta \rho_x \, dz.$$

A similar expression can be found for the derivative with respect to y. If it is assumed that the system is well-mixed, i.e. the density is constant in the vertical direction, this expression reduces to:

$$\frac{\partial \hat{P}}{\partial x} = \rho g \zeta_x \big|_{z=\zeta} + g \rho_x (\zeta - z). \tag{A.12}$$

Substitution of Eq. (A.12) in Eq. (A.11) and applying the Boussinesq approximation, given in Eq. (A.4), leads to the shallow-water equations:

$$\begin{cases} \frac{\partial \hat{u}}{\partial t} + \hat{U} \cdot \nabla \hat{u} + f_* \hat{w} - f \hat{v} = -g \zeta_x + \frac{g \rho'_x}{\rho_0} (\zeta - z) + \frac{\partial}{\partial z} \left(A_v \frac{\partial u}{\partial z} \right), \\ \frac{\partial \hat{v}}{\partial t} + \hat{U} \cdot \nabla \hat{v} + f \hat{u} = -g \zeta_y + \frac{g \rho'_y}{\rho_0} (\zeta - z) + \frac{\partial}{\partial z} \left(A_v \frac{\partial v}{\partial z} \right). \end{cases} \tag{A.13}$$

Note that the Boussinesq approximation does not warrant further simplification regarding density gradients because there is no term that dominates these contributions; All the gradients of the (constant) reference density vanished since they are by definition equal to zero. As a side note, we observe that the z-equation is no longer used to determine the vertical velocity profile, instead w will be completely determined by the free surface elevation and the change in the bottom profile and follows from the continuity equation.

A.2. Width-Averaged Shallow-Water Equations

A.2.1. Continuity Equation

To obtain the width-averaged continuity equation, Eq. (A.5) is integrated over the width of the estuary:

$$\int_{-B/2}^{B/2} \frac{\partial u}{\partial x} dy + \int_{-B/2}^{B/2} \frac{\partial v}{\partial y} dy + \int_{-B/2}^{B/2} \frac{\partial w}{\partial z} dy = 0. \tag{A.14}$$

Note that the boundaries of the integral depend on the longitudinal coordinate x. Using the Leibniz integral rule the first term in Eq. (A.14) can be rewritten as:

$$\int_{-B/2}^{B/2} \frac{\partial u}{\partial x} dy = \frac{\partial}{\partial x} \int_{-B/2}^{B/2} u \, dy - \frac{u}{2} \frac{\partial B(x)}{\partial x} \bigg|_{y=B/2} - \frac{u}{2} \frac{\partial B(x)}{\partial x} \bigg|_{y=-B/2}.$$

Using this expression, Eq. (A.14) becomes:

$$\frac{\partial}{\partial x} \int_{-B/2}^{B/2} u \, dy + \left(-\frac{u}{2} \frac{\partial B(x)}{\partial x} + v \right) \bigg|_{y=B/2} - \left(\frac{u}{2} \frac{\partial B(x)}{\partial x} + v \right) \bigg|_{y=-B/2} + \frac{\partial}{\partial z} \int_{-B/2}^{B/2} w \, dy = 0.$$

In this formulation we observe two boundary terms which represent mass fluxes across the upper and lower bank. To show this, take the outward pointing vectors perpendicular to the side banks:

$$\vec{n}_1 = \left(-\frac{1}{2} \frac{\partial B(x)}{\partial x}, 1, 0 \right),$$
$$\vec{n}_2 = \left(\frac{1}{2} \frac{\partial B(x)}{\partial x}, 1, 0 \right).$$

Then the fluxes across the banks are proportional to:

$$\bar{n}_1 \cdot \bar{U}\big|_{y=B/2} = \left(-\frac{u}{2}\frac{\partial B(x)}{\partial x} + v\right)\Big|_{y=B/2},$$
$$\bar{n}_2 \cdot \bar{U}\big|_{y=-B/2} = \left(\frac{u}{2}\frac{\partial B(x)}{\partial x} + v\right)\Big|_{y=-B/2}.$$

These terms vanish by Eq. (A.2) and the continuity equation reduces to:

$$\frac{\partial}{\partial x}\int_{-B/2}^{B/2} u\,dy + \frac{\partial}{\partial z}\int_{-B/2}^{B/2} w\,dy = 0.$$

Introduce the width-averaged velocities, denoted by a $\tilde{(\sim)}$, i.e.

$$\tilde{u} = \frac{1}{B(x)}\int_{B_2(x)}^{B_1(x)} u\,dy, \tag{A.15}$$

and similarly for the width-averaged vertical velocity $\tilde{w}$. Hence we can write:

$$\frac{\partial(B\tilde{u})}{\partial x} + \frac{\partial(B\tilde{w})}{\partial z} = 0,$$

or in short-hand notation:

$$(B\tilde{u})_x + (B\tilde{w})_z = 0.$$

Finally for a width defined by Eq. (A.1) the width-averaged continuity equation reads:

$$\tilde{u}_x + \tilde{w}_z - \frac{\tilde{u}}{L_b} = 0. \tag{A.16}$$

A.2.2. Momentum Equations

The first step in the derivation of the width-averaged momentum equations is neglecting the Coriolis effect. Being an inherently three-dimensional phenomena, the Coriolis effect has no 2DV counterpart. This assumption is made with the aim of deriving a width-averaged formulation, for the sake of simplicity. However, the Coriolis effect is in fact worthy of consideration, as can be seen from the several studies that exist regarding its influence on estuarine fluid flow, for example: Wong [1994], Valle-Levinson et al. [2003] and Huijts et al. [2006].

The x-momentum balance of Eq. (A.13) then reduces to:

$$u_t + uu_x + vu_y + wu_z + g\zeta_x + \frac{g\rho_x}{\rho_0}(\zeta - z) - (A_v u_z)_z = 0. \tag{A.17}$$

Integrating over the width and simplifying, using Eq. (A.15), leads to:

$$(B\tilde{u})_t + \int_{-B/2}^{B/2}\Big[uu_x + vu_y + wu_z\Big]\,dy + Bg\zeta_x + B\frac{g\rho_x}{\rho_0}(\zeta - z) - B(A_v\tilde{u}_z)_z = 0. \tag{A.18}$$

To further simplify, the velocity components shall be written as the sum of a width-averaged term and a residual term, denoted by an apostrophe:

$$u = \tilde{u}(t,x,z) + u'(t,x,y,z). \tag{A.19}$$

Similar decompositions can be made for v and w. Note that upon integrating over the width, the residual term vanishes. Thus we can write:

$$\begin{aligned}
\int_{-B/2}^{B/2} uu_x\,dy &= \frac{1}{2}\int_{-B/2}^{B/2}(uu)_x, \\
&= \frac{1}{2}\int_{-B/2}^{B/2}(\tilde{u}\tilde{u})_x + 2(\tilde{u}u')_x + (u'u')_x\,dy, \\
&= \frac{B}{2}(\tilde{u}\tilde{u})_x + \frac{1}{2}\frac{\partial}{\partial x}\left(\tilde{u}\int_{-B/2}^{B/2} u'\,dy\right) + \int_{-B/2}^{B/2} u'u'_x\,dy, \\
&= B\tilde{u}\tilde{u}_x + \underbrace{\int_{-B/2}^{B/2} u'u'_x\,dy}_{\mathrm{I}}.
\end{aligned}$$

$$\int_{-B/2}^{B/2} v u_y \, dy = \int_{-B/2}^{B/2} \tilde{v}\tilde{u}_y + \tilde{v}u'_y + v'\tilde{u}_y + v'u'_y \, dy,$$
$$= \underbrace{\tilde{v}u'_y\Big|_{-B/2}^{B/2}}_{\text{IV}} + \underbrace{\int_{-B/2}^{B/2} v'u'_y \, dy}_{\text{II}}.$$

$$\int_{-B/2}^{B/2} w u_z \, dy = \int_{-B/2}^{B/2} \tilde{w}\tilde{u}_z + \tilde{w}u'_z + w'\tilde{u}_z + w'u'_z \, dy,$$
$$= B\tilde{w}\tilde{u}_z + \underbrace{\int_{-B/2}^{B/2} w'u'_z \, dy}_{\text{III}}.$$

Upon evaluating the integral term of Eq. (A.18), we find four terms that contain residual terms: three velocity correlation terms (I, II and III) and one boundary contribution (IV). We assume that the velocity correlations can be parametrised by a diffusive process and that these contributions are accounted for by the eddy-viscosity term of Eq. (A.18). Further we take $\tilde{v} = 0$, hence term IV vanishes. With these simplifications we can write Eq. (A.18) in the width-averaged form:

$$\tilde{u}_t + \tilde{u}\tilde{u}_x + \tilde{w}\tilde{u}_z + g\zeta_x + \frac{g\rho_x}{\rho_0}(\tilde{\zeta} - z) - (A_v\tilde{u}_z)_z = 0. \tag{A.20}$$

Note that the cross-sectional momentum equation is identically zero and can therefore be omitted.

A.3. Boundary Conditions and Model Diagnostics

The set of differential equations describing the width-averaged water motion is given by Eqs. (A.16) and (A.20). This will now be complemented with suitable boundary conditions for the idealized geometry from Figure A.1. Moreover, further unknowns, such as the density gradient and spatial variation of the eddy viscosity, will be taken as diagnostic model variables.

The seaward boundary at $x = 0$ is taken to be forced by the semi-diurnal lunar (M_2) and solar (S_2) tidal constituents and their respective first overtides (M_4 and S_4):

$$\zeta(t,0) = \sum_{i\in\mathcal{G}} A_i \cos(\sigma_i t + \phi_i), \tag{A.21}$$

with $\mathcal{G} = (M_2,\ S_2,\ M_4,\ S_4)$ the set containing harmonic tidal constituents, A_i the tidal amplitude, σ_i the angular frequency and $\phi_i \in [0,\ 2\pi)$ a relative phase differences. At the landward boundary, $x = L$, we describe a constant river discharge $\tilde{Q} > 0$:

$$B(L)\int_{-H}^{\tilde{\zeta}} \tilde{u}(t,L,z) \, dz = -\tilde{Q}. \tag{A.22}$$

Next, the free surface at $z = \tilde{\zeta}$ is required to be stress-free:

$$A_v\tilde{u}_z = 0, \qquad \text{at } z = \tilde{\zeta}, \tag{A.23}$$

and we impose the kinematic boundary condition:

$$\tilde{w} = \tilde{\zeta}_t + \tilde{u}\tilde{\zeta}_x, \qquad \text{at } z = \tilde{\zeta}. \tag{A.24}$$

Further we require that the river bed is impermeable:

$$\tilde{w} = -\tilde{u}H_x, \qquad \text{at } z = -H(x). \tag{A.25}$$

Next, by definition the bed shear stress τ_b is proportional to the near-bed velocity squared. Following Zimmerman [1982], we replace this quadratic relation by the linearized bottom friction condition $\tau_b = \rho_0 s_f \tilde{u}$, with s_f the partial slip parameter. Using this, we can express turbulent stresses in terms of linearized friction at the bed:

$$A_v\tilde{u}_z = s_f\tilde{u}, \qquad \text{at } z = -H(x). \tag{A.26}$$

This comprises the formulation of the boundary conditions.

We continue by stating the model diagnostic parameters. Following Friedrichs and Hamrick [1996], we take the vertical eddy viscosity to be linearly proportional to the local water depth:

$$A_v = A_{v0}\frac{H(x)}{H_0}, \tag{A.27}$$

with A_{v0} the eddy viscosity coefficient and H_0 the depth at the entrance. This relation might be inferred if one considers that the scale of vertical turbulent momentum transfer can be taken as the product of a typical turbulent velocity scale $\mathcal{U}_{tur}$ with a typical depth scale $\mathcal{H}$, resulting in: $A_v \sim \mathcal{U}_{tur}\mathcal{H}$. Balancing of Eq. (A.26), we find a similar linear relation for the partial slip parameter:

$$s_f = s_{f0}\frac{H(x)}{H_0}, \tag{A.28}$$

with s_{f0} the bottom friction coefficient. Lastly, density is taken as a linear function of the tidally averaged salt concentration only [Chernetsky et al., 2010]. Introduce $\langle\cdot\rangle$ as the average over an M_2 constituent with period $P = 2\pi/\sigma_{M_2}$:

$$\langle\cdot\rangle \equiv \frac{1}{P}\int_0^P \cdot\, dt. \tag{A.29}$$

Then the along-channel density profile is given by:

$$\rho(x) = \rho_0\Big(1 + \beta_s\langle S(x)\rangle\Big), \tag{A.30}$$

with $\langle S(x)\rangle$ the tidal- and depth-averaged along-channel salinity profile and β_s the conversion factor from salinity to density. Following Talke et al. [2009b] we take the salinity profile as a hyperbolic tangent function of the longitudinal coordinate:

$$\langle S(x)\rangle = S_b + \frac{S_*}{2}\left(1 - \tanh\left(\frac{x - x_c}{L}\right)\right), \tag{A.31}$$

with S_b the base salinity as x approaches infinity, S_* the salinity scale and x_c the location of maximum salinity gradient. Note that we assumed that density is independent of any suspended load concentration. For a discussion regarding the influence of a suspended load dependent density on the formation of turbidity maxima, consult Talke et al. [2009b] or Chernetsky [2012].

B

Width-Averaged Sediment Dynamics

We assume that sediment consists of fine particles of uniform size suspended in water. Moreover we take the particles to be non-cohesive. Hence the suspended sediment can be modelled as concentration being advected by water flow.

B.1. Sediment Transport Equation

Conservation of mass for suspended sediment is given by:

$$\frac{\partial c}{\partial t} + \nabla \cdot \bar{J} = 0, \tag{B.1}$$

with $\bar{J}$ the total flux which consists of two parts: an advective flux $\bar{J}_a$, related to transport of sediment advected by water velocity and a settling flux $\bar{J}_s$, related to a constant falling velocity of suspended particles towards the bottom. Hence we can write:

$$\begin{aligned} \bar{J}_a &= c\bar{U}, \\ \bar{J}_s &= -c w_s \bar{e}_z, \end{aligned}$$

with $\bar{e}_x$, $\bar{e}_y$, $\bar{e}_z$ Cartesian unit vectors and w_s a constant settling velocity. To account for turbulent fluctuations we shall derive the Reynolds-averaged transport equation for the concentration of sediment, following the procedure of Section A.1.2. Substitute the Reynolds decomposition of Eq. (A.7) for c and u and proceed by taking the mean defined in Eq. (A.8), resulting in:

$$\frac{\partial \hat{c}}{\partial t} + \nabla \cdot (\hat{c}\hat{U}) - \nabla \cdot (\hat{c} w_s \bar{e}_z) + \nabla \cdot \langle c' \bar{U}' \rangle = 0. \tag{B.2}$$

Similarly to the eddy viscosity parametrisation, defined in Eq. (A.10), the correlation term '$c'\bar{U}'$' gives rise to turbulent mass transfer which can be parameterised by a diffusive flux $\hat{J}_d$ [Nieuwstadt et al., 2016]. Then the Reynolds-averaged fluxes read:

$$\begin{aligned} \hat{J}_a &= \hat{c}\hat{U}, \\ \hat{J}_s &= -\hat{c} w_s \bar{e}_z, \\ \hat{J}_d &= -K_h \left(\frac{\partial \hat{c}}{\partial x} \bar{e}_x + \frac{\partial \hat{c}}{\partial y} \bar{e}_y \right) - K_v \frac{\partial \hat{c}}{\partial z} \bar{e}_z, \end{aligned}$$

with K_h and K_v the horizontal and vertical turbulent diffusion coefficients, respectively. A distinction is made between directions of turbulent mixing in the horizontal and vertical direction because of different characteristic length scales. Then, in shorthand notation, the Reynolds-averaged form of Eq. (B.1) can be written as:

$$c_t + (uc)_x + (vc)_y + ((w - w_s)c)_z = (K_h c_x)_x + (K_h c_y)_y + (K_v c_z)_z.$$

The width-averaged form can be found by integrating over the width of the domain, and applying the Leibniz integral rule. This results in:

$$\frac{\partial}{\partial t}\int_{-B/2}^{B/2} c\,dy + \frac{\partial}{\partial x}\int_{-B/2}^{B/2} uc\,dy + \frac{\partial}{\partial z}\int_{-B/2}^{B/2}(w-w_s)c\,dy - \frac{\partial}{\partial x}\int_{-B/2}^{B/2} K_h c_x\,dy - \frac{\partial}{\partial z}\int_{-B/2}^{B/2} K_v c_x\,dy = \left[\frac{uc}{2}\frac{\partial B}{\partial x} - vc - \frac{K_h c_x}{2}\frac{\partial B}{\partial x} + K_h c_y\right]_{y=B/2} + \left[-\frac{uc}{2}\frac{\partial B}{\partial x} - vc + \frac{K_h c_x}{2}\frac{\partial B}{\partial x} + K_h c_y\right]_{y=-B/2}. \quad \text{(B.3)}$$

In this formulation, two boundary terms occur representing sediment fluxes across the upper and lower bank. To show this, take the outward pointing vectors perpendicular to the side banks:

$$\bar{n}_1 = \left(-\frac{1}{2}\frac{\partial B}{\partial x}, 1, 0\right),$$
$$\bar{n}_2 = \left(\frac{1}{2}\frac{\partial B}{\partial x}, 1, 0\right).$$

Then the sediment fluxes across the banks are proportional to:

$$\bar{n}_1 \cdot J|_{y=B/2} = \left[\frac{uc}{2}\frac{\partial B}{\partial x} - vc - \frac{K_h c_x}{2}\frac{\partial B}{\partial x} + K_h c_y\right]_{y=B/2},$$
$$\bar{n}_2 \cdot J|_{y=-B/2} = \left[-\frac{uc}{2}\frac{\partial B}{\partial x} - vc + \frac{K_h c_x}{2}\frac{\partial B}{\partial x} + K_h c_y\right]_{y=-B/2}.$$

These terms vanish by Eq. (A.2). Next we substitute the decomposition of Eq. (A.19) for the quantities u, v, w, c and continue, similarly to Section A.2.2, by integrating over the width of the domain to obtain:

$$(B\tilde{c})_t + (B\tilde{u}\tilde{c})_x + (B(\tilde{w}-w_s)\tilde{c})_z - (BK_h\tilde{c}_x)_x - (BK_v\tilde{c}_z)_z = 0. \quad \text{(B.4)}$$

The contribution of cross-correlation terms, i.e. terms containing products of residual terms, are all captured in the eddy-diffusivity parameters K_h and K_v. The argument for this is analogous to the justification of the width-averaged eddy-viscosity term A_v in Section A.2.2. Further, it is assumed that $c'|_{y=\pm B/2} = \tilde{c}$, see also Section A.2.2. The final step is to substitute the expression for the width B given by Eq. (A.1):

$$\tilde{c}_t + \tilde{u}\tilde{c}_x + (\tilde{w}-w_s)\tilde{c}_z = (K_h\tilde{c}_x)_x + (K_v\tilde{c}_z)_z - \frac{1}{L_b}K_h\tilde{c}_x. \quad \text{(B.5)}$$

B.2. Boundary Conditions and Concentration Equilibrium

For sediment transport at $z = \tilde{\zeta}$, we require that the flux across the free surface vanishes:

$$-w_s\tilde{c} - K_v\tilde{c}_z + K_h\tilde{c}_x\tilde{\zeta}_x = 0, \qquad \text{at } z = \tilde{\zeta}. \quad \text{(B.6)}$$

At the seaward boundary the sediment concentration is prescribed by constant value c_{sea} representing the depth- and tidal-averaged sediment concentration at the entrance. On the landward side, the tidal-averaged sediment transport is prescribed by a fluvial import $\mathcal{F}_{\text{river}}$ that can vary on a time-scale that is much longer than the tidal period.

Following Brouwer et al. [2018], the river bed is taken as an impermeable sandy layer not subjected to erosion. Due to sediment settling, an active layer of erodible mud can be deposited on the river bed. A tidal-averaged rate of sediment deposition exceeding the erosion results in the growth of a bottom pool, denoted by $\mathcal{S}$. The evolution of the bottom pool and sediment fluxes are thus governed by the difference in deposition and erosion fluxes, $\tilde{D}$ and $\tilde{E}$ respectively:

$$B\mathcal{S}_t = B\langle\tilde{D} - \tilde{E}\rangle \quad \text{(B.7)}$$

The deposition flux at the bottom, which is due to the constant settling velocity, can be written as:

$$\tilde{D} = w_s\tilde{c}_{\text{bed}}n_{z'}$$

with $\bar{n} = (n_{x'}, n_{y'}, n_{z'})$ the normal vector of the bottom profile (where the apostrophe denotes the Cartesian coordinate instead of the derivative) and $\tilde{c}_{\text{bed}}$ is the suspended sediment concentration just above the bed.

For erosion flux a distinction is made between two states: the availability-limited and the erosion-limited state. These states correspond to the absence or presence of the bottom pool. In the absence of a bottom pool, the rate of erosion is limited by the availability of sediment and therefore by the rate of deposition. However, in the presence of a bottom pool, when an abundant amount of sediment is available, the rate of erosion is limited by a maximum potential erosion that is related to bed shear stresses. This allows for the expression of the erosion flux $\tilde{E}$:

$$\tilde{E} = \begin{cases} \hat{E} & \text{if } \mathcal{S} > 0, \\ \min\left(\hat{E}, \tilde{D}\right) & \text{if } \mathcal{S} = 0, \end{cases} \tag{B.8}$$

with $\hat{E}$ denoting the potential erosion given by:

$$\hat{E} = \frac{w_s \rho_s \hat{M}}{\rho_0 g' d_s} |\tau_b(t,x)|, \tag{B.9}$$

with ρ_s, ρ_0 and d_s denoting sediment density, water density and grain size respectively, g' the reduced gravity and $\hat{M}$ the dimensionless erosion parameter. Further τ_b is the bottom shear stress given by:

$$\tau_b = \rho_0 A_v \tilde{u}_z = \rho_0 s_f \tilde{u}, \qquad \text{at } z = -H(x), \tag{B.10}$$

where the partial slip condition (A.26) was used. These two types of erosion can simultaneously occur within a single tidal period. Therefore Brouwer et al. [2018] introduced the dimensionless tidal-averaged erodibility function $0 \leq f(t,x) \leq 1$ to elegantly denote the tidal-averaged state of the bottom. Explicitly, a tidal-averaged erodibility $f = 1$ implies an erosion limited state for the entirety of the tidal period and thus the growth of a bottom pool, while $f < 1$ implies that the bed is sandy at least one point in the tidal period. Then the tidal-averaged erosion flux can be expressed as:

$$\tilde{E} = \hat{E} f. \tag{B.11}$$

Finally, we note that the erosion flux can be related to turbulent induced mixing at the bed. This process was parametrised by the macro-scale diffusive mixing parameters K_h and K_v, defined in Section B.1:

$$\tilde{E} = -K_h (\tilde{c}_{\text{bed}})_x n_{x'} - K_v (\tilde{c}_{\text{bed}})_z n_{z'} \tag{B.12}$$

Next, we will use Eq. (B.4), to relate the bottom fluxes to the sediment concentration, by integrating over depth and invoking the Leibniz integral rule:

$$\begin{aligned} \frac{\partial}{\partial t}\int_{-H}^{\tilde{\zeta}} B\tilde{c}\, dz + \frac{\partial}{\partial x}\int_{-H}^{\tilde{\zeta}} B\tilde{u}\tilde{c}\, dz - \frac{\partial}{\partial x}\int_{-H}^{\tilde{\zeta}} BK_h\tilde{c}_x\, dz = B\tilde{c}(\tilde{\zeta}_t + \tilde{u}\tilde{\zeta}_x - \tilde{w})\Big|_{z=\tilde{\zeta}} + \dots \\ B(w_s\tilde{c} - K_h\tilde{c}_x\tilde{\zeta}_x + K_v\tilde{c}_z)\Big|_{z=\tilde{\zeta}} + B\tilde{c}(\tilde{u}H_x + \tilde{w})\Big|_{z=-H} - B\left(w_s\tilde{c} + K_h\tilde{c}_x H_x + K_v\tilde{c}_z\right)\Big|_{z=-H}. \end{aligned} \tag{B.13}$$

This expression can be simplified by applying boundary conditions from Eqs. (A.24), (A.25) and (B.6). The only remaining boundary term corresponds to the width-averaged sediment flux across the bed. Since $H_x \ll 1$, this flux can be written as $-B(\tilde{D} + \tilde{E}_s)$. Hence we can formulate Eq. (B.13) as:

$$\frac{\partial}{\partial t}\int_{-H}^{\tilde{\zeta}} B\tilde{c}\, dz + \frac{\partial}{\partial x}\int_{-H}^{\tilde{\zeta}} B(\tilde{u}\tilde{c} - K_h\tilde{c}_x)\, dz = -B(\tilde{D} - \tilde{E}_s).$$

Next, we impose that the concentrations are in a tidally averaged steady-state. This condition is called the concentration equilibrium [Dijkstra et al., 2019] and it implies:

$$-\frac{\partial}{\partial x}\left\langle \int_{-H}^{\tilde{\zeta}} B(\tilde{u}\tilde{c} - K_h\tilde{c}_x) dz \right\rangle = B\langle \tilde{D} - \tilde{E} \rangle, \tag{B.14}$$

Combining Eqs. (B.7) and (B.14) results in the following relation for bottom pool formation:

$$B\mathcal{S}_t = -\left\langle B\int_{-H}^{\tilde{\zeta}} (\tilde{u}\tilde{c} - K_h\tilde{c}_x)\, dz \right\rangle_x. \tag{B.15}$$

For the seaward boundary condition, a prescribed erodibility f_{sea} is given by:

$$f_{\text{sea}} = \frac{H_0 \tilde{c}_{\text{sea}}}{\langle \hat{C} \rangle_{x=0}}, \tag{B.16}$$

with $\tilde{c}_{\text{sea}}$ the prescribed depth- and width-averaged seaward concentration and $\langle \hat{C} \rangle$ the subtidal carrying capacity, that is the maximum tidal-averaged amount of sediment that can be in suspension locally for given hydrodynamic conditions:

$$\langle \hat{C} \rangle = \left\langle \int_{-H}^{0} \tilde{c}(t,x,z)\Big|_{f=1} dz \right\rangle. \tag{B.17}$$

At the landward boundary a fluvial import of sediment $\mathcal{F}_{\text{river}}$ is prescribed:

$$(BTf + BFf_x)_{x=L} = -\mathcal{F}_{\text{river}}. \tag{B.18}$$

C

Perturbation Analysis

A perturbation method is used to find (semi-)analytical approximations of solutions of the width-averaged system of equations, Eqs. (A.16), (A.20) and (B.5) with their corresponding boundary conditions. The first step in this procedure is non-dimensionalizing the equations using typical scales. Then we define a perturbation parameter ε and express magnitudes of the non-dimensional parameters in orders of ε. Finally, we expand the solution as an asymptotic series in terms of ε and group terms of equal order in their respective order equations. To obtain an approximation, we systematically solve the (linear) order equations up to a desired order. Further analysis of these approximations will bring clarity to the qualitative behaviour of the true (non-linear) solution at specific orders.

Table C.1: Scales of the model parameters

Variable	Typical Scale	Symbol	Expression
t	M_2 tidal frequency	σ	$t = \sigma^{-1} t^*$
ζ	M_2 tidal amplitude	A_{M_2}	$\zeta = A_{M_2}\zeta^*$
z	Water depth at entrance	H_0	$z = H_0 z^*$
x	Minimum of L_b or L	$\mathcal{L}$	$x = \mathcal{L}x^*$
u	Balancing the continuity equation	$\mathcal{U} = \frac{\sigma \mathcal{L} A_{M_2}}{H_0}$	$u = \mathcal{U}u^*$
w	Balancing the continuity equation	$\mathcal{W} = \frac{H_0}{\mathcal{L}}\mathcal{U}$	$w = \mathcal{W}w^*$
c	Seaward sediment concentration	c_{sea}	$c = c_{\text{sea}} c^*$
$\langle S \rangle$	Seaward salinity	S_*	$\langle S \rangle = S_* \langle S^* \rangle$
$\mathcal{S}$	Balancing the M.Eq. condition	$\mathcal{S}_0$	$\mathcal{S} = \mathcal{S}_0 \mathcal{S}^*$

Typical scales can be found in Table C.1. The typical scale of the horizontal and vertical velocities can be found by requiring a mass balance of the depth-integrated continuity equation [Chernetsky, 2012]. Using the Leibniz integral rule and boundary conditions (A.24) and (A.25), the depth-integrated continuity equation in non-dimensional form reduces to:

$$A_{M_2}\sigma\zeta^*_{t^*} + \frac{\mathcal{U}H_0}{\mathcal{L}}\hat{u}^*_{x^*} - \frac{\mathcal{U}H_0}{\mathcal{L}}\hat{u}^* = 0, \tag{C.1}$$

with $\hat{u}$ the depth-integrated horizontal velocity. By requiring the typical scale to be of the same magnitude we find $\mathcal{U}$. Then, a similar mass balance in the (non-depth-integrated) continuity equation produces $\mathcal{W}$.

With the typical scales defined, the non-dimensional forms of Eqs. (A.16) and (A.20) becomes:

$$u^*_{x^*} + w^*_{z^*} - \frac{\mathcal{L}}{L_b} u^* = 0, \tag{C.2a}$$

$$u^*_{t^*} + \frac{\mathcal{U}}{\sigma\mathcal{L}}(u^* u^*_{x^*} + w^* u^*_{z^*}) + \left(\frac{L_w}{\mathcal{L}}\right)^2 \zeta^*_{x^*} - \frac{\mathcal{U}_d}{\mathcal{U}} \langle S^* \rangle_{x^*} \left(z^* - \frac{A_{M_2}}{H_0}\zeta^*\right) = \left(\frac{A_v}{\sigma H_0^2} u^*_{z^*}\right)_{z^*}, \tag{C.2b}$$

with L_w the the frictionless tidal wavelength and $\mathcal{U}_d = \frac{g H_0 \beta_s S_*}{\sigma}$ a typical scale for density driven velocities. The non-dimensional boundary condition at the entrance becomes:

$$\zeta^*(t^*, 0) = \sum_{i \in \mathcal{G}} \frac{A_i}{A_{M_2}} \cos\left(\frac{\sigma_i}{\sigma_{M_2}} t^* + \phi_i\right) \tag{C.3}$$

Further, at the landward boundary we find:

$$\int_{-H/H_0}^{(A_{M_2}/H_0)\zeta^*} u^* \, dz^* = -\frac{Q}{\mathcal{U} H_0 B}, \qquad \text{at } x^* = \frac{L}{\mathcal{L}}. \tag{C.4}$$

Note that in dimensionless terms, the free surface is located at $z^* = (A_{M_2}/H_0)\zeta^*$. The corresponding boundary conditions are:

$$A_v u^*_{z^*} = 0, \qquad \text{at } z^* = (A_{M_2}/H_0)\zeta^*, \tag{C.5}$$

and

$$w^* = \zeta^*_{t^*} + \frac{A_{M_2}}{H_0} u^* \zeta^*_{x^*} \qquad \text{at } z^* = (A_{M_2}/H_0)\zeta^*. \tag{C.6}$$

The non-dimension sediment transport equation is given by:

$$c^*_{t^*} + \frac{\mathcal{U}}{\sigma\mathcal{L}}(u^* c^*_{x^*} + w^* c^*_{z^*}) - \frac{w_s}{\sigma H_0} c^*_{z^*} - \frac{K_h}{\sigma\mathcal{L}^2} c^*_{x^* x^*} - \frac{K_v}{\sigma H_0^2} c^*_{z^* z^*} - \frac{K_h}{\sigma\mathcal{L} L_b} c^*_{x^*} = 0. \tag{C.7}$$

The non-dimensional no flux condition becomes:

$$\frac{w_s}{\sigma H_0^2} c^* + \frac{K_v}{\sigma H_0^2} c^*_{z^*} = \frac{K_h}{\sigma\mathcal{L}^2} \frac{A_{M_2}}{H_0} c^*_{x^*} \zeta^*_{x^*}, \qquad \text{at } z^* = \frac{A_{M_2}}{H_0}\zeta^*. \tag{C.8}$$

The non-dimensional partial slip condition is given by:

$$u^*_{z^*} = \frac{s_f H_0}{A_v} u^*,$$

with the dimensionless slip parameter $s_f H_0 / A_v$. If this parameter is much larger than unity, then the bottom is close to a no-slip condition and if the dimensionless slip parameter is much smaller than unity then the bottom can be regarded as frictionless.

Finally, the non-dimensional form of the concentration equilibrium is given by:

$$\frac{\sigma\mathcal{L}\mathcal{S}_0}{H_0 c_{\text{sea}}} B^* \mathcal{S}^*_{t^*} = -\left\langle B^* \int_{-H/H_0}^{(A_{M_2}/H_0)\zeta^*} \mathcal{U} u^* c^* - \frac{K_h}{\mathcal{L}} c^*_{x^*} \, dz^* \right\rangle_{x^*}. \tag{C.9}$$

For many estuaries, including the Ems, the ratio of the M_2 tidal amplitude and the characteristic depth is small. Therefore we take our perturbation parameter to be this ratio: $\varepsilon = A_{M_2}/H_0 \ll 1$. Now, we can express the magnitude of non-dimensional parameters in orders of ε. The orders and numerical values of the non-dimensional parameters are shown in Table C.2.

Table C.2: Orders expressed in ε and values of non-dimensional parameters.

Parameter	Order	Value
$\varepsilon \equiv A_{M_2}/H_0$	$\mathcal{O}(\varepsilon)$	0.13
$\mathcal{U}/(\sigma\mathcal{L})$	$\mathcal{O}(\varepsilon)$	0.13
$\mathcal{U}_d/\mathcal{U}$	$\mathcal{O}(\varepsilon)$	0.29
$w_s/(\sigma H_0)$	$\mathcal{O}(1)$	3.57
$\mathcal{L}/L_b$	$\mathcal{O}(1)$	1
$A_v/(\sigma H_0^2)$	$\mathcal{O}(1)$	0.86
$K_v/(\sigma H_0^2)$	$\mathcal{O}(1)$	0.86
$K_h/(\sigma\mathcal{L}^2)$	$\mathcal{O}(\varepsilon^3)$	$7.9\cdot10^{-4}$
$K_h/(\sigma\mathcal{L}L_b)$	$\mathcal{O}(\varepsilon^3)$	$7.9\cdot10^{-4}$
$K_h/(\mathcal{L}\mathcal{U})$	$\mathcal{O}(\varepsilon^2)$	$6\cdot10^{-3}$
$K_h/(\sigma\mathcal{L}^2H_0)$	$\mathcal{O}(\varepsilon^4)$	$1.1\cdot10^{-4}$
A_{M_4}/A_{M_2}	$\mathcal{O}(\varepsilon)$	0.14
A_{S_2}/A_{M_2}	$\mathcal{O}(1)$	*
A_{S_4}/A_{M_2}	$\mathcal{O}(\varepsilon)$	*
$Q/(\mathcal{U}H_0B)$	$\mathcal{O}(\varepsilon)$	*

* These parameters are variable, albeit with fixed order, throughout this research.

Finally, we expand our solution as an asymptotic series:

$$\begin{aligned}
u^* &= u^{0*} + \varepsilon u^{1*} + \varepsilon^2 u^{2*} + \ldots,\\
w^* &= w^{0*} + \varepsilon w^{1*} + \varepsilon^2 w^{2*} + \ldots,\\
\zeta^* &= \zeta^{0*} + \varepsilon \zeta^{1*} + \varepsilon^2 \zeta^{2*} + \ldots,\\
c^* &= c^{0*} + \varepsilon c^{1*} + \varepsilon^2 c^{2*} + \ldots,
\end{aligned}$$

with u^{k*} representing the non-dimensional k^{th} order term of the approximation of u^*, similar for w^{k*}, ζ^{k*} and c^{k*}. After substituting these expressions in the non-dimensional width-averaged equations and boundary conditions, we can collect terms corresponding to equal powers of ε in their respective order equations. The quantities determining the concentration equilibrium, are all contained in to the first two orders. Hence the higher order interactions will be neglected. The leading and first order equations and respective solutions are described in Sections C.1 and C.2.

The introduction of the asymptotic series results in leading and first order contribution to the potential erosion $\hat{E}$. Note that the magnitude of the bed shear stress can be written as:

$$\begin{aligned}
|\tau_b| &= \rho_0 s_f |u^0 + u^1|,\\
&= \rho_0 s_f \sqrt{(u^0+u^1)^2},\\
&\approx \rho_0 s_f \sqrt{(u^0)^2 + 2u^0u^1},\\
&= \rho_0 s_f |u^0| \sqrt{1 + 2\frac{u^1}{u^0}},\\
&\approx \rho_0 s_f \left(|u^0| + \operatorname{sgn}(u^0)u^1\right),
\end{aligned}$$

where a Taylor expansion was used to obtain the last approximation. Using this we can formulate the leading and first order potential erosion contributions:

$$\hat{E}^0 = \frac{w_s \rho_s s_f \hat{M}}{g' d_s} |u^0|, \tag{C.10}$$

$$\hat{E}^1 = \frac{w_s \rho_s s_f \hat{M}}{g' d_s} \operatorname{sgn}(u^0) u^1. \tag{C.11}$$

C.1. Leading Order System of Equations

From here on, we continue with the dimension-full equations, since all the parameters are of equal order. Further, we have omitted the distinction for width-averaged quantities, for notational convenience. Furthermore, besides the first superscript, denoting the order of ε, a second superscript is given denoting the corresponding tidal forcing, e.g. u^{02} is the leading order longitudinal velocity forced by the M_2 and S_2 tidal constituents.

The leading order hydrodynamics are solely forced by M_2 and S_2 tidal waves at the seaward boundary. Therefore the leading order hydrodynamics are given by:

$$u_x^{02} + w_z^{02} - \frac{u^{02}}{L_b} = 0, \tag{C.12a}$$

$$u_t^{02} + g\zeta_x^{02} - (A_v u_z^{02})_z = 0. \tag{C.12b}$$

With the leading-order boundary conditions at the landward- and seaward-side:

$$\zeta^{02}(t,0) = A_{M_2}\cos(\sigma_{M_2}t + \phi_{M_2}) + A_{S_2}\cos(\sigma_{S_2}t + \phi_{S_2}), \tag{C.13}$$

$$\int_{-H(L)}^{0} u^{02}\,dz = 0. \tag{C.14}$$

Note that in Eq. (C.14) the domain of the integral is from the river bed to the undisturbed water level. Including the free surface elevation in this domain introduces $\mathcal{O}(\varepsilon)$ terms, this can be seen by substituting the Taylor expansion of u^{02} around $z = 0$ in Eq. (C.4). Hence for leading order river discharge, we only need to account for the $z = 0$ upper integration bound. This also holds for the boundary conditions, hence we take the boundary condition for $z = 0$ as the leading order contribution of the free surface boundary conditions:

$$w^{02} = \zeta_t^{02}, \qquad \text{at } z = 0, \tag{C.15}$$

$$A_v u_z^{02} = 0, \qquad \text{at } z = 0. \tag{C.16}$$

The bottom boundary conditions read:

$$w^{02} = -u^{02}H_x, \qquad \text{at } z = -H(x), \tag{C.17}$$

$$A_v u_z^{02} = s u^{02}, \qquad \text{at } z = -H(x). \tag{C.18}$$

In leading order the sediment transport equation reduces to a balance of local inertia, settling and vertical mixing:

$$c_t^0 - w_s c_z^0 = \left(K_v c_z^0\right)_z \tag{C.19}$$

The leading order contribution of the no-flux condition is given by:

$$w_s c^0 + K_v c_z^0 = 0, \qquad \text{at } z = 0. \tag{C.20}$$

The erosion boundary condition at $z = -H(x)$, is given in terms of a tidally averaged erodibility parameter $f(t,x)$

$$\begin{aligned} -K_v c_z^0 &= \hat{E}^0 f(t,x), \\ &= \frac{w_s \rho_s s_f \hat{M}}{\rho_0 g' d_s} |u^0(t,x,-H)| f(t,x). \end{aligned} \tag{C.21}$$

Leading Order Solution

A direct approach to solving the system of equations, as proposed by Chernetsky [2012], conflicts with the tidal average defined in Eq. (A.29) because the S_2 constituent cannot be averaged over the M_2 wave period since it has a slightly longer wave period. In order to maintain the applicability of the M_2 tidal average we propose a multiple time-scale approach for finding an approximation for the leading order solution in terms of the M_2 frequency only. Start by rewriting Eq. (C.13) in complex exponential form:

$$\begin{aligned} \zeta^{02}(t,0) &= \Re\left\{A_{M_2}e^{i\sigma_{M_2}t} + A_{S_2}e^{i\sigma_{S_2}t + i\phi_{S_2}}\right\}, \\ &= \Re\left\{\left(A_{M_2}e^{i\phi_{M_2}} + A_{S_2}e^{i(\sigma_{S_2}-\sigma_{M_2})t + i\phi_{S_2}}\right)e^{i\sigma_{M_2}t}\right\}, \end{aligned} \tag{C.22}$$

where $\Re\{\cdot\}$ denotes the real part. Thus the seaward boundary condition can be interpreted as an M_2 forcing with time-varying amplitude, this is known as the spring-neap tidal cycle. Next we expand time in two distinct time-scales $t = t_1 + t_2$ with $t_1 \ll t_2$. Thus t_1 corresponds to a short time-scale, $t_1 = \sigma_{M_2} t$, related to the ebb-flood cycle and t_2 corresponds to a long time-scale, $t_2 = (\sigma_{S_2} - \sigma_{M_2})t$, related to the spring-neap cycle. From inspection of the relative orders we find $(\sigma_{S_2} - \sigma_{M_2})/\sigma_{M_2} \sim \mathcal{O}(\varepsilon^2)$, hence the contribution of the time-derivative in leading order can be expressed as:

$$\left.\frac{d}{dt}\right|_{\mathcal{O}(1)} = \sigma_{M_2}\frac{\partial}{\partial t_1}. \tag{C.23}$$

Next, observe that Eqs. (C.12a) and (C.12b) are linear and separable, hence the solutions are of the following form:

$$(u^{02},\, w^{02},\, \zeta^{02}) = \Re\left\{\left(\hat{u}^{02}(x,z),\, \hat{w}^{02}(x,z),\, \hat{\zeta}^{02}(x,z)\right)\cdot A_{SN_2}(t_2)\cdot e^{i t_1}\right\}. \tag{C.24}$$

Substitution of Eqs. (C.23) and (C.24) into Eqs. (C.12a) and (C.12b) results in a system of ordinary differential equations for $(\hat{u}^{02},\, \hat{w}^{02},\, \hat{\zeta}^{02})$:

$$\hat{u}^{02}_x + \hat{w}^{02}_z - \frac{\hat{u}^{02}}{L_b} = 0, \tag{C.25a}$$

$$i\sigma_{M_2}\hat{u}^{02} + g\hat{\zeta}^{02}_x - (A_v\hat{u}^{02}_z)_z = 0. \tag{C.25b}$$

Solving Eq. (C.25b) with the boundary conditions at $z = 0$ and $z = -H(x)$ from Eqs. (C.16) and (C.18) results in the following expression of $\hat{u}^{02}$ in terms of the free surface elevation $\hat{\zeta}^{02}$:

$$\hat{u}^{02} = -\frac{g\hat{\zeta}^{02}_x}{i\sigma_{M_2}}\left(1 - \alpha(x)\cosh\beta(x)z\right), \tag{C.26}$$

with:

$$\alpha(x) = \frac{s}{A_v\beta\sinh\beta H + s\cosh\beta H},$$
$$\beta(x) = \sqrt{\frac{i\sigma_{M_2}}{A_v}}.$$

Next, solving Eq. (C.25b) with the boundary condition at $z = 0$ from Eq. (C.15) results in the expression for $\hat{w}^{02}$ in terms of the free surface elevation $\hat{\zeta}^{02}$:

$$\hat{w}^{02} = \frac{g}{i\sigma_{M_2}}\left(\frac{\hat{\zeta}^{02}_x}{L_b} - \hat{\zeta}^{02}_{xx}\right)\left(z - \frac{\alpha}{\beta}\sinh\beta z\right) + \frac{g\hat{\zeta}^{02}_x}{i\sigma_{M_2}\beta}\left(\alpha_x + \alpha\beta_x\left(z\coth\beta z - \frac{1}{\beta}\right)\right) + i\sigma_{M_2}\hat{\zeta}^{02}. \tag{C.27}$$

We have expressed both the longitudinal and vertical velocity profiles in terms of the free surface elevation. These expressions are related through Eq. (C.17). Then by substitution of the expressions for the velocity profiles, we find that the boundary condition is satisfied if $\hat{\zeta}^{02}$ satisfies the following differential equation:

$$T_1\hat{\zeta}^{02}_{xx} + T_2\hat{\zeta}^{02}_x + T_3\hat{\zeta}^{02} = 0, \tag{C.28}$$

with the coefficients given by:

$$T_1 = \frac{\alpha}{\beta}\sinh\beta H - H,$$
$$T_2 = -\frac{T_1}{L_b} - \frac{\alpha_x\sinh\beta H}{\beta} - \frac{\alpha\beta_x\sinh\beta H + \alpha\beta\beta_x H\cosh\beta H}{\beta^2} - H_x(1 - \alpha\cosh\beta H),$$
$$T_3 = -\frac{\sigma^2_{M_2}}{g}.$$

The equation for $\hat{\zeta}^{02}$ can be solved analytically for only a few limiting cases, for example in the case of constant depth we can simplify by $H_x = 0$ and the quantities A_v and s become constants. However in general, Eq. (C.28) has to be solved numerically, for example using finite-difference schemes. Then by back-substitution we find

the semi-analytical expressions for the leading order velocity profiles. Finally, from Eq. (C.22) it follows that the t_2-dependency is determined by:

$$A_{SN_2}(t_2) = A_{M_2} e^{i\phi_{M_2}} + A_{S_2} e^{it_2 + i\phi_{S_2}}. \tag{C.29}$$

This concludes the solution of the leading order hydrodynamics.

From an inspection of the bottom boundary condition, Eq. (C.21), it follows that leading order concentrations contain a residual (M_0) and an overtide (M_4) component, see Appendix D for the derivation. This allows the formulation:

$$c^0 = |A_{SN_2}(t_2)| \cdot \hat{c}^{00}(x,z) + \Re\left\{ \hat{c}^{04}(x,z) \cdot \frac{A_{SN_2}(t_2)}{A^*_{SN_2}(t_2)} |A_{SN_2}(t_2)| \cdot e^{2it_1} \right\}, \tag{C.30}$$

with $A^*_{SN_2}(t_2)$ denoting the complex conjugate of $A_{SN_2}(t_2)$. Since the order equations are linear and separable, one can find:

$$\hat{c}^{00} = \hat{E}^{00} f(t_2, x) e^{-\frac{w_s}{K_\nu}(H+z)},$$
$$\hat{c}^{04} = C_1 e^{r_1 z} + C_2 e^{r_2 z},$$

with the characteristic values:

$$r_{1,2} = \frac{-w_s \pm \lambda_{M_4}}{2K_\nu},$$

with $\lambda_{M_4} = \sqrt{w_s^2 + 8i\sigma_{M_2} K_\nu}$ and the coefficients:

$$C_1 = \frac{A_2(\lambda_{M_4} - w_s)}{\lambda_{M_4} + w_s},$$
$$C_2 = \frac{4(\lambda_{M_4} - w_s)\hat{E}^{04} f(t_2, x)}{(\lambda_{M_4} + w_s)^2 e^{-r_2 H} - (\lambda_{M_4} - w_s)^2 e^{-r_1 H}}.$$

Note that we have taken f to be a function of t_2. This is justified since f represents the tidal-averaged erodibility and hence it is independent of the short time-scale.

C.2. First Order System of Equations

The first order system contains the non-linearities expressed in terms of the leading order quantities, hence these terms can be interpreted as prescribed forcing. The first order equations describing the hydrodynamics are given by:

$$u^1_x + w^1_z - \frac{u^1}{L_b} = 0, \tag{C.31a}$$
$$u^1_t + u^{02} u^{02}_x + w^{02} u^{02}_z + g\zeta^1_x - g\beta\langle S\rangle_x z = (A_\nu u^1_z)_z. \tag{C.31b}$$

In the first order, we have the following landward- and seaward-side boundary conditions:

$$\zeta^1(t,0) = A_{M_4}\cos(\sigma_{M_4} t + \phi_{M_4}) + A_{S_4}\cos(\sigma_{S_4} t + \phi_{S_4}), \tag{C.32}$$
$$\int_{-H(L)}^{0} u^1 \, dz + \frac{H_0}{A_{M_2}} \zeta^{02} u^{02}\Big|_{z=0} = \frac{Q}{B}. \tag{C.33}$$

Where the second term of Eq. (C.33) follows from a Taylor expansion of the upper integration boundary around $z = 0$. However, from substitution of Eq. (C.26) in Eq. (C.14) it follows that $u^{02} = 0$ at $x = L$, hence this term vanishes and the seaward boundary condition reads:

$$\int_{-H(L)}^{0} u^1 \, dz = -\frac{Q}{B}. \tag{C.34}$$

The boundary conditions at the free surface are given by a Taylor expansion around $z = 0$, resulting in:

$$w^1 = \zeta^1_t - \zeta^{02} w^{02}_z + u^{02}\zeta^{02}_x, \qquad \text{at } z = 0, \tag{C.35}$$
$$A_\nu u^1_z + A_\nu \zeta^{02} u^{02}_{zz} = 0, \qquad \text{at } z = 0. \tag{C.36}$$

The bottom boundary conditions read:

$$w^1 = -u^1 H_x, \qquad \text{at } z = -H(x), \tag{C.37}$$

$$A_v u_z^1 = s u^1, \qquad \text{at } z = -H(x). \tag{C.38}$$

This concludes the first order hydrodynamics.

In first order, advective contributions enter the sediment transport equation as linear source terms:

$$c_t^1 - w_s c_z^1 - K_v c_{zz}^1 = -u^0 c_x^0 - w^0 c_z^0. \tag{C.39}$$

The first order contribution of the no-flux condition is given by:

$$w_s c^1 + K_v c_z^1 = -\zeta^0 c_t^0, \qquad \text{at } z = 0. \tag{C.40}$$

The erosion boundary condition at $z = -H(x)$, is given in terms of an tidally averaged erodibility parameter $f(t,x)$

$$\begin{aligned} -K_v c_z^1 &= \hat{E}^1 f(t,x), \\ &= \frac{w_s \rho_s s_f \hat{M}}{\rho_0 g' d_s} \mathrm{sgn}(u^0) u^1 \cdot f(t,x). \end{aligned} \tag{C.41}$$

First Order Solution

The first order system of equations is forced by the seaward boundary and by linear forcing in terms of leading order quantities. Using the same time-scales as for the leading order solution, $t = t_1 + t_2$, we rewrite the seaward boundary contribution at first order as:

$$\begin{aligned} \zeta^1(t,0) &= \Re\left\{ A_{M_4} e^{i\sigma_{M_4} t + i\phi_{M_4}} + A_{S_4} e^{i\sigma_{S_4} t + i\phi_{S_4}} \right\}, \\ &= \Re\left\{ \left(A_{M_4} e^{i\phi_{M_4}} + A_{S_4} e^{i(\sigma_{S_4} - \sigma_{M_4})t + i\phi_{S_4}} \right) e^{i\sigma_{M_4} t} \right\}, \\ &= \Re\left\{ \left(A_{M_4} e^{i\phi_{M_4}} + A_{S_4} e^{2it_2 + i\phi_{S_4}} \right) e^{2it_1} \right\}. \end{aligned} \tag{C.42}$$

Similar to the leading-order spring-neap cycle, we define the following subtidal amplitude function:

$$A_{SN_4}(t_2) = \left(A_{M_4} e^{i\phi_{M_4}} + A_{S_4} e^{2it_2 + i\phi_{S_4}} \right). \tag{C.43}$$

To show that the other forcing terms contain residual (M_0) and overtide (M_4) components we observe what happens to a typical forcing quantity: $\gamma(x,z,t_1,t_2) = w^{02}(x,z,t_1,t_2) u^{02}(x,z,t_1,t_2)$. Neglecting t_2-dependency for the moment, this can be written as:

$$\begin{aligned} \gamma &= \frac{1}{4}\left(\hat{w}^{02} e^{it_1} + \hat{w}^{02*} e^{-it_1} \right)\left(\hat{u}^{02} e^{it_1} + \hat{u}^{02*} e^{-it_1} \right), \\ &= \frac{1}{4}\left(w^{02} u^{02*} + w^{02*} u^{02} \right) + \frac{1}{4}\left(w^{02} u^{02} e^{2it_1} + w^{02*} u^{02*} e^{-2it_1} \right), \\ &= \langle \gamma \rangle + [\gamma]. \end{aligned}$$

Hence we find that the source γ induces an M_0, denoted by $\langle\cdot\rangle$, and an M_4, denoted by $[\cdot]$, contribution.

Using above remarks, we write the first order solution in terms of residual flow and a first overtide:

$$\chi^1 = \chi^{10} + \chi^{14},$$

with $\chi = (u, w, \zeta)$. We will separate the equations according to these tidal constituent.

Residual Flow

The first order system can be reduced to a system describing the residual flow by taking the tidal-average defined by Eq. (A.29). Note that due to the introduction of two time-scales the tidal-average is well-defined. Further, the forcing terms are denoted by an underbrace accompanied by a physical interpretation. Hence we find:

$$u_x^{10} + w_z^{10} - \frac{u^{10}}{L_b} = 0, \tag{C.44a}$$

$$\underbrace{\langle u^{02}u_x^{02} + w^{02}u_z^{02}\rangle}_{\text{adv}} + g\zeta^{10}\underbrace{-g\beta\langle S\rangle_x z}_{\text{grav-circ}} = (A_v u^{10})_z. \tag{C.44b}$$

There is a forcing term due to the residual advective contribution and the time-independent contribution due to a salinity gradient is named gravitational circulation. Further, the residual component of the boundary conditions at the free surface are given by:

$$w^{10} = \underbrace{-\langle \zeta^{02}w_z^{02} + u^{02}\zeta_x^{02}\rangle}_{\text{stokes}}, \qquad \text{at } z = 0, \tag{C.45}$$

$$A_v u_z^{10} + \underbrace{\langle A_v\zeta^{02}u_{zz}^{02}\rangle}_{\text{no-stress}} = 0, \qquad \text{at } z = 0. \tag{C.46}$$

These forcing terms can be interpreted as the residual contribution of Stokes drift and a term corresponding to the no-stress condition imposed at the free surface. The residual component of the boundary conditions at the bottom are given by:

$$w^{10} = -u^{10}H_x, \qquad \text{at } z = -H(x), \tag{C.47}$$

$$A_v u_z^{10} = su^{10}, \qquad \text{at } z = -H(x). \tag{C.48}$$

The river discharge forces the residual flow at the weir by:

$$\int_{-H(L)}^{0} u^{10}\,dz = \underbrace{-\frac{Q}{B}}_{\text{river}}. \tag{C.49}$$

Where the forcing term corresponds to the river discharge. Lastly, the residual forcing at the seaward boundary vanishes:

$$\zeta^{10}(t_1, t_2, L) = 0. \tag{C.50}$$

Due to linearity these equations can be solved by considering the sources independently, thus allowing a formulation:

$$\chi^{10} = \chi^{10}_{\text{adv}} + \chi^{10}_{\text{grav-circ}} + \chi^{10}_{\text{stokes}} + \chi^{10}_{\text{no-stress}} + \chi^{10}_{\text{river}}. \tag{C.51}$$

The individual components can be found analogously to the first order solutions. See the electronic supplement of Dijkstra et al. [2017].

First Overtide

The M_4 contribution to the first order solution is found by solving:

$$u_x^{14} + w_z^{14} - \frac{u^{14}}{L_b} = 0, \tag{C.52a}$$

$$u_{t_1}^{14} + \underbrace{[u^{02}u_x^{02} + w^{02}u_z^{02}]}_{\text{adv}} + g\zeta_x^{14} = (A_v u^{10})_z, \tag{C.52b}$$

containing a forcing term due to an advective contribution. Further at the boundary conditions at the free-surface are given by:

$$w^{14} = \zeta_{t_1}^{14} + \underbrace{[u^{02}\zeta_x^{02} - \zeta^{02}w_z^{02}]}_{\text{stokes}}, \qquad \text{at } z = 0, \tag{C.53}$$

$$A_v u_z^{10} + \underbrace{[A_v\zeta^{02}u_{zz}^{02}]}_{\text{no-stress}} = 0, \qquad \text{at } z = 0, \tag{C.54}$$

where we find the M_4 contributions due to Stokes drift and the no-stress condition. Further, at the bottom we find:

$$w^{14} = -u^{14} H_x, \qquad \text{at } z = -H(x), \tag{C.55}$$

$$A_v u_z^{14} = s u^{14}, \qquad \text{at } z = -H(x). \tag{C.56}$$

The externally prescribed M_4 tidal forcing at the seaward boundary is given by Eq. (C.42). Finally it must hold that the M_4 contribution of the river-discharge vanishes:

$$\int_{-H(L)}^{0} u^{14}\, dz = 0. \tag{C.57}$$

Due to linearity these equations can be solved by considering the sources independently, thus allowing a formulation:

$$\chi^{14} = \chi^{14}_{\text{adv}} + \chi^{14}_{\text{stokes}} + \chi^{14}_{\text{no-stress}} + \chi^{14}_{\text{tide}}. \tag{C.58}$$

Where the individual components can be found analogously to the first order solutions. See the electronic supplement of Dijkstra et al. [2017].

Sediment dynamics

Only the semi diurnal concentration component leads to a non-zero tidal-averaged contribution to the mopho-dynamic equilibrium condition, hence $c^1 \equiv c^{12}$. It follows that first order sediment dynamics is forced by linear estimates for sediment advection (C.39), a surface correction term (C.40) and first order erosion (C.41). Due to linearity of the order equations we can write:

$$c^{12} = c^{12}_{\text{ero}} + c^{12}_{\text{no-flux}} + c^{12}_{\text{sedadv}}. \tag{C.59}$$

Where the individual components can be found analogously to the first order solutions. See the electronic supplement of Dijkstra et al. [2017].

C.3. Solution of the Concentration Equilibrium

Following the general trend of the perturbation analysis, we will find the leading order solution of bottom pool evolution. This section serves as a concise overview of a detailed study on the topic given by Brouwer et al. [2018].

In the previous sections we derived that solutions to the tidal constituents u, c and ζ are composed by tidal components:

$$u = u^{02} + u^{10} + u^{14}, \tag{C.60}$$

$$\zeta = \zeta^{02} + \zeta^{10} + \zeta^{14}, \tag{C.61}$$

$$c = c^{00} + c^{04} + c^{12}. \tag{C.62}$$

Further, by inspecting the expressions for leading and first order concentration we find that these quantities solely contain components that scale linearly with f or f_x:

$$c = f c_f + f_x c_{f_x}, \tag{C.63}$$

with c_f denoting the component of c that scales linearly with f, similarly for c_{f_x}. This allows the formulation:

$$\begin{aligned} c_f &= c_f^{00} + \hat{c}_f^{04} + c_f^{12}, \\ c_{f_x} &= c_{f_x}^{12}. \end{aligned} \tag{C.64}$$

Now we start our analysis of Eq. (B.15). First, isolate the higher-order contribution of the free surface by expanding the upper integration bound as a Taylor series around $z = 0$ to obtain:

$$B\mathcal{S}_t = -\left\langle B \int_{-H}^{0} (uc - K_h c_x)\, dz + B\left[\zeta (uc - K_h c_x)\right]_{z=0} \right\rangle_x. \tag{C.65}$$

Since the flux-balance, i.e. the right-hand-side, is defined in terms of a tidal-average we will only consider terms containing residual components. These terms correspond to products of M_0-components and products of like tidal constituents, because the square of a sinusoidal function always contains a residual term. Next, by inspecting the orders of the flux-balance (Eq. (C.9)) we find that the leading order of the concentration equilibrium corresponds to $\mathcal{O}(\varepsilon^2)$ and is given by:

$$B\mathcal{S}_t = -(BTf + BFf_x)_x, \tag{C.66}$$

with:

$$T = \left\langle \int_{-H}^{0} u^{02} c_f^{12} + u^{14} c_f^{04} + u^{10} c_f^{00} - K_h (c_f^{00})_x \, dz + [\zeta^{02} u^{02} c_f^{00}]_{z=0} \right\rangle, \tag{C.67a}$$

$$F = \left\langle \int_{-H}^{0} u^{02} c_{f_x}^{12} - K_h c_f^{00} \, dz \right\rangle. \tag{C.67b}$$

The functions T and F are fully determined by leading and first order water motion. Finally, an initial condition obeying the boundary conditions for f needs to be supplied. Then Eq. (C.66) combined with boundary condition from Eqs. (B.16) and (B.18) can be solved by applying numerical time-integration and finite-difference methods.

D

Subtidal Transport Capacity

To derive the influence of the spring-neap amplitude modulation on the transport capacities we will first define the notion of subtidal dependency. Then we give derivations of the subtidal dependencies of the water motion and the suspended sediment concentration.

Definition of Subtidal Dependency

We remind the reader that the order equations (derived in Appendix C) are linear and separable resulting in a predefined form of the solutions in terms of complex functions. For example leading order horizontal velocity is given by:

$$u^{02}(t_1,t_2,x,z) = \Re\left\{u^{02}(x,z)\cdot A_{SN_2}(t_2)\cdot e^{it_1}\right\}.$$

Then the subtidal dependency is defined as the component of the argument of the real part that is proportional to function of t_2. For example the subtidal dependency of u^{02} is given by the spring-neap modulation function $A_{SN_2}(t_2)$, this will be denoted as:

$$u^{02} \propto A_{SN_2}.$$

For quantities that do not fluctuate on the subtidal time scale, e.g. the velocity induced by the river discharge u^{10}_{river}, the subtidal dependency is given by:

$$u^{10}_{\text{river}} \propto 1.$$

Water Motion

The leading order water motion is linearly proportional with the leading order amplitude function, see Eq. (C.24):

$$u^{02} \propto A_{SN_2}, \tag{D.1}$$

$$\zeta^{02} \propto A_{SN_2}. \tag{D.2}$$

First order hydrodynamical components typically arise due to the products of leading order quantities, see Appendix C. For example, the component related to the no-stress condition is solely forced by $A_v\zeta^{02}u^{02}_{zz}$. By writing out this product, assuming eddy-viscosity is independent of t_2, we can find the following temporal dependency of the forcing term that results in the no-stress component:

$$\begin{aligned}
\zeta^{02}u^{02}_{zz} &= \frac{1}{4}\left(\hat{\zeta}^{02}A_{SN_2}e^{it_1} + \hat{\zeta}^{02*}A^*_{SN_2}e^{-it_1}\right)\left(\hat{u}^{02}_{zz}A_{SN_2}e^{it_1} + \hat{u}^{02*}_{zz}A^*_{SN_2}e^{-it_1}\right),\\
&= \frac{1}{4}\left(|A_{SN_2}|^2(\hat{\zeta}^{02}\hat{u}^{02*}_{zz} + \hat{\zeta}^{02*}\hat{u}^{02}_{zz}) + (A_{SN_2})^2\hat{\zeta}^{02}\hat{u}^{02}_{zz}e^{2it_1} + (A^*_{SN_2})^2\hat{\zeta}^{02*}\hat{u}^{02*}_{zz}e^{-2it_1}\right),\\
&= \frac{1}{2}\underbrace{\Re\left(|A_{SN_2}|^2\hat{\zeta}^{02}\hat{u}^{02*}_{zz}\right)}_{D_0\text{ component}} + \frac{1}{2}\underbrace{\Re\left((A_{SN_2})^2\hat{\zeta}^{02}\hat{u}^{02}_{zz}e^{2it_1}\right)}_{D_4\text{ component}}.
\end{aligned} \tag{D.3}$$

Hence $u^1_{\text{no-stress}}$ consists of D_0 and D_4 components which vary on the subtidal time scale according to:

$$u^{10}_{\text{no-stress}} \propto |A_{SN_2}|^2,$$
$$u^{14}_{\text{no-stress}} \propto (A_{SN_2})^2.$$

Due to linearity, similar expressions can be found for $\zeta^1_{\text{no-stress}}$, $(u^1,\zeta^1)_{\text{adv}}$ and $(u^1,\zeta^1)_{\text{stokes}}$. Further, it is assumed that the residual velocities due to gravitational circulation and river discharge do not dependent on the long time scale t_2. Lastly, the resulting water motion forced by the first order external forcing scales with A_{SN_4}. Table D.1 gives an overview of the subtidal dependencies of the various water motion contributions.

Table D.1: Overview of subtidal hydrodynamical dependencies

(u^{02},ζ^{02})	$\propto$	A_{SN_2}
$(u^{10},\zeta^{10})_{\text{grav-circ}}$	$\propto$	1
$(u^{10},\zeta^{10})_{\text{river}}$	$\propto$	1
$(u^{10},\zeta^{10})_{\text{adv}}$	$\propto$	$\lvert A_{SN_2}\rvert^2$
$(u^{10},\zeta^{10})_{\text{stokes}}$	$\propto$	$\lvert A_{SN_2}\rvert^2$
$(u^{10},\zeta^{10})_{\text{no-stress}}$	$\propto$	$\lvert A_{SN_2}\rvert^2$
$(u^{14},\zeta^{14})_{\text{adv}}$	$\propto$	$(A_{SN_2})^2$
$(u^{14},\zeta^{14})_{\text{stokes}}$	$\propto$	$(A_{SN_2})^2$
$(u^{14},\zeta^{14})_{\text{no-stress}}$	$\propto$	$(A_{SN_2})^2$
$(u^{14},\zeta^{14})_{\text{tide}}$	$\propto$	A_{SN_4}

Sediment Dynamics

The leading order suspended sediment concentration is forced by erosion at the river bed, given by:

$$\hat{E}^0 = \frac{w_s \rho_s s_f}{g' d_s} \left| u^{02} \right|.$$

To express this in tidal constituents, the absolute value of the velocity h to be decomposed as a Fourier series:

$$\left| u^{02} \right| = a_0 + \sum_{m=1}^{\infty} \left(a_m e^{2imt_1} + a_m^* e^{-2imt_1} \right), \tag{D.4}$$

where the coefficients for all integer m (including zero) are given by

$$a_m = \frac{2}{\pi} \left| \hat{u}^{02} A_{SN_2} \right| \left(\frac{\hat{u}^{02} A_{SN_2}}{\left| \hat{u}^{02} A_{SN_2} \right|} \right)^{2m} \frac{(-1)^m}{1-4m^2}. \tag{D.5}$$

Since the forcing suspended sediment concentration is at leading order and since the first order water motion only contains D_0 and D_4 components, we find that only the contributions corresponding to $m = 0$ and $m = 1$ result in nonzero tidally averaged sediment transport. Thus, by omitting the higher order harmonics, we find that the subtidal dependencies of the leading order concentrations of interest are given by:

$$c^{00}_{\text{ero}} \propto |A_{SN_2}|, \text{ corresponding to } m = 0, \tag{D.6}$$

$$c^{04}_{\text{ero}} \propto |A_{SN_2}| \frac{A_{SN_2}}{A^*_{SN_2}}, \text{ corresponding to } m = 1. \tag{D.7}$$

First order concentration has contributions due to sediment advection, the no-flux condition at the surface and erosion. The subtidal dependency of the sediment advection term can be found by:

$$\begin{aligned} u^{02}c^{00}_{\text{ero},x} &= \frac{1}{4}\left(\hat{u}^{02}A_{SN_2}e^{it_1} + \hat{u}^{02*}A^*_{SN_2}e^{-it_1}\right)\cdot\left(|A_{SN_2}|c^{00}_{\text{ero},x} + |A_{SN_2}|c^{00*}_{\text{ero},x}\right), \\ &= \Re\left\{\hat{u}^{02}\cdot A_{SN_2}|A_{SN_2}|\cdot c^{00}_{\text{ero},x}\cdot e^{it_1}\right\}, \\ &\propto A_{SN_2}|A_{SN_2}|. \end{aligned} \tag{D.8}$$

The subtidal dependency due to the no-flux condition at the surface is given by:

$$\begin{aligned} u^{02}c^{04}_{x,\text{no-flux}} &= \frac{1}{4}\left(\hat{u}^{02}A_{SN_2}e^{it_1} + \hat{u}^{02*}A^*_{SN_2}e^{-it_1}\right)\left(\hat{c}^{04}_{x,\text{no-flux}}|A_{SN_2}|\frac{A_{SN_2}}{A^*_{SN_2}}e^{2it_1} + \hat{c}^{04*}_{x,\text{no-flux}}|A_{SN_2}|\frac{A^*_{SN_2}}{A_{SN_2}}e^{-2it_1}\right), \\ &= \frac{1}{2}\Re\left\{\hat{u}^{02*}\hat{c}^{04}_{x,\text{no-flux}}\cdot A^*_{SN_2}|A_{SN_2}|\frac{A_{SN_2}}{A^*_{SN_2}}\cdot e^{it_1}\right\} + h.o.h., \\ &\propto A^*_{SN_2}|A_{SN_2}|\frac{A_{SN_2}}{A^*_{SN_2}}, \\ &\propto A_{SN_2}|A_{SN_2}|. \end{aligned} \tag{D.9}$$

With $h.o.h.$ denoting the higher order harmonics, i.e. terms containing $e^{\pm 3it_1}$. Since these terms do not lead to non-zero tidally averaged sediment transport, they will be omitted.

The first order contribution due to erosion is given by:

$$\hat{E}^1 = \frac{w_s\rho_s s_f}{g'd_s}\text{sgn}\left(u^{02}\right)[u^{10}+u^{14}].$$

Similar to the leading order erosion, we make a harmonic decomposition:

$$\text{sgn}\left(u^{02}\right) = \sum_{m=1}^{\infty}\left(b_m e^{i(2m-1)t_1} + b^*_m e^{-i(2m-1)t_1}\right), \tag{D.10}$$

with the coefficients given by:

$$b_m = \frac{2}{\pi}\frac{(-1)^{(m-1)}}{2m-1}\left(\frac{\hat{u}^{02}A_{SN_2}}{|\hat{u}^{02}A_{SN_2}|}\right)^{2m-1}. \tag{D.11}$$

Leading order water motion only contains an D_2 component, therefore only contributions to the first order suspended sediment concentration resulting from $m=1$ and $m=2$, corresponding to D_2 and D_6 components respectively, result in non-zero tidally averaged sediment transport. In this section, only the contribution corresponding with $m=1$ is analyzed. The respective subtidal dependencies is given by $\text{sgn}(A_{SN_2})$. To obtain the D_2 component of the suspended sediment concentration, the D_2 component must be multiplied with each term contained in u^{10} and u^{14}. The resulting subtidal dependencies of the first order sediment concentration due to erosion is given in Table D.2.

Table D.2: Overview of subtidal dependencies of individual concentration components*

c^{00}_{ero}	$\propto$	$\lvert A_{SN_2}\rvert$	due to u^{02}
c^{04}_{ero}	$\propto$	$\lvert A_{SN_2}\rvert\frac{A_{SN_2}}{A^*_{SN_2}}$	due to u^{02}
c^{12}_{sedadv}	$\propto$	$A_{SN_2}\lvert A_{SN_2}\rvert$	
$c^{12}_{\text{no-flux}}$	$\propto$	$A_{SN_2}\lvert A_{SN_2}\rvert$	
c^{12}_{ero}	$\propto$	$\text{sgn}(A_{SN_2})$	due to u^{10}_{river} and $u^{10}_{\text{grav-circ}}$
c^{12}_{ero}	$\propto$	$A_{SN_2}\lvert A_{SN_2}\rvert$	due to u^{10}_{adv}, u^{10}_{stokes} and $u^{10}_{\text{no-stress}}$
c^{12}_{ero}	$\propto$	$A_{SN_2}\lvert A_{SN_2}\rvert$	due to u^{14}_{adv}, u^{14}_{stokes} and $u^{14}_{\text{no-stress}}$
c^{12}_{ero}	$\propto$	$\text{sgn}(A_{SN_2})^* A_{SN_4}$	due to u^{14}_{tide}

*For first order concentration due to erosion, only the dominant contribution is analyzed.

Transport Capacity

Now that the subtidal dependencies of the water motion and sediment concentration have been obtained, we turn our attention towards the transport capacity. In this appendix, we only derive the subtidal dependencies of the six dominant transport mechanisms in the interior of the domain, namely transport due to Stokes-forcing, the no-stress condition at the surface, sediment advection, river discharge, gravitational circulation and the tidal forcing. Subtidal dependencies of other transport mechanisms can be obtained analogously.

The transport capacity due to Stokes-forcing T_{stokes} consists of two components, transport due to Stokes-drift $T_{\text{stokes-drift}}$ and the tidal return flow $T_{\text{return-flow}}$. These components have similar subtidal behaviour given by:

$$\begin{aligned} T_{\text{stokes-drift}} &= \left\langle \left[\zeta^{02} u^{02} c^{00}_{\text{ero}}\right]_{z=0} + \left[\zeta^{02} u^{02} c^{04}_{\text{ero}}\right]_{z=0} \right\rangle, \\ &= A_{SN_2} A^{*}_{SN_2} |A_{SN_2}| \cdot \Re\left\{ \frac{1}{2}\left[\hat{\zeta}^{02} \hat{u}^{02*} \hat{c}^{00}_{\text{ero}}\right]_{z=0} + \frac{1}{4}\left[\hat{\zeta}^{02} \hat{u}^{02} \hat{c}^{04*}_{\text{ero}}\right]_{z=0} \right\}, \\ &\propto |A_{SN_2}|^3. \end{aligned} \tag{D.12}$$

and

$$\begin{aligned} T_{\text{return-flow}} &= \int_{-H}^{0} u^{10}_{\text{stokes}} c^{00}_{\text{ero}} + \left\langle u^{14}_{\text{stokes}} c^{04}_{\text{ero}} + u^{02} c^{12}_{\text{ero,stokes}} \right\rangle \, dz. \\ &= \int_{-H}^{0} |A_{SN_2}|^3 \cdot \left(\hat{u}^{10}_{\text{stokes}} \hat{c}^{00}_{\text{ero}} + \frac{1}{2} \cdot \Re\left\{ \hat{u}^{14}_{\text{stokes}} \hat{c}^{04*}_{\text{ero}} + \hat{u}^{02} \hat{c}^{12*}_{\text{ero,stokes}} \right\} \right) dz, \\ &\propto |A_{SN_2}|^3, \end{aligned} \tag{D.13}$$

Hence we conclude:

$$T_{\text{stokes}} = (T_{\text{stokes-drift}} + T_{\text{return-flow}}) \propto |A_{SN_2}|^3. \tag{D.14}$$

Since the subtidal dependencies of the horizontal water velocity components due to Stokes-forcing and the no-stress condition are equal (see Table D.1), it also follows that $T_{\text{no-stress}} \propto |A_{SN_2}|^3$.

In an analogous manner, we find that the transport capacity due to sediment advection T_{sedadv} is given by:

$$\begin{aligned} T_{\text{sedadv}} &= \int_{-H}^{0} \left\langle u^{02} c^{12}_{\text{sedadv}} \right\rangle \, dz. \\ &\propto |A_{SN_2}|^3. \end{aligned} \tag{D.15}$$

For the transport capacity due to river discharge T_{river} we find:

$$\begin{aligned} T_{\text{river}} &= \int_{-H}^{0} u^{10}_{\text{river}} c^{00}_{\text{ero}} + \left\langle u^{02} c^{12}_{\text{river}} \right\rangle \, dz, \\ &= \int_{-H}^{0} |A_{SN_2}| \cdot \left(\hat{u}^{10}_{\text{ero, river}} \hat{c}^{00}_{\text{ero}} + \frac{1}{2} \cdot \Re\left\{ \hat{u}^{02} \hat{c}^{12}_{\text{ero, river}} \right\} \right) dz, \\ &\propto |A_{SN_2}|. \end{aligned} \tag{D.16}$$

Since the subtidal dependency of u^{10}_{river} and $u^{10}_{\text{grav-circ}}$ is equal, it also follows that $T_{\text{grav-circ}} \propto |A_{SN_2}|$.

The transport capacity due to externally prescribed tidal forcing will be decomposed in D_2 and D_4 contributions. First the spring-neap amplitude functions will be written as:

$$\begin{aligned} A_{SN_2} &= |A_{SN_2}| e^{i\phi_{SN_2}}, \\ A_{SN_4} &= |A_{SN_4}| e^{i\phi_{SN_4}}, \end{aligned}$$

with ϕ_{SN_2} and ϕ_{SN_4} the respective t_2-dependent phases of the externally prescribed tidal wave and the first overtide. Using this, the subtidal dependency for $T_{\text{ext.-}D_2}$ can be expressed as:

$$\begin{aligned} T_{\text{ext.-}D_2} &= \int_{-H}^{0} \left\langle u^{02} c^{12}_{\text{ero,tide}} \right\rangle \, dz, \\ &= \int_{-H}^{0} \frac{1}{2} \cdot \Re\left\{ |A_{SN_2}| \cdot |A_{SN_4}| e^{-i(\phi_{SN_4} - 2\phi_{SN_2})} \cdot \hat{u}^{02} \hat{c}^{12*}_{\text{ero,tide}} \right\} dz, \\ &\propto |A_{SN_2}| \cdot |A_{SN_4}| e^{-i(\phi_{SN_4} - 2\phi_{SN_2})}. \end{aligned} \tag{D.17}$$

In a similar fashion, the dependency of $T_{\text{ext.-}D_4}$ is obtained:

$$\begin{aligned} T_{\text{ext.-}D_4} &= \int_{-H}^{0} \left\langle u_{\text{tide}}^{14} c_{\text{tide}}^{04} \right\rangle \, dz, \\ &= \int_{-H}^{0} \frac{1}{2} \cdot \Re \left\{ |A_{SN_2}| \cdot |A_{SN_4}| e^{i(\phi_{SN_4} - 2\phi_{SN_2})} \hat{u}_{\text{tide}}^{14} \hat{c}_{\text{tide}}^{04*} \right\} \, dz, \\ &\propto |A_{SN_2}| \cdot |A_{SN_4}| e^{i(\phi_{SN_4} - 2\phi_{SN_2})}. \end{aligned} \tag{D.18}$$

Table D.3 contains an overview of these results.

Table D.3: Overview of subtidal dependencies of the dominant contributions to the transport capacity

T_{stokes}	$\propto$	$\lvert A_{SN_2}\rvert^3$
$T_{\text{no-stress}}$	$\propto$	$\lvert A_{SN_2}\rvert^3$
T_{sedadv}	$\propto$	$\lvert A_{SN_2}\rvert^3$
T_{river}	$\propto$	$\lvert A_{SN_2}\rvert$
$T_{\text{grav-circ}}$	$\propto$	$\lvert A_{SN_2}\rvert$
$T_{\text{ext.-}D_2}$	$\propto$	$\lvert A_{SN_2}\rvert \cdot \lvert A_{SN_4}\rvert e^{-i(\phi_{SN_4} - 2\phi_{SN_2})}$
$T_{\text{ext.-}D_4}$	$\propto$	$\lvert A_{SN_2}\rvert \cdot \lvert A_{SN_4}\rvert e^{i(\phi_{SN_4} - 2\phi_{SN_2})}$

Bibliography

G.P. Allen, J.C. Salomon, P. Bassoullet, Y. du Penhoat, and C. de Grandpre. Effects of tides on mixing and suspended sediment transport in macrotidal estuaries. *Sedimentary Geology*, 1980.

R.L. Brouwer, G.P. Schramkowski, Y.M. Dijkstra, and H.M. Schuttelaars. Time evolution of estuarine turbidity maxima in well-mixed tidally dominated estuaries: the role of availability- and erosion-limited conditions. *Journal of Physical Oceanography*, 2018.

H. Burchard. *Applied Turbulence Modelling in Marine Water*. 2002.

H. Burchard, H.M. Schuttelaars, and D.K. Ralston. Sediment trapping in estuaries. *Annual review of Marine Science*, 2018.

A. S. Chernetsky, H. M. Schuttelaars, and S. A. Talke. The effect of tidal asymmetry and temporal settling lag on sediment trapping in tidal estuaries. *Ocean Dynamics*, 2010.

A.S. Chernetsky. Trapping of sediment in tidal estuaries, 2012.

F. Colijn. Light absorption in the waters of the ems-dollard estuary and its consequences for the growth of phytoplankton and microphytobenthos. *Netherlands Journal of Sea Research*, 1982.

R. Costanza, R. d'Arge, R. de Groot, S. Farber, M. Grasso, B. Hannon, K. Limburg, S. Naeem, R.V. O'Neill, J. Paruelo, R.G. Raskin, P. Sutton, and M. van den Belt. The value of the world's ecosystem services and natural capital. *Nature*, 1997.

B. Cushman-Roisin. *Introduction to Geophysical Fluid Dynamics*. 1994.

V.N. de Jonge, H.M. Schuttelaars, J.E.E. van Beusekom, S.A. Talke, and H.E. de Swart. The influence of channel deepening on estuarine turbidity levels and dynamics as exemplified by the ems estuary. *Estuarine, Coastal and Shelf Science*, 2014.

R.J. Diaz and R. Rosenberg. Introduction to environmental and economic consequences of hypoxia. *Water Resources Development*, 2011.

Y.M. Dijkstra. Regime shifts in sediment concentrations in tide-dominated estuaries, 2019.

Y.M. Dijkstra, R.L. Brouwer, H.M. Schuttelaars, and G.P. Schramkowski. The iflow modelling framework v2.4: a modular idealized process-based model for flow and transport in estuaries. *Geoscientific Model Development*, 2017.

Y.M. Dijkstra, H.M. Schuttelaars, and G.P. Schramkowski. Modeling the transition to high sediment concentration as a response to channel deepening in the ems river estuary. *JGR Oceans*, 2019.

R.W. Fairbridge. *The estuary: its definition and geochemical role*. 1980.

C. L. Fefferman. *Existence and Smoothness of the Navier-Stokes Equations*. 2000.

J.F. Festa and D.V. Hansen. Turbidity maxima in partially mixed estuaries: a two-dimensional numerical model. *Estuarine and Coastal Marine Science*, 1978.

C.T. Friedrichs and J.M. Hamrick. Effects of channel geometry on cross sectional variations in along channel velocity in partially stratified estuaries. *Coastal and Estuarine Studies*, 1996.

K.M.H. Huijts, H.M. Schuttelaats, H.E. de Swart, and A. Valle-Levinson. Lateral entrapment of sediment in tidal estuaries: An idealized model study. *Journal of Geophysical Research*, 2006.

Stephen Hunt, Karin R. Bryan, and Julia C. Mullarney. The effect of wind waves on spring-neap variations in sediment transport in two meso-tidal estuarine basins with contrasting fetch. *Geomorphology*, 2017.

Ming Li, Wei Liu, Robert Chant, and Arnoldo Valle-Levinson. Flood-ebb and spring-neap variations of lateral circulation in the james river estuary. *Continental Shelf Research*, 2017.

C. Meerman, V. Rottschafer, and H.M. Schuttelaars. Influence of geometrical variations on morphodynamic equilibria in short tidal basins. *Ocean Dynamics*, 2019.

P. Meire, T. Ysebaert, S. van Damme, E. van den Bergh, T. Maris, and E. Struyf. The scheldt estuary: a description of a changing ecosystem. *Springer Hydrobiologia*, 2005.

A. B. Murray. Contrasting the goals, strategies and predicitions associated with simplified numerical models and detailed simulations. *Prediction in Geomorphology*, 2003.

F. T. M. Nieuwstadt, B. J. Boersma, and J. Westerweel. *Turbulence: Introduction to Theory and Application of Turbulent Flows*. 2016.

R. Pawlowicz, B. Beardsley, and S. Lentz. Classial tidal harmonic analysis including error estimates in matlab using t-tide. *Computers and Geosciences*, 2002.

D.W. Pritchard. What is an estuary: a physical viewpoint. *American Association for the Advancement of Science*, 1967.

M. Rahman. *Water Waves*. 1995.

H.G. Savenije. *Salinity and Tides in Alluvial Estuaries*. 2012.

G.P. Schramkowksi, H.M. Schuttelaars, and H.E. de Swart. The effect of geometry and bottom friction on local bed forms in a tidal embayment. *Continental Shelf Research*, 2002.

D.A. Sutherland and P. MacCready. A model study of the salish sea estuarine circulation. *Journal of Physical Oceanography*, 2011.

S.A. Talke, H.E. de Swart, and V.N. de Jonge. An idealized model and systematic process study of oxygen depletion in highly turbid estuaries. *Estuaries and Coasts*, 2009a.

S.A. Talke, H.E. de Swart, and H.M. Schuttelaars. Feedback between residual circulations and sediment distribution in highly turbid estuaries: An analytical model. *Continental Shelf Research*, 2009b.

A. Valle-Levinson, C. Reyes, and R. Sanay. Effects of bathymetry, friction and rotation on estuary-ocean exchange. *Journal of Physical Oceanography*, 2003.

J.C. Winterwerp and Z.B. Wang. Man-induced regime shifts in small estuaries - 1: theory. *Ocean Dynamics*, 2013.

R.C. Wofsy. A simple model to predict extinction coefficients and phytoplankton biomass in eutrophic waters. *Limnology and Oceanography*, 1983.

K. C. Wong. On the nature of transverse variability in coastal plain estuary. *Journal of Geophysical Research*, 1994.

J.T.F. Zimmerman. On the lorentz linearization of a quadratically damped forced oscillator. *Physics Letters A*, 1982.